How Large Immobile Particles Impact Sediment Transport and Bed Morphology in Gravel Bed Rivers

by

Christopher William McKie

A thesis
presented to the University of Waterloo
in fulfillment of the
thesis requirement for the degree of
Master of Applied Science
in
Civil Engineering

Waterloo, Ontario, Canada, 2019

Author's Declaration

I hereby declare that I am the sole author of this thesis. This is a true copy of the thesis, including any required final revisions, as accepted by my examiners.

I understand that my thesis may be made electronically available to the public.

Abstract

Large particles can be deposited in natural stream channels as a result of failed erosion protection measures or geological deposits. The impacts these large particles have on the natural systems have been studied, however the previous literature that has been completed either has a very narrow scope applicable only to alpine rivers or are simplified and do not fully capture the processes that occur in a natural channel system. Additionally, the results often contradict each other, and give an unclear understanding of the effects these large particles have on bed morphology and sediment transport.

This thesis utilizes a laboratory experiment to evaluate the effects that varying densities of large immobile particles in a gravel-bed channel have on sediment transport and bed morphology. The objective of this study is to gain further understanding and to consolidate existing literature to provide a more holistic overview of the effects of these large particles on a channel bed. It was expected that large immobile particles would cause an increase in channel roughness, and that the impacts to sediment transport and bed morphology would reflect this.

The laboratory experiment consisted of 5 test cases with varying densities of large immobile particles, and one base case with no large particles present. In each case, the flume bed was composed of a poorly sorted gravel mixture with a bi-modal distribution of sand and gravel meant to be representative of a natural gravel-bed channel. The large particles were sized to be representative of common engineering principles by applying a factor of safety to a minimum stable particle size. Each experimental case consisted of a single hydrograph with continuous sediment input scaled to the flow rate.

The results of the test cases and the base case proved that relating the large particle density to an increase in channel roughness was too simplistic to explain the trends found within this study. At low densities of large immobile particles, the transported material and the bed material both became coarser. At medium densities of large immobile particles, the bed material size and erosion reached a maximum, and the system also approached equal mobility. Finally, at high densities of large immobile particles, the size of transported material and bed material sizes were similar to that of the base case, and the sediment transport also had the strongest clockwise hysteresis trend. These results indicate the difficult of relating large immobile particle density to channel roughness to explain the effects on sediment transport and bed morphology.

In an effort to provide a more holistic explanation, and to consolidate the existing literature, a more complex explanation was developed using the findings of previous research and relating it to the results found within this study. This complex model is made up of 3 main points:

1. Isolated large immobile particles create localized areas of increased erosive forces, and localized protected areas (Brayshaw et al., 1983).
2. At a narrow range of large immobile particle spacings, flow structures build upon each other and amplify their erosive forces (Tan and Curran, 2012).

3. Densely spaced large immobile particles causes high energy skimming flow that is able to create powerful eddies in gaps between the large particles (Hassan and Reid, 1990).

This complex model explains the trends and results found within this study. Additionally, the results of this research were used to form the framework for predicting or understanding the impacts to a natural channel system caused by the introduction of large immobile material. Finally, the results of this study can be used to further research and develop design criteria for engineered in-channel structures to remedy imbalanced channel processes.

Acknowledgements

I would like to begin by thanking my supervisor, Dr. William Annable, for his guidance and support. He introduced me to river science and has helped me gain understanding and knowledge in this field, not only during this masters thesis, but also through the experiences which began in my 2B co-op term. Without this mentorship, I would not be where I am today.

I would also like to thank many people at the Laboratory of Hydraulic Constructions at École polytechnique fédérale de Lausanne (EPFL) for their help with my lab experiment. Specifically I would like to thank Dr. Mário Franca and Dr. Carmelo Juez who helped my formulate the experiments presented here, and gave me guidance while the experiments were being run, when the data was being processed and analyzed, and during the writing of this thesis. While they were both extremely helpful in my guiding my thesis, they also welcomed me and provided support for the 3 months I spent away from home. Finally, I would also like to thank Dr. Anton Schleiss who provided me with the laboratory equipment and the resources to complete my experiment.

Ben Plumb deserves thanks for many reasons. He has provided me with a great deal of guidance, review and motivation throughout this entire process. From being available to talk through the experimental setup all the way to giving this thesis a read through before being submitted, this thesis would not be what it is today without his help. Although the circumstances were unfortunate, I would be amiss not to thank Ben for providing the opportunity to study in Switzerland for three months, and also helping to nudge me in the right direction to seize it.

I would like to thank the Natural Sciences and Engineering Research Council of Canada (NSERC) for providing funding through the IPS scholarship. I would also like to thank John Beebe (JTB Environmental Systems) for providing funding as a part of the IPS program, but also for encouraging me to take the opportunity go to study in Switzerland.

Finally, I would like to thank my wife Katherine for supporting me through this process. She was understanding during all of the evenings and weekends I spent writing this thesis. She even brought me the occasional beer to help get me through it.

Table of Contents

List of Figures

List of Tables

List of Symbols

$\frac{D_i}{D_x}$	Relative sediment size [−]
$\frac{p_i}{f_i}$	Fractional transport ratio [−]
$\frac{q_{bi}p_i}{f_i}$	Scaled fractional transport rate $[\frac{M}{L \cdot T}]$
γ	Specific weight of water $[\frac{M \cdot L}{L^2 \cdot T^2}]$
λ	Distance between particle centers $[L]$
ρ_s	Sediment density $[\frac{M}{L^3}]$
ρ_w	Water density $[\frac{M}{L^3}]$
τ_m^*	Dimensionless shear stress on mobile sediment [−]
τ_t^*	Dimensionless total shear stress [−]
τ^*	Dimensionless shear stress [−]
τ_C^*	Dimensionless critical shear stress [−]
τ_{cm}^*	Dimensionless critical shear stress for mobile sediment [−]
τ_0	Bed shear stress $[\frac{M \cdot L}{L \cdot T^2}]$
τ_{ci}^*	Dimensionless critical shear stress of specific size class [−]
A_m	Area of mobile sediment on channel bed $[L^2]$
A_t	Total area of channel bed $[L^2]$
D	Particle diameter $[L]$
D_i	i$^{\text{th}}$ particle diameter $[L]$
d_i	Grain diameter $[L]$
D_x	reference particle size $[L]$
D_{gi}	Geometric mean of the sediment size class diameter $[L]$
f_i	Fraction of size class in bed material [−]
G	Specific gravity of material [−]
h	Depth of flow $[L]$
n	Manning's roughness coefficient $[\frac{T}{L^{1/3}}]$

p_i Fraction of size class in transported material $[-]$

q^* Dimensionless discharge $[-]$

q^* Einstein's dimensionless bedload transport rate $[-]$

q^*_{sm} Dimensionless sediment transport rate for mobile sediment $[-]$

q_s Dimensional bedload transport rate $[\frac{M}{L \cdot T}]$

q_{bi} Transport rate of material size class $[-]$

q_{bi} Unit bedload transport rate of specific size fraction $[\frac{M}{L \cdot T}]$

$Q_{s,in}$ Sediment flow rate entering the system $[M/T]$

$Q_{s,out}$ Sediment flow rate leaving the system $[M/T]$

R_h Hydraulic Radius $[L]$

S Bed slope $[-]$

S_f Friction slope $[-]$

V Average channel velocity $[\frac{L}{T}]$

1 Introduction

Channel erosion, either due to natural processes or as it adjusts due to a disturbance such as urbanization, can often increase infrastructure or other human interests to higher levels of risk. In the past, infrastructure proximal to stream channels were generally protected using hard-engineering approaches, often concrete walls or concrete channel linings. Despite industry advancements away from these practices, other hard approaches such as the lining of channel banks with riprap or other large material are commonplace (Province of British Columbia, 2000; MTO, 1997; Colorado Department of Transportation, 2004; U.S. Department of Transportation, Federal Highway Administration, 1989; IOWA Department of Natural Resources, 2006; New Jersey State Soil Conservation Committee, 2014; United States Geological Survey, 1986; Vermont Department of Environmental Conservation, 2013; Scottish Environment Protection Agency, 2008). Large material is used for constructing scour protection measures for many features including culvert outlets, bridge piers, and grade control structures.

While the use of large material in river engineering works is aimed at providing erosion protection and stability, it often does not address the channel processes that created the initial issues. Without addressing these issues, stabilization and protection efforts can fail through processes such as particle erosion, transitional slides, and slumping (Blodgett and McConaughy, 1986). Additionally, installation errors can cause failure of these stabilization efforts (Sutton, 2008). Regardless of the exact method of failure, the use of large material in channel remediations often result in large material being deposited on the channel bed.

The impacts of large particles once they have reached the bed of a channel have been studied with varying outcomes. Brayshaw et al. (1983) proposed that at higher densities of large particles on the channel bed, resistance to flow would increase and sediment transport rates would decrease. More recent studies have found that intermediate densities of large particles experienced a peak in resistance rather than large particle density being proportional to resistance (Hassan and Reid, 1990; Yager et al., 2007). There is disagreement in the trends of sediment transport with changes in large particle density, with some studies finding that sediment transport follows a decreasing trend with increasing large particle density (Ghilardi, 2014) and others finding the trend to be complex and not following a consistently increasing or decreasing trend when compared to either resistance to flow or large particle density (Hassan and Reid, 1990).

While the topic of research related to the effects of large immobile particles on sediment transport and bed morphology has been explored by many researchers, their conflicting findings emphasize the need for further study. Many of the studies relevant to this topic use over simplified conditions to gain understanding of a complex process such as steady flow (Hassan and Reid, 1990; Church et al., 1998; Hassan and Church, 2000), uniform sediment (Strom et al., 2004), or no sediment inflow (Hassan and Reid, 1990). Additionally, many studies have examined the isolated effects of a single roughness element or a small group of them (Brayshaw et al., 1983; Church et al., 1998; Strom et al., 2004; Tritico and Hotchkiss, 2005), which is often difficult to use for understanding of larger scale processes. Finally, many of the studies completed to date were based upon a narrow set of conditions,

emulating high-gradient river systems typically found in alpine settings (Ghilardi, 2014; Aristide Lenzi et al., 2006; Yager et al., 2007, 2012).

In order to gain further understanding of the effects of large particles on sediment transport and bed morphology on gravel-bed channel processes, further research is merited to provide insight on a more holistic system that emulates more naturally occurring conditions. Further work is needed to confirm that results found in high-gradient systems are applicable in moderate-to-low gradient systems found in many gravel bed rivers. In order to address this research gap, this study undertook flume experiments, with a moderate channel slope, a bi-modal sand gravel bed composition and variable water and sediment inflow rates to emulate a typical hydrographic flood event. Data related to sediment transport and bed morphology were collected throughout the experiment. The specific objectives of this research are: 1) to evaluate the effects that varying densities of large immobile particles (ie. rip-rap that has failed from its intended location and is contributing to the bed material) in a gravel-bed channel have on sediment transport and bed morphology and 2) to provide a more holistic overview of these effects of large particles to consolidate the findings of existing literature.

2 Background

This section provides a background on the pathways in which large particles find their way into channel systems, as well as a background overview of analysis methodologies and previous work related to large particles in channel systems. The first subsection examines the modes that large particles are introduced into stream corridors, and then further provides information on how such particles become part of the bed material compliment. The remaining subsections provide background on previous research completed on the effects that large particles may have on sediment transport and bed morphology. In the process of looking at these studies, the development of the related science is briefly presented. The topics covered include:

- roughness and shear stress,
- a general overview of sediment transport,
- hysteresis, and
- fractional transport and equal mobility.

These topics are useful for analyzing the effects of large particles and their impacts to bed morphology and sediment transport.

2.1 Introducing large particles into the stream corridor

While large particles can be found in streams resulting from the geological units they have been carved within, they are often introduced anthropogenically as a means of erosion protection. When a stream channel becomes unstable due to urbanization or natural or artificial disturbances, the resulting erosion can pose a risk to or damage of adjacent infrastructure. When this occurs, practitioners have traditionally applied hard-engineering approaches to mitigate or remedy site specific problems. This has included methods such as concrete walls, concrete channel linings, gabion walls or other engineered structures. More recently, softer, more natural approaches are being undertaken to provide a more dynamic and resilient approach to channel stabilization. These rehabilitation methods range from vegetation plantings on channel banks to vegetated buttress linings. An approach that has been used commonly to solve erosion or stabilization issues is the application of riprap or larger, more stable particles to the bank or area of interest. Riprap or roundstone lining is prevalent worldwide as evidenced through numerous design manuals from Canada (Province of British Columbia, 2000; MTO, 1997), the United States (Colorado Department of Transportation, 2004; U.S. Department of Transportation, Federal Highway Administration, 1989; IOWA Department of Natural Resources, 2006; New Jersey State Soil Conservation Committee, 2014; United States Geological Survey, 1986; Vermont Department of Environmental Conservation, 2013) and internationally (Scottish Environment Protection Agency, 2008). In addition to riprap used for erosion protection, armouring is often installed at culvert outlets, bridge piers or other stream side locations to protect underlying infrastructure such as watermains, sanitary sewers or pipelines. Examples of installed riprap or large particles in channel settings are shown in Figures 1, 2 and 3.

Figure 1: This photo shows the placement of riprap material on a channel bank for erosion protection (Province of British Columbia, 2000).

Figure 2: Large particles placed on the outside of a channel bend for erosion protection. These particles have been integrated with vegetation for further stability (IOWA Department of Natural Resources, 2006).

With riprap and armouring frequently used for small patchwork applications without addressing the problems that caused the erosive forces within the channel system, these stabilization and protection measures can be insufficient to arrest channel processes and fail. Many different forms of riprap failure are understood, including particle erosion, transitional slides, and slumping (Blodgett and McConaughy, 1986). While these failures may be the result of inadequate design or understanding of river system processes, they

Figure 3: This photo shows the placement of riprap material on a channel bank for erosion protection (New Jersey State Soil Conservation Committee, 2014).

may also be the result of improper installation (Sutton, 2008). These failures are not limited to riprap bank protection but also frequently occur for other types of revetments such as culvert outfalls or bridge piers and abutments.

Regardless of the method of failure, all of these channel responses result in the introduction of large material into the channel bed. Some of the methods of introduction, such as bank slumping of a riprap lined bank would introduce the material as a tightly spaced matrix on the channel bed. Alternatively, the erosion of a riprap bank or the failure of material at a culvert outlet, such as in Figure 4, might be dispersed loosely on the channel bed. Another example of this is shown in Figure 5, which depicts large particles downstream of a bridge crossing on Etobicoke Creek, located in Mississauga, Ontario.

2.2 Roughness and shear stress

In order to provide the broad picture of the effects large particles may have on a channel beds, roughness and shear stress must first be addressed. Channel roughness represents a channel's resistance to flow. This is commonly defined by assigning a channel roughness to a given reach of channel, such as the Darcy-Weisbach friction factor, Manning's coefficient or Chézy coefficient which is then considered to be representative of the net channel resistance. In general the roughness coefficients are generated by calibrating an at-a-station discharge or velocity with the parameters of slope, depth and cross sectional area, such as in the form of the Manning's equation (Manning, 1891):

$$V = \frac{1}{n} R_h^{2/3} S_f^{1/2} \tag{1}$$

where V $[\frac{L}{T}]$ is the average channel velocity, n $[\frac{T}{L^{1/3}}]$ is Manning's roughness coefficient, R_h $[L]$ is the hydraulic radius, and S_f $[-]$ is the friction slope. This method of determining the roughness coefficient is often impossible due to the lack of the required flow data for calibration, however Cowan (1956) developed a procedure for estimating the roughness coefficient:

$$n = (n_b + n_1 + n_2 + n_3 + n_4)m \tag{2}$$

where

- n_b is a base value for straight, uniform channels,
- n_1 is a coefficient to represent channel irregularity,
- n_2 is a coefficient for variation in cross sectional shape,
- n_3 is a coefficient for obstructions in the channel,
- n_4 is a coefficient for vegetation, and
- m is a coefficient for the meandering of the channel.

Several documented works provide tables or visual references to guide the process of selecting appropriate parameters for Cowan's method (Cowan, 1956), but the key component to note is that the presence of large particles on a channel bed impacts three of

Figure 4: A photo of material placed for erosion protection at a culvert outlet, which is located behind the tree in the image. The photo depicts material that has been washed away due to improper installation. Originally the material was placed uniformly across the bank, but the material in the center has since washed into the channel.

Figure 5: A photo of artificial large immobile particles deposited downstream of a culvert crossing. The channel in the picture is Etobicoke Creek in Mississauga, Ontario.

the modifying parameters. Large particles increase the channel irregularity (n_1), increase the obstructions present in the cross section (n_3), and finally alter the base value (n_b) by changing the characterization of the channel substrate. All of these possible changes caused by the introduction of large particles results in an increased estimation in the roughness value.

Shear stress is the measure of force applied by moving water on a body in the path of the flow. In general, bed shear stress is the force of water acting on the grains of the channel bed. Bed shear stress (τ_0 $[\frac{M}{L \cdot T^2}]$) can be calculated using (Te Chow, 1959):

$$\tau_0 = 0.97 \gamma R S_f \tag{3}$$

where γ $[\frac{M \cdot L}{L^2 \cdot T^2}]$ is the weight density of water and h (L) is the depth of flow.

On a flat uniform channel bed, shear stress is distributed approximately equally along all grains on the bed surface. However, large particles protruding from the channel bed experience a proportionately greater amount of the total shear stress due to being more predominantly in the flow path and deflecting flow away from the other bed material (Hassan and Church, 2000). As a result, the large particles tend to be more mobile than expected at a given flow, whereas the remaining smaller bed material will be shielded and therefore less mobile.

2.3 Sediment transport

Sediment transport has been studied for thousands of years, with evidence presented in engineering works completed on waterways in Mesepotamia as early as 5200 B.C., in Egypt

in 3000 B.C., as well as in China in 2278 B.C. (Graf, 1984). While most of these early works are documented through the observation of their practical works, Pierre DuBuat produced the first known formal writings of experimentation of hydraulics and sediment transport named "Principes d'Hydraulique" in 1786 (Du Buat, 1786). Despite this early work, the first formal sediment transport equation was presented by DuBoys in 1879 (DuBoys, 1879). By the time Ashworth and Ferguson (1989) were studying gravel bed rivers, it was well known that sediment transport rates are a function of sediment transport capacity, sediment supply and sediment size. Figure 6 depicts common impacts of channel flow and sediment transport on a gravel bed river system.

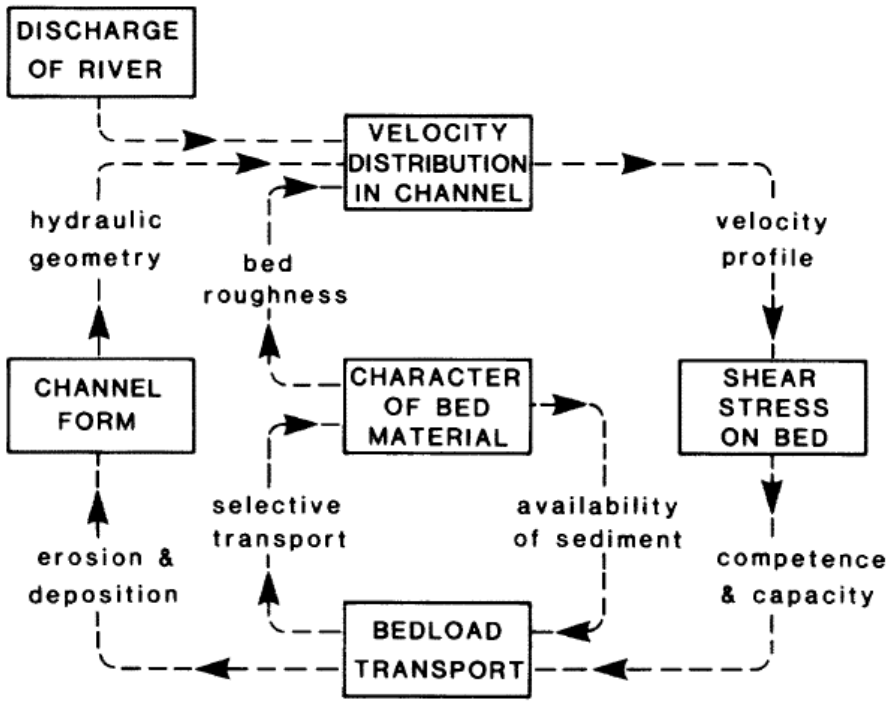

Figure 6: Interrelationships amongst form, flow, and sediment in active gravel-bed rivers (Ashworth and Ferguson, 1986)

Numerous sediment transport formulae have been developed in order to quantify the bedload transport rates over varying conditions. Most formulae have been formulated in dimensionless form to allow for broad ranges in application:

$$q^* = \frac{q_s}{\sqrt{(G-1)gd_i^3}} \tag{4}$$

where q^* is Einstein's dimensionless bedload transport rate, q_s $[\frac{M}{L \cdot T}]$ is the dimensional bedload transport rate, G $[-]$ is the specific gravity of the transported material, and d_i $[L]$ is a discrete grain diameter.

One of the most commonly applied bedload transport equations for gravel size fractions is that presented by Meyer-Peter and Müller (1948) of the form:

$$q^* = 8(\tau^* - \tau_C^*)^{\frac{3}{2}} \tag{5}$$

where τ^* is the dimensionless shear stress being applied to the channel bed, and τ_C^* is the critical shear stress required for the initiation of motion of the material. This equation was developed from experimental data in a flume, using a well-sorted gravel bed as the transport material. Wong and Parker (2006) identified an error in the Meyer-Peter and Müller (1948) formula, which was corrected to:

$$q^* = 4.93(\tau^* - \tau_C^*)^{1.6} \tag{6}$$

Numerous other equations have been developed that fit a similar format. Some examples of these were developed by Einstein (1950), Ashida and Michiue (1972), Engelund and Fredsøe (1976), Luque and Beek (1976), and Parker (1979).

2.3.1 Hysteresis

Bedload hysteresis has been studied since the work of Einstein (1950), which identifies trends in sediment transport across hydrographic events from the rising to the falling limbs. Generally speaking, hysteresis is the comparison of sediment transport occurring on the rising limb to sediment transport on the falling limb. A clockwise hysteresis identifies greater amounts of sediment transport on the rising limb, whereas a counter-clockwise hysteresis identifies great sediment transport occurring on the falling limb. Common hysteresis trends are shown in Figure 7

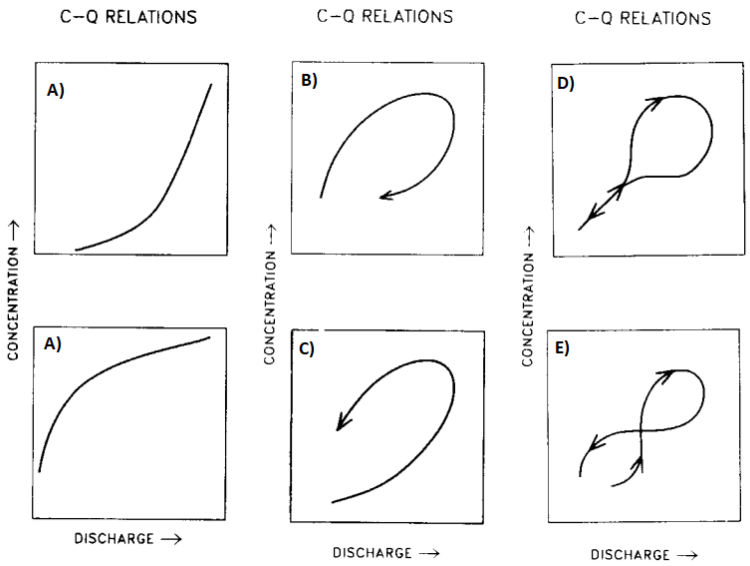

Figure 7: Common hysteresis trends where A) is a single value line B) is clockwise hysteresis C) is counter-clockwise hysteresis D) is a single value line plus a loop and E) is a figure eight (Williams, 1989).

Williams (1989) outlined a framework for the physical reasons for the different hysteresis patterns and likely causes of each as shown in Table 1. Supplementing the trends depicted by Williams (1989), Kuhnle (1982) predicted that clockwise loops are caused by lags in the

formation and destruction of bed roughness elements during the rising and falling limbs. It was also postulated that counterclockwise loops are a result of greater flow strengths required to mobilize sediment on the rising limb than the falling limb, possibly due to the breaking up of the armour layer or other such processes.

Table 1: Hysteresis Patterns as Outlined by Williams (1989)

Class	Relation	Cause
A	Single value line	Uninterrupted sediment supply
B	Clockwise loop	Depletion of available sediment or formation of armour layer prior to water flow peak
C	Counterclockwise loop	Faster propagation of water wave than sediment wave, high sediment erodibility with prolonged erosion, or seasonal variability of rainfall distribution and sediment production within basin
D	Single Value line plus loop	Combination of causes from 1, 2 and 3
E	Figure eight	Combination of causes from 2 and 3

Numerous studies have published the measured hysteresis of experiments both in the field (Humphries et al., 2012; Wang et al., 2015) as well as in a flume (Mao, 2012; Waters and Curran, 2015). In general, a clockwise trend for sediment transport was more common within both systems, with studies indicating the deposition of coarse material during the falling limb, reducing the bed mobility (Mao, 2012; Humphries et al., 2012). Interestingly, it was found that coarse material generally followed a clockwise hysteresis trend whereas fine material followed a counterclockwise hysteresis trend (Wang et al., 2015). Finally, specific to flume experiments, it was found that a counterclockwise hysteresis was found on the first hydrograph on a channel bed due to the flow history commonly run prior to the experiments. The flow history, which created patches of fine sediment and patches of coarse sediment resulted in sediment transport lag due to patchy sediment availability (Waters and Curran, 2015).

2.3.2 Bed Armouring and Imbrication

As channel beds experience more flow events, a process of channel armouring occurs. Channel armouring is the condition of finer material being washed from the channel bed, while the coarser, less mobile material remains on the bed surface (Melville and Chin, 1986). This coarse material layer, called the armour layer, protects fine sediment below it, resulting in a limited sediment supply for flow events unable to move the coarse material (Melville and Chin, 1986). It was later discovered that while the erosion of fine material was the primary process behind armour layer development, the creep of subsurface material to the surface also contributes to it's development (Ferdowsi et al., 2017). Despite channel armouring protecting the material below it, and limiting sediment availability, it was found that channel armouring co-exists with the transport of all sizes of surface grains (Wilcock and DeTemple, 2005).

Adding further to the channel bed resilience is the process of particle imbrication. Imbrication is the alignment of armour particles with their flatter faces sloping upwards in the downstream direction (Friedman and Sanders, 1978; Melville and Chin, 1986). A schematic depicting imbrication is found in Figure 8.

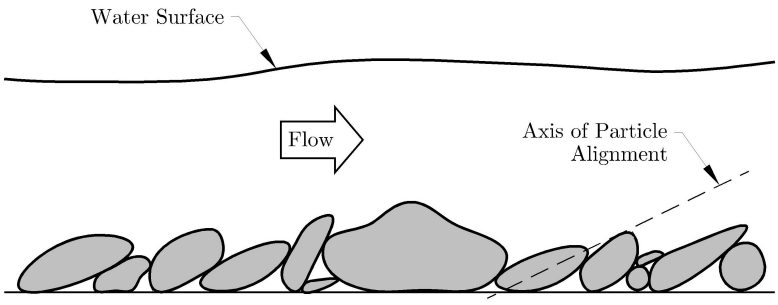

Figure 8: Schematic of particle imbrication in channel settings. The schematic is the profile of a channel or flume.

Even though both channel armouring and imbrication increase the resilience and stability of the channel bed, sufficient flows or disturbances can be achieved to break-up the coarse surface layer of bed material. This armour layer break-up initially causes fining of the surface material, followed by an almost immediate increase in sediment transport. After the armour layer break-up has occurred, the resultant reformation typically creates an even coarser armour layer (Orrú et al., 2016).

2.3.3 Fractional transport and equal mobility

A particle strictly in isolation is mobilized based upon shear stresses being applied on the particle and the resistance forces to that particle. Based strictly upon size and weight, a smaller particle is easier to mobilize than a larger particle. However, when particles are integrated into a mixture of different sizes and weights, their mobility now relates to the mobility of the mixture as a whole rather than the mobility of the individual particles. It has been suggested that a condition, referenced to as equal mobility, occurs when all particle sizes in a mixture are mobilized and transported equally (Parker et al., 1983). Conversely, size selective transport refers to the mobility of particles based upon the absolute diameter of the given particle, rather than the diameter relative to other material on the bed. The condition for equal mobility, according to Parker et al. (1983), is that the pavement layer must be broken prior to this occuring. Wilcock and Southard (1988) later determined using a laboratory experiment at steady state flow that all sediment sizes within a mixture begin motion at approximately the same dimensional bed shear stress.

Ashworth and Ferguson (1989) studied the results presented by Parker et al. (1983) to determine if the results could be replicated at the field scale. While it was found that the bedload transport approached a scenario of equal mobility at the highest tested flows and shear stresses, ultimately, selective transport processes were identified in all cases examined. It was accepted that the initiation of motion was more reliant upon relative

particle size effects rather than absolute size effects. They also discussed that size selective transport occurs before the largest particles on a channel bed are mobilized and only exposed particles are transported. Once coarse particles on the surface begin motion, bedload transport approaches equal mobility.

Wilcock and McArdell (1997) offered a partial transport mechanism which identified that a shear stress that is insufficient for equal mobility may cause some size fractions to be in a state of partial mobility. Despite a range in sizes of material being fully mobile based upon a given shear stress, the transport rates are independent of the size of the material, and are dependent on the amount of material present on the channel bed. They also found that the shear stress that is able to fully mobilize the coarsest particles in the bed sediment mixture is the same shear stress in which equal mobility also occurs. Smaller grains, however, may be fully mobile prior to equal mobility, but may be hidden under coarser sediment in this scenario. The mechanism in which partial mobility occurs is the trapping of a mobile particle size between larger particle sizes, reducing their proportion of active grains in the mobile fraction.

Church and Hassan (2002) further expanded fractional transport rate research by presenting the fractional transport ratio p_i/f_i and the scaled fractional transport ratio $q_{bi}p_i/f_i$ $[\frac{M}{L \cdot T}]$. Examples of these are taken from Church and Hassan (2002) and are shown in Figure 9 to provide definitions and delineations of the transport modes. A fractional transport ratio (p_i/f_i) of 1 for a range in particle sizes indicates that the system is at equal mobility, and the deviation from this horizontal line is indicative of an overrepresentation of some size classes, and an underrepresentation of others when comparing their fraction of the bedload to their fractions in the bed material. The scaled fractional transport ratio multiplies the fractional transport ratio by the sediment transport rate of each size fraction. This is done to provide weighting to the sediment transport rates of each size fraction to its over- or under-representation in the bedload.

2.3.4 Hiding functions and relative size effects

In order to better account for the complex processes in regards to sediment transport, many studies have focused on developing formulae to predict the relative size effects within sediment mixtures. This often takes the form of a hiding function, which determines the transportability of a specific size class based on the difference in size between that size class and a representative material size.

Egiazaroff (1965) identified that the mobility of sediment in a non-uniform sediment mixture was dependent on the relative size of the sediment. To account for this effect, a generalized power-law was suggested for determining the critical shear stress (τ^*_{ci}) using the relative size of the sediment (D_i/D_x) (Egiazaroff, 1965):

$$\tau^*_{ci} = a(D_i/D_x)^b \tag{7}$$

where D_i $[L]$ is the particle diameter of interest, D_x $[L]$ is the reference particle size, and a and b are fitting parameters.

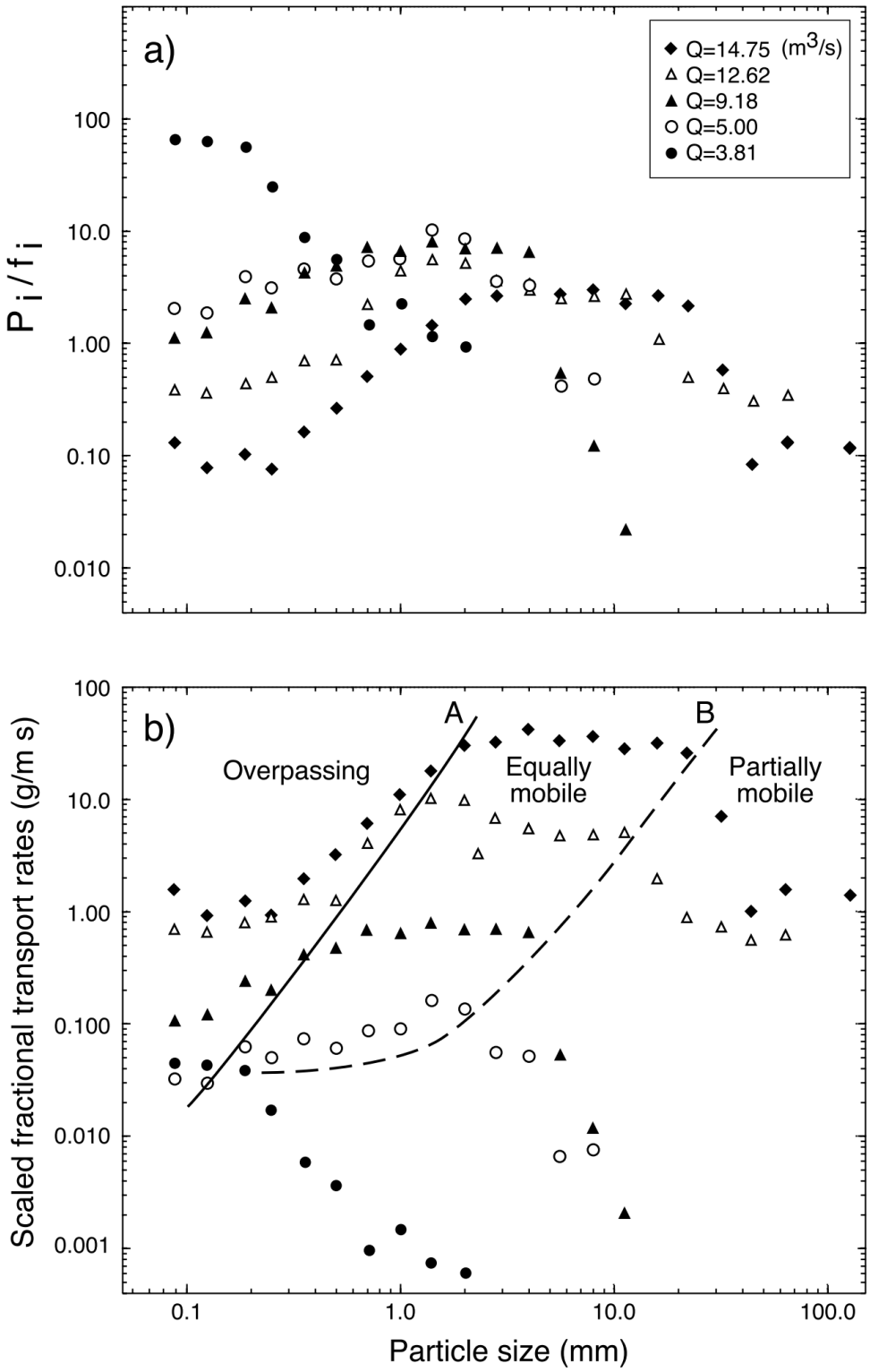

Figure 9: Examples of plots depicting a) the fractional transport ratio p_i/f_i and b) the scaled fractional transport rate $q_{bi}p_i/f_i$.

Early attempts to parameterize D_x on D_i in equation 7 utilized the relationship between the bed material size and a representative size found within the subsurface sediment of the channel bed (Andrews, 1983), as subsurface material is typically more representative of the material gradation found within bedload. Andrews (1983) determined the critical shear stress for a specific particle size in a mixture by normalizing equation 7 by the median particle size of the subpavement material (d_{50}) of the form:

$$\tau^*_{ci} = 0.0834(d_i/d_{50})^{-0.872} \tag{8}$$

Many variations of the above equation can be found (Ashworth and Ferguson, 1989; Marion and Weirich, 2003; Petit, 1994; Aristide Lenzi et al., 2006), however, it was suggested that using a size of material other than the median particle size might be beneficial. The use of the D_{90} has been recommended since the coarsest material determines the hiding effects on the bed.

2.4 Previous studies on the effects of large particles

2.4.1 Sediment transport research related to large particles

Numerous studies have examined the effects of roughness elements on alluvial channels, specifically regarding impacts to stability, sediment transport and roughness. While few studies specifically look at the effects of immobile keystones on alluvial channels, other work has been completed on particle clusters, either naturally formed (Church et al., 1998; Hassan and Church, 2000; Buffin-Blanger et al., 2000; Tan and Curran, 2012) or seeded using coarse material found typically in a stream bed (Hassan and Reid, 1990). Despite differences between the large immobile particles examined on a given channel bed or particle clusters examined in other studies, both are isolated roughness elements, and are similar enough to provide valuable insight into the responses caused by either the presence of these features or the effects of different spacings on bedform responses.

Laboratory studies have typically been employed to accurately control flow rates and sediment sizes, and for increased resolution and accuracy in data collection. Some laboratory studies have utilized a sediment feed into the flume (Hassan and Church, 2000; Yager et al., 2007; Tan and Curran, 2012), however many studies had examined effects in the absence of sediment feeds and relied upon sediment eroded from upstream regions in the flume for sediment resupply (Brayshaw et al., 1983; Hassan and Reid, 1990; Church et al., 1998; Buffin-Blanger et al., 2000). Field studies have evaluated the impacts of roughness elements on natural stream channels, and have looked at the resultant flow structures on the channel bed created by the roughness elements (Buffin-Blanger et al., 2000) or have been used to confirm results previously found in laboratory experiments (Yager et al., 2012).

2.4.2 Large particle interaction

Brayshaw et al. (1983) studied the effects of varying the proximity of multiple particles and the impacts to flow structures around the large particles. These relationships can be used

to infer changes to sediment transport in a stream containing particle clusters at varying densities on the stream bed. The study showed that mobile particles experience less drag and lift when they were positioned closer to the wake side of obstructions or other large particles. A particle on the upstream side of an obstruction experienced increased lift as it was positioned closer, which would result in the particle being mobilized more readily. These results were tested using seeded particles to examine the differences in mobility at various locations around an obstruction. Counter to the previous result, particles downstream of the large particle cluster were noted to be more frequently mobilized despite their predicted lower lift and drag forces compared to upstream particles. However, upstream particles were found to have greater travel distances, perhaps being a better indication of their greater instability on the stream bed.

A study completed by Tritico and Hotchkiss (2005) undertook a more detailed examination into the changes in hydrodynamics around a flow obstruction such as a protruding boulder. They found that flow upstream of an obstruction, while lower in energy than an unobstructed scenario, generally followed the log-wake law (Nezu et al., 1993) and maintains turbulent flow structures. On the downstream side of the obstruction, a near field vortex street can be found at the edges of the obstruction, resulting in increases in kinetic energy and lateral turbulence. The results of the study completed by Tritico and Hotchkiss (2005) are illustrated in Figure 10.

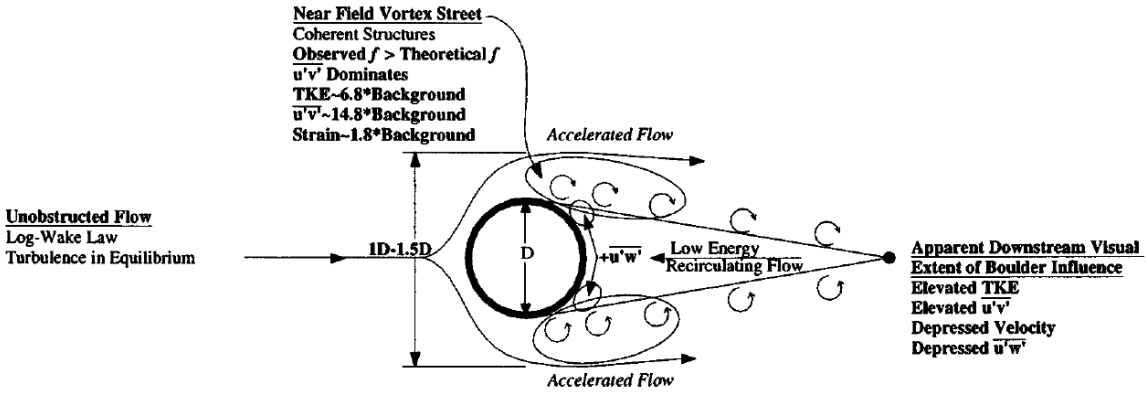

Figure 10: Summary of hydrodynamic changes around a placed boulder obstruction (Tritico and Hotchkiss, 2005)

While the study completed by Brayshaw et al. (1983) identified that the lift and drag forces on the downstream side of a protruding particles is reduced, Tritico and Hotchkiss (2005) clearly showed that turbulence and total kinetic energy is infact increased on the wake side of the particles. This explains the increased mobilization of particles on the downstream side found by Brayshaw et al. (1983), and points to the possibility of increased mobilization of particles on the downstream side of a flow obstruction.

A study completed by Tan and Curran (2012) examined the effects different configurations of particle clusters had on flow structure. Their experiments were studies with an armoured bed consisting of either the absence of bedform particle clusters, one isolated

cluster, two clusters or a group of three clusters. The study identified that the difference in scenarios were able to depict the effects of clusters for various spatial densities. When a single cluster was evaluated, peak kinetic energy Reynolds shear increased downstream of the cluster when related to a condition with no clusters. The peak kinetic energy as much as doubled when compared to the peak kinetic energy when no clusters were present. Coupled clusters were shown to experience a further increase in turbulence, with peak turbulence resulting from recirculation between the clusters. The coupled clusters are representative of a cluster density where the hydraulic interference of adjacent clusters build on each other rather than interfere with the flow patterns. Group clusters, which is at a greater density than the coupled clusters, were found to reduce the Reynolds shear. Their dense cluster spacing caused the flow patterns to interfere with each other and resulted in skimming flow. Skimming flow contains very similar characteristics to flow over a rough bed with no bedforms.

2.4.3 Large particle impacts on sediment transport

Hassan and Reid (1990) completed a laboratory study on the effects of varying densities of large particle clusters on roughness and sediment transport. The study consisted of a flume experiment in which particle clusters were seeded and run under steady flow conditions with no sediment inputs. They found that as the cluster density increased, flow resistance increased, however once cluster densities increased past a critical point, flow resistance began to decrease. This observation was explained using the three flow types defined by Morris (1955), being:

- isolated roughness, where the flow patterns around each obstruction do not significantly interefere with each other;
- wake-interference, where vortex generation and dissipation is not completed prior to the next element; and
- skimming, where small vortices form between elements, allowing flow to skim over the top of elements without impinging on the channel bed.

When relating the bedload transport to the flow resistance, it was found that flow resistance was inversely proportional to transport rates, with the minimum bedload transport being observed at the instance of the highest flow resistance (Hassan and Reid, 1990). Once cluster density was increased past the maximum flow resistance, bedload transport rates were found to increase, despite being within the skimming phase. It was observed that powerful, yet sporadic, eddies were impinging upon the channel bed in isolated areas due to the unevenly scattered clusters. Upon further increase in cluster densities, bedload transport rates decreased. This consequence was identified to arise from a greater coverage of skimming flow and less opportunities for eddy complexes to impinge on the channel bed. Hassan and Reid (1990) suggested that the bedload transport was impacted by both the excess energy available for transport, as well as the amount of area unprotected from skimming flow.

Church et al. (1998) conducted a flume study on the effects of particle clusters on gravel-bed streams with mobile bed sediment in which the clusters were allowed to form

naturally under varying steady flow conditions. They found that the presence of particle clusters reduced sediment transport by orders of magnitude and improved the channel bed stability. Additionally, they found that particle clusters generated more flow roughness the longer they were allowed to develop under low flow conditions. They also found that the strength of the clusters increased with increasing shear stress until a point where the shear stress was sufficient to destroy the clusters.

Hassan and Church (2000) undertook a study on the impacts of channel bed surface structure of a gravel bed river where the bed was allowed to develop without an initial sediment feed and allowing for stone cluster formation. They found that the bed structure and clusters were maintained once a sediment feed began, but the bed surface generally fined over time. This fining supported the trend that excess shear stress was consumed by the particle clusters, allowing for the deposition of finer materials once the sediment feed was added. Eventually, with the sediment feed added, the surface structure developed to reach a state where sediment continuity was maintained, suggesting that the formation of particle clusters on the channel bed continued until equilibrium was reached. Hassan and Church (2000) suggested, based upon the observations of this study, that naturally occurring bed structures, such as particle clusters or large particles, were resulting in sediment transport equations over predicting transport rates by an order of magnitude.

A study completed by Strom et al. (2004) using uniform spheres to observe the characteristics of cluster formation and their disintegration in relation to the Shields parameter (τ^*). They found that clusters formed at $1.25 \leq \tau^* \leq 2$ times the Shields parameter for the sediment, and the clusters disintegrated at $\tau^* \geq 2.25$ times. They found that there were three phases of cluster development: a sink phase at low shear stresses where material is added to the clusters, a neutral phase where sediment removed from structures is equivalent to that added to structures, and a source phase where the clusters begin to break apart. They observed that clusters increased the magnitude of sediment fluctuations despite the phase of formation they were currently experiencing, however, the largest fluctuations were observed during partial or complete cluster disintegration.

Yager et al. (2007) conducted a laboratory flume study on steep channels with large immobile grains by implementing various boulder densities in addition to altering the sediment flow rates to the system to examine alterations in roughness, sediment retention and protrusion of the immobile grains. Their study was designed to emulate mountain streams. The difference between total shear stress and the portion of shear stress imparted on the mobile sediment found in their study is shown in Figure 11. As shown, a greater proportion of the total shear stress (τ_t^*) is imparted on the immobile particles when the protrusion of immobile particles above the streambed increased, or when the density of the immobile particles increased. Yager et al. (2007) used the parameter of λ/D to quantify the density of large immobile grains on the channel bed, where λ $[L]$ is the distance between the particle centers, and D $[L]$ is the particle diameter.

Yager et al. (2007) found that for a given sphere spacing, as sediment input increased, bed roughness decreased, the proportion of the bed covered by mobile sediments increased, and the protrusion of immobile particles decreased. Additionally, they found intermediate levels of immobile particle densities ($1.7 \leq \lambda/D \leq 2$) were found to have the highest

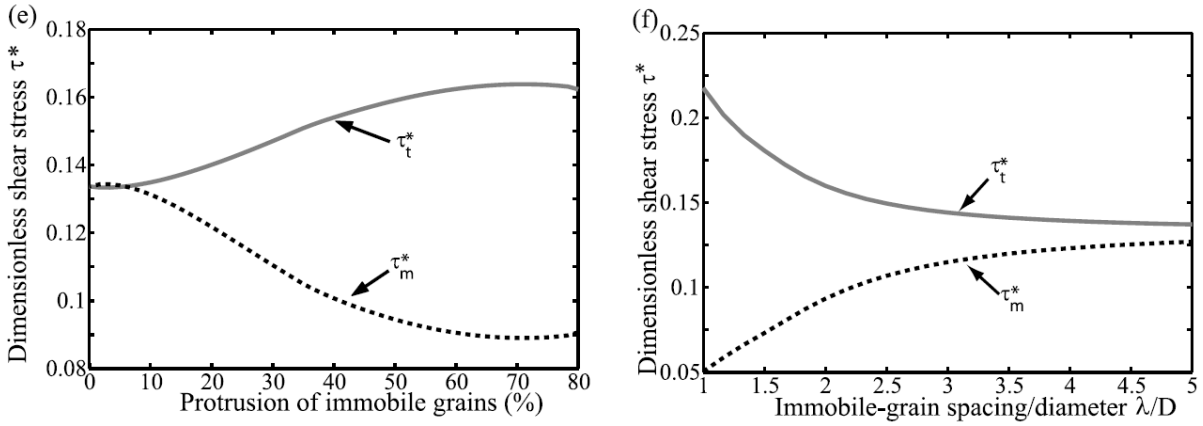

Figure 11: Dimensionless total shear stress and stress on mobile sediments (e) as a function of protrusion of immobile grains or (f) as a function of immobile grain density (Yager et al., 2007). τ_t^* is the total shear stress and τ_m^* is the shear stress acting on mobile bed sediment.

bed surface area covered by gravel and the largest values of roughness. The reason the higher density cases did not experience greater levels of roughness or gravel deposition were identified to be the result of skimming flow, and a low total area for gravel material to deposit between the large immobile particles. The lower densities of immobile particles exhibited a large bed surface area of gravel deposition, but the higher velocities and reduced inter-matrix opportunities for protected areas around the larger immobile particles resulted in less gravel retention as immobile particle density decreased.

Yager et al. (2007) developed a sediment transport equation for beds containing large immobile particles by incorporating the stress that is borne by the immobile grains, and accounts for the limited availability of the mobile sediment. The basis for this formulation was the excess stress based equation for sediment transport presented by Luque and Beek (1976):

$$q_s^* = 5.7(\tau_t^* - \tau_c^*)^{1.5} \tag{9}$$

This equation was then modified to use the shear stress acting on the mobile sediment, and to determine the critical shear stress of the median mobile material rather than the median size of the entire bed material. Additionally, the proportional area that the mobile sediment occupies was also incorporated in the form:

$$q_{sm}^* = 5.7(\tau_m^* - \tau_{cm}^*)^{1.5}\frac{A_m}{A_t} \tag{10}$$

where q_{sm}^* is the dimensionless sediment transport rate for mobile sediment, τ_{cm}^* is the dimensionless critical shear stress for mobile sediment, A_m is the area of mobile sediment on the channel bed, and A_t is the total area of the channel bed. They found that the difference between the equation accounting for the mobile sediment and that which ignored the effects of the large immobile particles were similar in results when $\lambda/D \geq 2.0$. However, when $\lambda/D < 2$, the modified equation by Yager et al. (2007) predicted the sediment transport rates at least an order of magnitude less.

Finally, a flume study completed by Ghilardi (2014) examined the impacts of various sizes and spatial densities of keystone particles. Experiments were conducted under a constant flow rate and a constant sediment feed rate throughout for all experimental runs, however, the slope ranged between 6.7% and 13% due to the focus of the study being on mountain streams. This study reaffirmed previous studies that sediment transport decreases with increased density of large particles on the channel bed. They also found that as $\lambda/D \Rightarrow 2$, there was a significant reduction in sediment transport and was identified to coincide with the change in flow regime from isolated roughness elements to wake interference flow. They also found that for a given λ/D, the sediment transport capacity increased with an increase in large particle sizes. This observation suggests that sediment capacity is more sensitive to the number of flow roughness elements per unit area rather than the size of the roughness elements.

Following the findings of Ghilardi (2014), where it was found that discharge was a more useful metric than bed shear stress for determining sediment transport rates on a bed containing immobile particles, the following sediment transport equation was proposed:

$$q_s^* = 4.69 S^{2.10} \sqrt{q^* - q_{cr}^*} \tag{11}$$

where q^* is the dimensionless discharge, S is the bed slope, and q_{cr}^* is the dimensionless critical discharge as calculated using:

$$q_{cr}^* = \frac{q_{cr}}{\sqrt{g d_{50}^3}} = S^{-0.46} \left(1 - \frac{D}{\lambda}\right)^{-0.7} \tag{12}$$

The previous studies completed on the effects of large particles on a channel bed provide pieces of information that create an incomplete description of the impacts to sediment transport and bed morphology. While each of the different studies fill in gaps in knowledge, the wide variety of input parameters and data collection do not provide a holistic understanding of the effects large particles have on bed morphology and sediment transport. This study undertook a series of flume experiments to gain a holsitic overview of the effects large particles have on sediment transport and bed morphology in a moderate gradient gravel-bed channel.

3 Methods

3.1 Overview and basis

This study consists of a flume experiment to examine the impacts to bed morphology and sediment transport caused by varying densities of large, immobile particles on a channel bed. To do this, the experimental setup is based on a previous laboratory configuration that was aimed at evaluating the impacts to channel morphology and sediment transport caused by urbanization induced by hydomodification (Plumb, 2017). Since Plumb (2017) designed the experimental setup to mimic a natural channel in terms of flow, sediment and geometry, using a similar setup allows this study to be related to natural channel processes more easily .

While the study completed by Plumb (2017) consisted of varying hydrographs over many flow events, this experiment contains a single hydrograph passing over a channel bed with a known sediment supply, and repeating the experiment with varying densities of large particles protruding from the channel bed. The hydrograph and the bed material were sized such that the D_{90} of the bulk material was mobile at peak discharge (Plumb, 2017). The distribution of this material is a bimodal sand-gravel distribution.

To focus on changes in bed morphology and sediment transport, emphasis was put on collecting the following data:

- bedload transport mass and texture using a sediment trap and analyzing the samples collected,
- bed surface texture using topographic photo analysis,
- bed surface profile using topographic scans collected using the echo-sounder, and
- water surface profile and flow rates using manual measurements and ultrasonic sensors at the limits of the study reach and within the head tank.

This information provides both the assurance that input parameters and initial conditions were equivalent for each test case and a detailed examination of the impacts of the large particle density in each test case.

3.2 Experimental facilities

Laboratory experiments were conducted at the Laboratory of Hydraulic Constructions (LCH) at École Polytechnique Fédérale de Lausanne (EPFL) in Lausanne, Switzerland. The flume setup consisted of a 9 m long by 0.5 m wide channel (Figure 12), with a flow stabilization tank and v-notch weir at the upstream end, and a sediment trap at the downstream end. The v-notch weir was verified to be accurate within +/- 10% based upon a calibrated valve-discharge relationship (Plumb, 2017). Flow parallelisers were included at the upstream end of the flume to remove turbulence created by the v-notch weir and to ensure parallel flow lines entering the flume. A sediment feeder utilizing an Archimedes

screw feed introduced a bed material mix at the upstream end, while a valve-adjustable sediment trap collected sediment at the downstream limit of the flume. The adjustable sediment trap outlets to a sediment collection basin, where the sediment was separated from the water and dried prior to analysis.

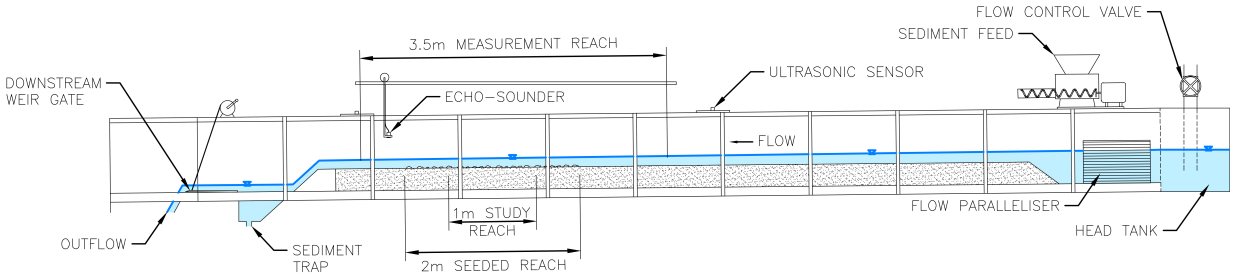

Figure 12: Flume apparatus and profile with the measurement reach identified. Flume width is 0.50 meters

The flume was equipped with sensors to flow depth and bed topography. An ultrasonic sensor located in the head tank was used for discharge calculations relating depth to the v-notch weir. The flume was also equipped with an echo-sounder on a motorized rail system for the measurement of bed topography within the study reach limits of the flume to a vertical accuracy of +/- 1 mm. Finally, a rail and camera mounting platform positioned over top of the flume was employed to allow for bed photos using a 12 MP mapping camera, which was used for bed material characterization.

3.3 Experimental Design

The current experiment was designed to assess the impacts to sediment transport and bed morphology based solely upon changes in the density of large immobile particles on the channel bed. The conditions being emulated were those pertaining to failed rip-rap supplies to stream channels. As such, all variables not pertaining to the spatial density of these large particles were kept constant for all test cases, including:

- input flow hydrograph,
- sediment input rates,
- bed and input material distributions,
- bed slope,
- large particle sizes and protrusion, and
- data collection methods.

Based upon the methods used by Ghilardi (2014), the density of large immobile particles was defined by:

$$\frac{\lambda}{D} = \frac{distance\ between\ centers\ of\ particles}{median\ diameter}$$

A schematic showing example measurements of λ and D is shown in Figure 13. The range in large particle density for the experiment was based off of the result of Ghilardi (2014), where it was shown that a maximum density of $\lambda/D = 2$ was dense enough to capture all abrupt changes in sediment transport and bed morphology. As such, this experiment was completed with a range of densities between approximately $\lambda/D = 2$ to $\lambda/D = 10$. Additionally a base-case scenario was also completed, that contained no large particles on the bed. The test cases and their relevant parameters are shown in Table 2.

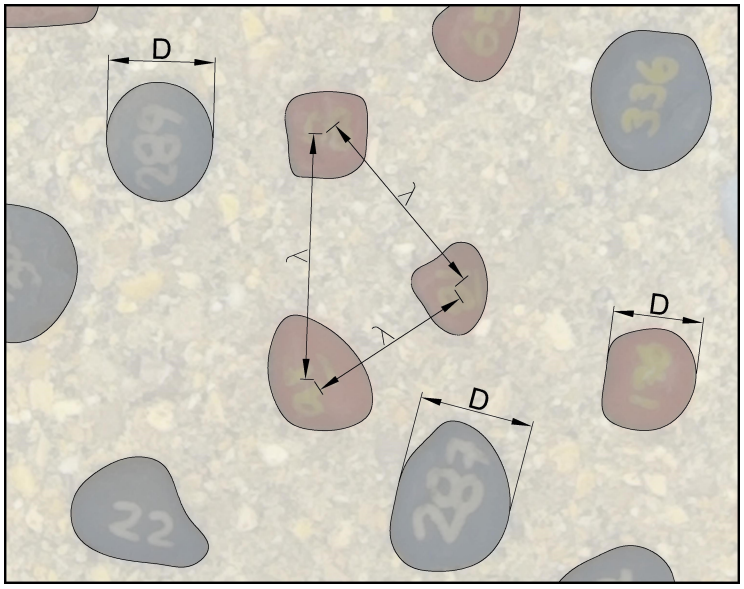

Figure 13: Schematic showing example measurements of λ and D off of a topographic photo of the flume bed.

Table 2: Particle size (D), particle spacing (λ), and number of particles per square meter(N/m^2), and area occupied by the particles as a percentage of total area (A_i/A_t) for each of the cases tested in this study

Experiment Case	λ/D	D (mm)	λ (mm)	N/m^2	A_i/A_t (%)
Base Case	N/A	N/A	N/A	0	0
Test Case 1	1.92	24.1	46	465	24.6%
Test Case 2	2.63	24.4	64	244	13.2%
Test Case 3	3.82	25.6	98	105	6.2%
Test Case 4	5.17	25.0	129	60	3.4%
Test Case 5	6.75	25.4	171	34	2.0%

The large, immobile particles were sized to follow standard practices where the material is sized to a factor of safety of 2, by doubling the diameter of the incipient particle size at a peak discharge. Since the bed material was sized to ensure the maximum particle size (10 mm diameter) was slightly larger than the incipient particle size at peak discharge, the size of the large immobile particles were sized to be approximately 20 mm in diameter.

Table 2 lists the spatial densities of the large particles for each test case run during this experiment.

Protrusion depths of the large particles were set such that 50% of each large immobile particle was protruding. Yager et al. (2007) found that the shear stress measured on the channel bed was significantly impacted by changes in the particle protrusion, with an increase in protrusion causing a decrease in bed shear stress on the mobile sediment. The results presented by Yager et al. (2007) showed that a protrusion of 50% significantly impacts bed shear stress while maintaining large particle stability, ensuring the effects of varying large particle density could be be fully observed.

3.4 Experimental procedure

The overall experimental procedure is presented in Figure 14, with each test beginning by establishing consistent initial conditions. Sediment was wetted prior to its addition to the channel bed to avoid vertical sorting of dry sediment during the leveling and moving of the sediment. The material was then graded longitudinally to achieve the same consistent bed slope for the entire flume, and leveled laterally to avoid the formation of lateral bed features during the experiment. 0.01 m/m was the bed slope determined by Plumb (2017) to provide equilibrium sediment transport through the study reach in a case with no large immobile particles on the bed.

Large immobile particles were subsequently introduced onto the channel bed. In order to capture the full effects of the placement of large particles on the bed within the 3.5 m measurement reach in the flume, a total of 2 m of the flume bed was seeded with the large particles. Additionally, only the central 1 m of this 2 m reach was used for analysis to avoid impacts of the flow transitions at the upstream and downstream ends. This 1 m of the flume is referred to as the study reach. The large particles were numbered prior to their addition to the flume, and an inventory of their a, b and c axes was created. This information was gathered for determining the keystone density during the data analysis, as the average diameter of the placed particles was not exactly 20 mm in diameter. The particles were randomly selected and hand placed within the study reach with a distance between each particle corresponding to the current test case. Once all particles were placed, the particles were pressed into the bed until each particle was approximately 50% buried. Visual observation of the protrusion was sufficient, as Yager et al. (2007) demonstrated that bed shear stress was not sensitive to small variations in protrusion with the protrusion around 50% of the particle diameter.

Once the bed was prepared, bed photos were taken using a top mounted camera. A series of 12 plan-view photos representing 50 cm of channel length were taken along the 3 m stretch of channel containing the study reach, with 10 cm of overlap with each of the adjacent photos.

Once the bed was prepared and the bed photos were taken, a flow history was established in a similar manner to other studies (Waters and Curran, 2015; Mao, 2012). A flow history allows the bed material to reach more stable positions, and for the fine, unprotected sediment to flush away to allow for a slight armour layer to form (Waters and Curran, 2015;

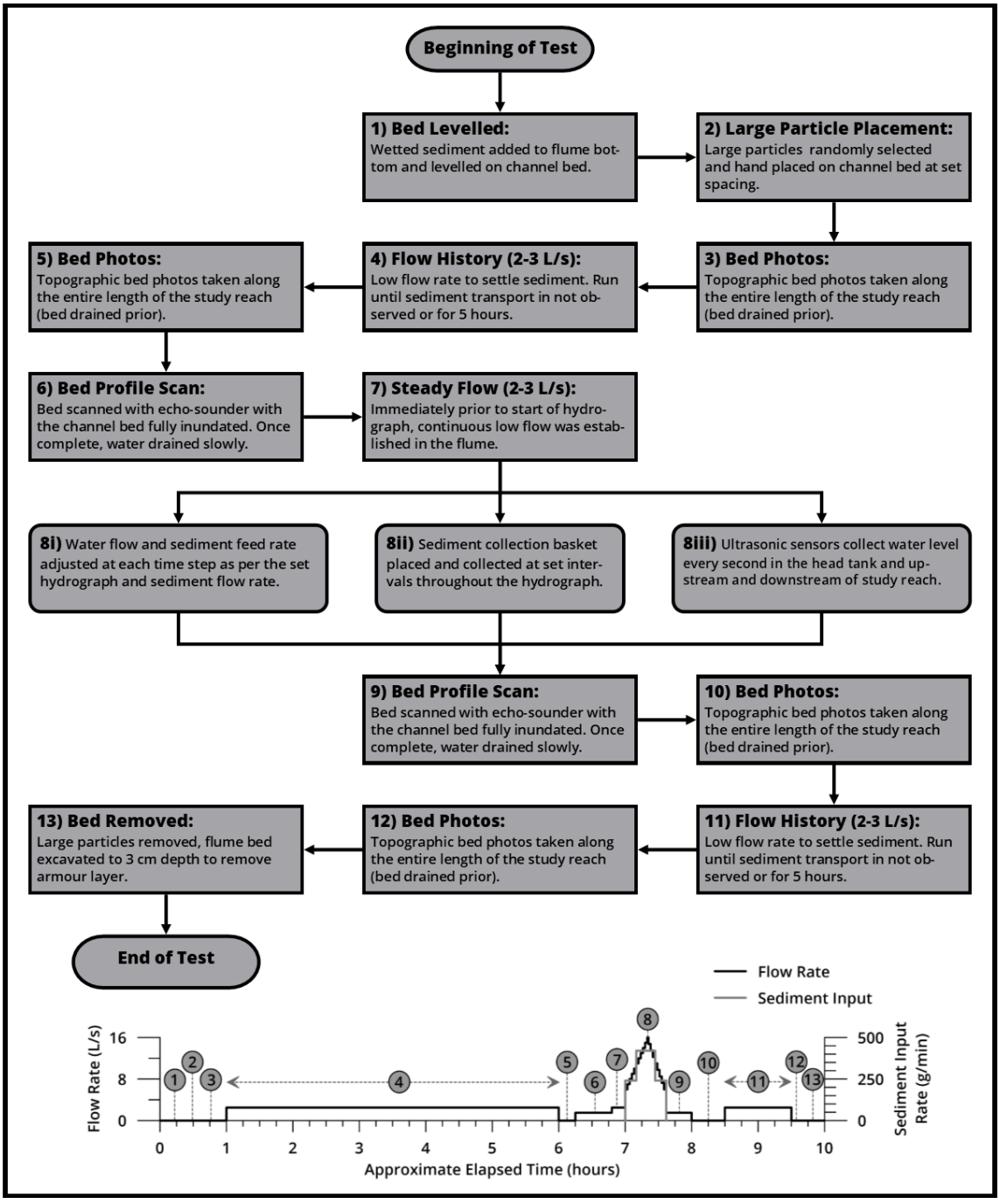

Figure 14: A) flow chart outlining the general experimental procedure for an experiment, and B) water flow rate and the sediment input rate for the duration of each test case. Numbered items in the flow chart are depicted in the bottom plot at the time in which they occur.

Mao, 2012) The flow history was run at a small discharge (2-3 L/s), which was below the initial discharge for the experiment's hydrograph. This was run for approximately five

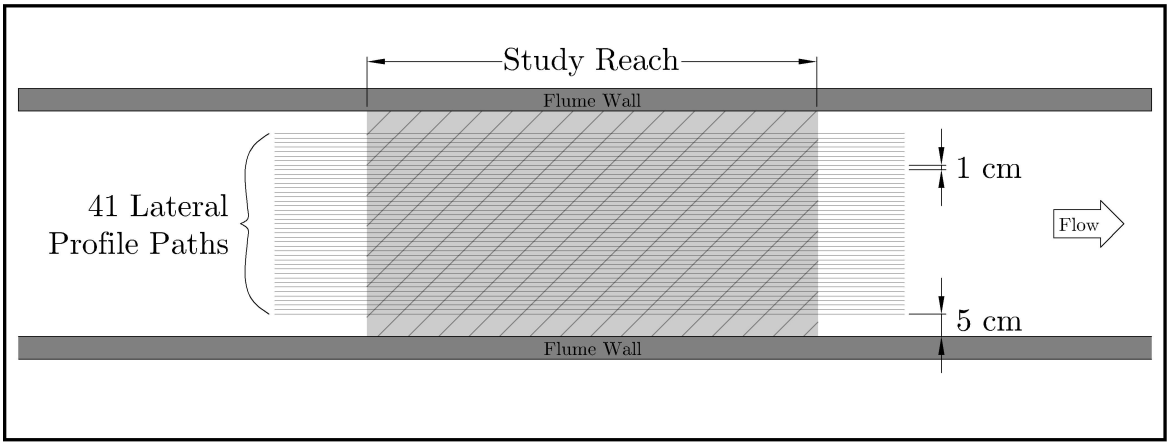

Figure 15: Top view flume schematic showing the location of the 41 lateral bed profile scans.

hours or until there was no sediment being collected in the bedload trap, and no mobility in the channel was observed. Photos were taken after the completion of the flow history, once the bed had been allowed to drain and dry to avoid reflections caused by standing water and wet particles.

Bed profile scans were conducted immediately before beginning the hydrograph. Scans were completed by backwatering the channel as the echosounder required the bottom of the instrument to be submersed. Backwater the channel involved closing the bedload trap, running a low discharge through the channel, and raising the downstream gate. Once the water level had reached the bottom of the echosounder, profile data along the entire 3 m instrumented reach was collected every 1 cm for the 40 cm width at the center of the channel. Profiles were not collected within 5 cm of the channel walls due to the physical limitations of the echosounder. Figure 15 depicts the location of the 41 lateral profiles. Once the entire bed had been profiled, the channel was drained slowly by turning off the pump and opening the bedload sediment trap.

To commence the hydrograph, the downstream gate was lowered, the bedload sediment trap valve was opened, and the channel was wetted using a low discharge equivalent to the flow used during the flow history. Once the flow had achieved steady-state along the entire channel length, the discharge was increased to the first stage of the hydrograph, the sediment feeder was started, and a collection basket was placed at the bedload trap. Figure 16 illustrates the flow rate, sediment input rate, and bedload collection samples for the hydrograph used in each experimental case.

During each hydrograph, the ultrasonic sensors were used to monitor flow rates. A side-mounted camera and a top-mounted camera obtained photos of the 1 m study reach

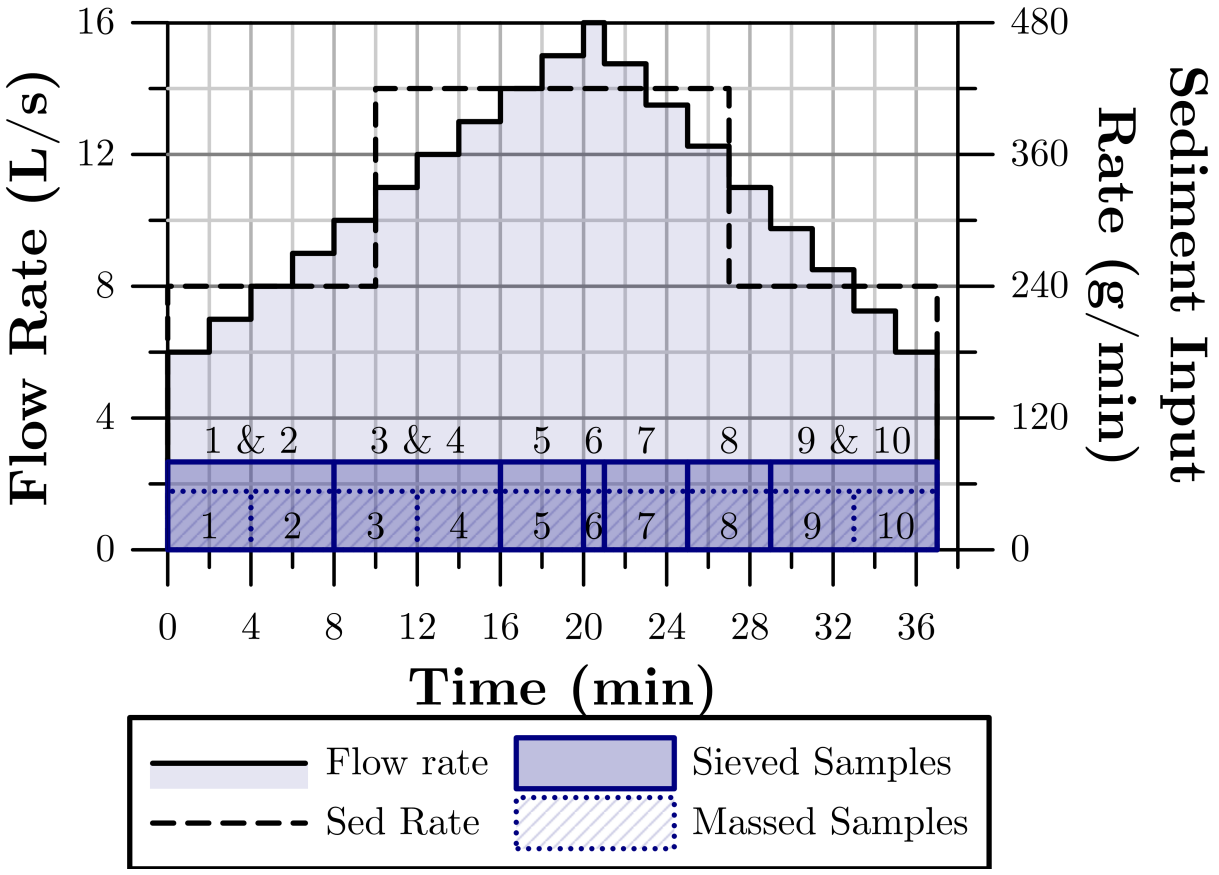

Figure 16: Flume experiment flow rates, sediment input rates and the sample collection schedule for each hydrograph. Numbers within the shaded boxes represent the bulk samples that were massed, and the numbers above the shaded boxes represent the bulk samples that were consolidated prior to size analysis.

at 10 second intervals throughout each experiment. On the opposite side of the flume from the side mounted camera, a 10x1 cm grid was installed in order to provide scale for the photos. An example photo from the side-mounted camera is shown in Figure 17, and an example photo from the top-mounted camera is shown in Figure 18. Upon completion of the hydrograph, profile scans were completed with the echosounder, and bed photos were taken.

A second flow history was conducted at the end of each experiment for a brief period of time (1 hour) in order to allow the sediment to settle and fines to wash away. This procedure was conducted to reproduce field results, in which an extended low flow period would occur after a flow event and before sampling could be completed on the site. After the second flow history, another set of bed photos was taken.

After all photos and scans were completed for each experiment, keystone particles were removed and the bed material was excavated to a depth of 3 to 5 cm to allow for a reset of the bed material composition and initial depth and slope conditions.

The procedure outlined above was completed for each of the 5 test cases and the base

Figure 17: Side view of the flume in the middle of the study reach during a hydrograph. The grid behind the flume was defined at 1 cm and 10 cm vertical and horizontal spacings, respectively.

Figure 18: Planimetric view of bed material sediment and numbered immobile particles.

case containing no large particles. Subsequent to each experiment, sediment samples were processed to obtain masses and grain size distributions. Bedload sediment collected at the bedload trap was also processed at the end of each experiment.

This experimental procedure was conducted in a similar fashion to those of Plumb (2017), with the following differences:

- Large particles were introduced in varying densities for the five test cases,

- only one hydrograph was performed for each test case,
- the study reach was truncated to 1 meter (however 2 meters of the reach was seeded with large particles), rather than the 3 meter reach used by Plumb (2017),
- an increased resolution of profile data was collected with the echosounder, doubling the number of profiles measured across the flume width,
- bedload trap samples were collected at approximately half the frequency during the hydrograph, and
- fine sediment from the beginning of the rising limb and the end of the falling limb were further binned into groups of 4 hydrograph steps prior to the grain size analysis to reduce processing time (samples were massed prior to combining).

3.5 Post-processing methods

In order to compare the sediment transport rates between data from the different test cases, sediment transport ratios and bedload hysteresis were compared. The sediment transport ratio (STR) evaluates the balance of sediment through the system, and was determined by:

$$STR = \frac{Q_{s,out}}{Q_{s,in}} \tag{13}$$

where $Q_{s,in}$ $[M/T]$ and $Q_{s,out}$ $[M/T]$ are the sediment transport rates entering and leaving the flume limits, respectively. STR is a measure of the level of sediment storage within the flume, indicating erosive or depositional trends. Bedload hysteresis was calculated by evaluating the hysteresis ratio, which is defined as the ratio of total bedload transport on the rising limb to the total bedload transport on the falling limb. The hysteresis ratio was then plotted against the large particle density (λ/D) to determine any trends amongst the test cases (Plumb, 2017).

To accompany the analysis of the bedload transport rates, the size of the transported material was also measured and compared between the test cases and the base case. The bedload transport rates and the size of the transported material were compared based on the average values over each hydrograph as well as for just the peak discharge.

3.5.1 Bed Surface Grain Size Distribution

In order to evaluate the impact of varying densities of large particles over a hydrograph on the channel bed morphology, the channel surface grain size distribution was compared. To do this, photographs of the channel bed were taken and analyzed for each of the test cases. The post-hydrograph bed material was compared rather than changes over the course of a hydrograph. This was done due to observed variability of initial conditions, with varying amounts of fine material being present on the channel bed after the flow history. Photo analysis was completed using a similar method to that presented by Mao (2012). The analysis involved taking 5 photos of the channel bed equally spaced along the study reach. The images were scaled using CAD software, and an 8 by 8 grid was superimposed over a 0.30 m x 0.30 m area at the center of each photo (leaves 0.1 m at each side of the flume

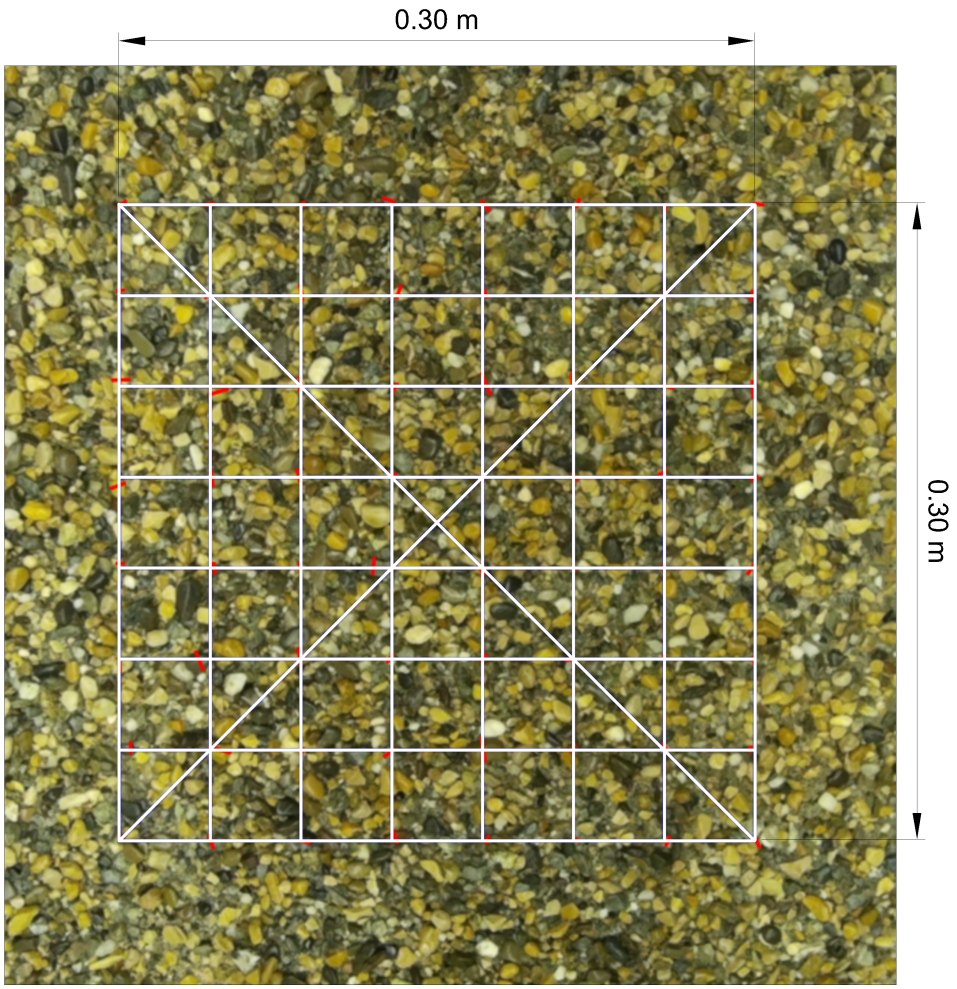

Figure 19: Superimposed sampling grid on bed surface photo. Red lines indicate the b-axis measurements of each particle at the points of the grid.

to avoid edge effects and avoids overlap between photos). The particle located at each intersection of the grid, as shown in Figure 19, was measured electronically to determine each particles' b-axis. Once a full set of 5 photos were analyzed, the b-axis measurements were tabulated into a grain size distribution.

The analysis of each set of photos produced a maximum of 320 measured particles. However, when a grid intersection corresponded to the location of a large, immobile particle, the intersection was skipped to avoid skewing the results based on an increased density of large particles. Therefore, the analysis resulted in each photo set containing between 247 and 310 particle measurements .

3.5.2 Particle Clustering Analysis

Particle clustering analysis was completed to determine how coarse bed material clustered or disbursed due to the impacts of the large immobile particles. While the bed surface grain size distributions provide a good metric for evaluating changes in overall bed surface

texture, a more detailed approach was required for the particle clustering analysis to depict the micro-scale changes in bed texture. To provide this more detailed approach, the software program BASEGRAIN (Detert and Weitbrecht, 2013) was utilized to obtain the B-axis measurements for all visible particles in the bed surface photos. A 50 cm x 50 cm area in the center of the study reach was used for the analysis. Due to software constraints and photo resolution, only particles with a b-axis greater than 2 mm were able to be measured. The b-axis measurements were manually inspected and modified to remove the measurements of the large immobile particles as well as to fix any incorrect measurements provided by the software.

The particle clustering analysis began by associating each particle's b-axis measurement produced by BASEGRAIN to the spatial coordinate of the particle center. This was then turned into a density heat map, showing the spatial density of coarse bed material, by summing the square of all b-axis measurements within a 1.5 cm radius of each pixel on the heat map. The b-axis measurements were squared prior to the summation to provide more weight to coarser particles. The areas overlapping the large immobile particles were removed from the analysis.

To observe the particle clustering over the course of a hydrograph in each test case, the heat map correlating to before the hydrograph was subtracted from the heat map from after the hydrograph. The result was a map where positive values indicated areas where more coarse material clustered over the hydrograph, and negative values indicating the opposite trend. An example of this resultant heat map, as well as the heat maps of before and after the hydrograph, are shown in Figure 20.

Using the final heat map, the following three metrics of comparing the particle clustering data were used to compare the test cases and the base case:

- the mean ratio; the ratio of the average positive pixel values to the average negative pixel values, to depict whether the increases in particle clustering were more or less substantial than the decreases in particle clustering,
- the increasing/decreasing area ratio; the ratio of positive pixels to negative pixels, to show the proportion of bed area that experienced increased clustering to the bed area that experienced decreased clustering, and
- the sum ratio; the ratio of the sum of all positive pixels to the sum of all negative pixels, to depict whether the overall trend was increased or decreased particle clustering.

3.5.3 Profile scan data

In order to evaluate the 41 longitudinal profiles collected laterally across the flume both before and after each hydrograph, the profiles were averaged to create one composite profile for the entire flume width over the 1 m study reach. The profiles were averaged rather than compared discreetly since the analysis was completed to get an overall understanding of whether there were elevation or slope changes. An example of the resulting composite profiles is shown in Figure 21, which shows the profiles from before and after the hydrograph

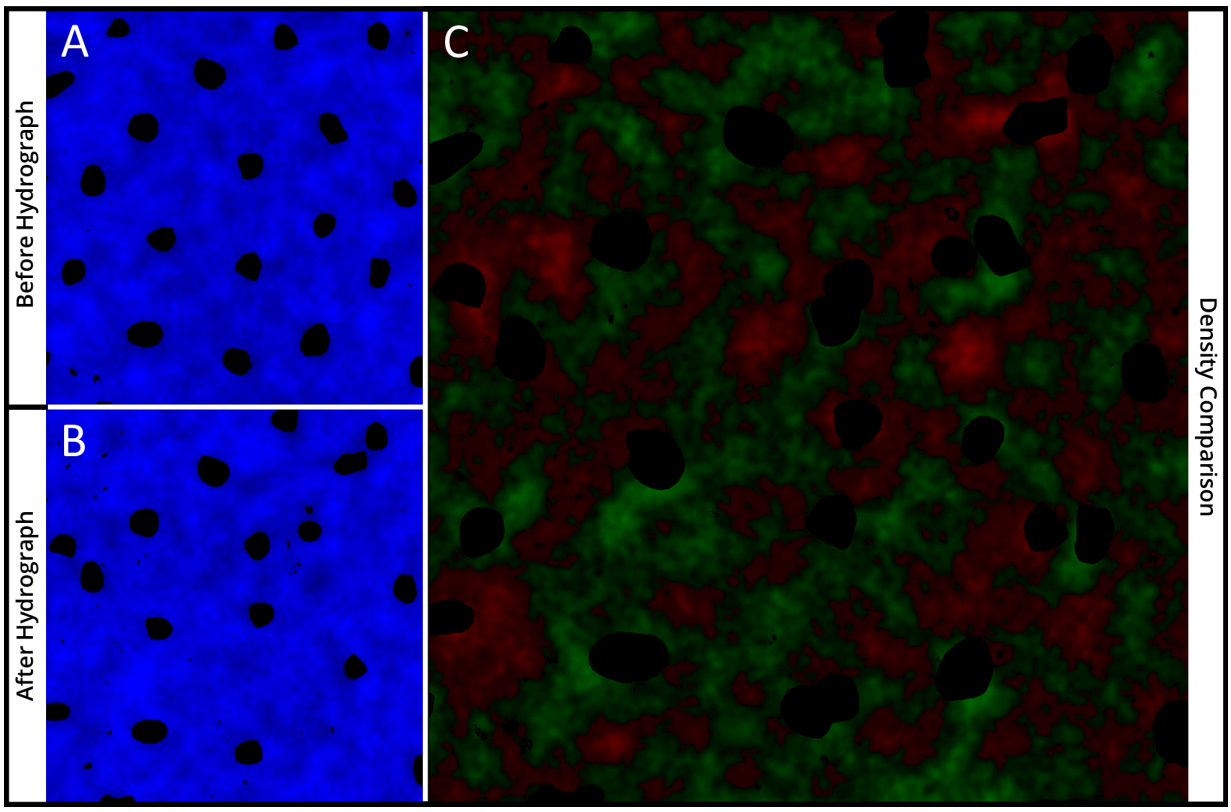

Figure 20: Processed images from Test Case 3. Images A) and B) are processed images for before and after the hydrograph, respectively. The blue intensity represents coarse material density and black areas represent the large immobile particle locations. Image C) is the comparison of image A) and B), where green represents an increase in particle clustering, and red a decrease. Black in this image is the removed areas where large particles were located.

in Test Case 1, as well as the resultant difference profile. The profiles were evaluated for the average change in channel elevation as well as the final bed slope for each of the five test cases and the base case.

3.5.4 Fractional transport analysis

To further compare the test cases and the base case, fractional transport (P_i/f_i) analysis was used to evaluate the relative mobility of the different particle size classes within the bedload samples (Parker et al., 1983; Wilcock and Southard, 1988; Church and Hassan, 2002). Following the methods presented by Wilcock and Southard (1988) and Church and Hassan (2002), P_i/f_i is defined as the ratio between a size fraction i's proportion in the bedload material (P_i) and it's proportion in the bulk bed material (f_i). The scaled fractional transport ratio ($q_{bi}P_i/f_i$) is then scaled by the unit bedload discharge (q_{bi}) of size fraction i. Bulk material characteristics were employed here for reasons consistent with Church and Hassan (2002) who found that the bulk material was more representative of the reference material for fractional transport analysis. They found that this observation was

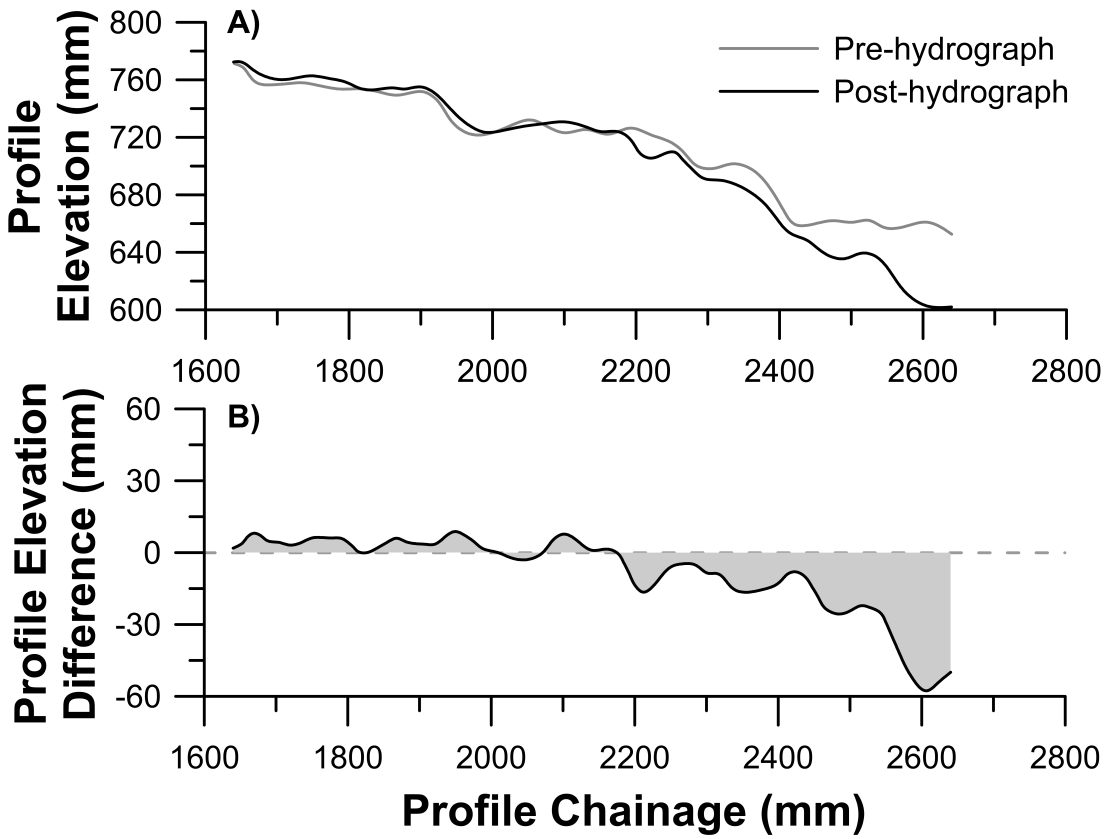

Figure 21: Example of profile comparison between pre- and post-hydrograph profiles isolated for the 1 m study reach. In the top plot, the Base Data profile is the pre-hydrograph profile, with the Comparison Data profile being the post-hydrograph profile. The bottom plot depicts the change in profile elevation, with the horizontal yellow line indicating the value of no change in elevation

attributed to the uncertainty in the surface material composition at the time of transport, as well as the lack of fines within the surface material that is prevalent in the bedload material.

Scaled fractional transport was evaluated by employing the dimensionless unit bedload flux (q^*_{bi}), which is a method presented by Parker et al. (1983). The dimensionless unit bedload flux is defined as (Parker et al., 1983):

$$q^*_{bi} = \frac{q_{bi} f_i^{-1}}{\sqrt{[(\rho_s/\rho_w) - 1] g D_{gi}} D_{gi}} \tag{14}$$

where q_{bi} $[\frac{M}{L \cdot T}]$ is the unit bedload transport rate of the given grain size fraction of interest, f_i is the fraction of the size class in the bed surface material, ρ_s is the sediment density ($2650 kg/m^3$), ρ_w is the water density ($1000 kg/m^3$), and D_{gi} $[L]$ is the geometric mean of the sediment size class diameter. This method is compared against the modified Meyer-Peter and Müller equation (Wong and Parker, 2006) as defined by:

$$q^* = 4.93(\tau^*_b - 0.0470)^{1.6} \tag{15}$$

The shear stress was determined at each flow step by using the depth collected using the ultrasonic sensors and the bed slope with the following equation (Julien, 2002):

$$\tau = \gamma R_h S_0 \tag{16}$$

where γ is the specific weight of water ($9806 N/m^3$), R_h is the hydraulic radius, and S_0 is the flume bed slope (0.01 m/m).

Equation 15 determines which size classes are either being over represented or under represented in the bedload composition when compared to the sediment in the bed material. Results are compared against other test cases, the base case and Equation 15. By determining the representation of the size classes, inferences can be made about the hiding of material by the large immobile particles, and the effects that large immobile particles have on the applicability of typical sediment transport equations.

4 Results

4.1 Bedload transport data

The sediment transport rates for each of the steps of the hydrographs were measured during the experiment. The raw data from the sieved samples can be found in Appendix A. The sediment transport ratio (STR) of each case shows that increasing the spacing between the large immobile particles is related to an increase in the sediment transport rate. Figure 22 shows the sediment transport ratio for the bulk sample, but also for the fine and coarse fractions of the bed material (separated by a particle diameter of 2 mm). There is an increase in the sediment transport rate from a large particle density of $\lambda/D = 2.63$ to $\lambda/D = 1.92$ for both the peak discharge (Figure 22B) as well as the entire hydrograph (Figure 22A). This increase is a result of increased fine material transport, as the coarse fraction has a decreasing STR as λ/D decreases over this range. Interestingly, the coarse sediment transport ratio is lower for Test Case 5 ($\lambda/D = 6.75$) than it is for Test Case 4 ($\lambda/D = 5.17$) at the peak discharge.

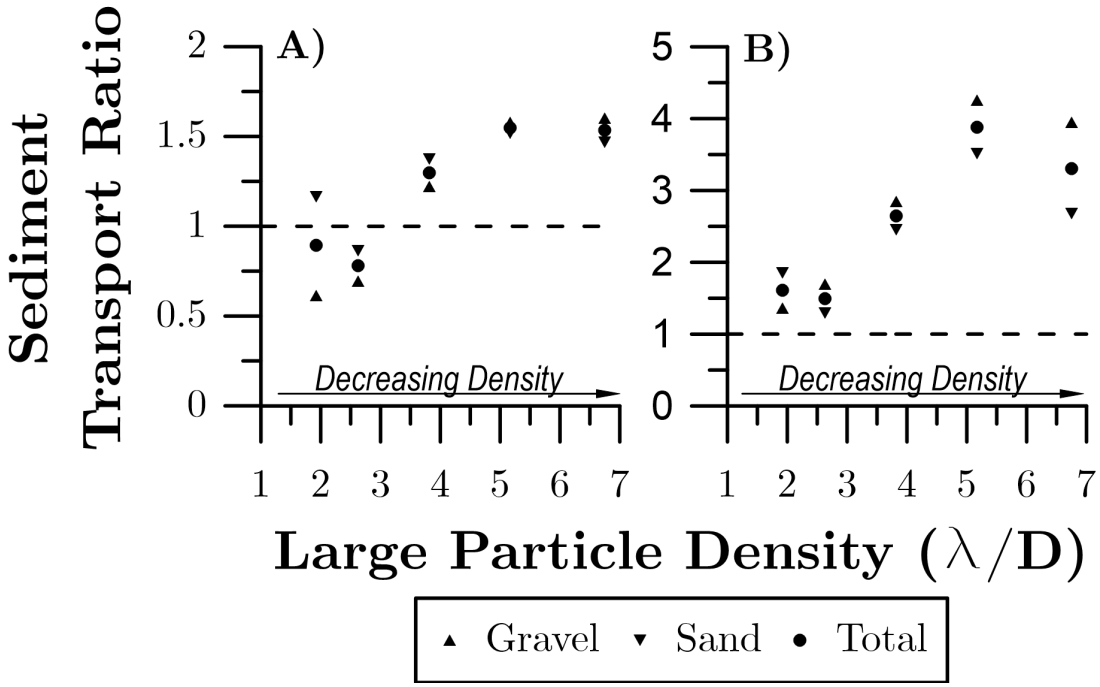

Figure 22: Sediment transport ratio for sediment transported over the entire hydrograph in each test case. The horizontal dashed lines indicates a value where sediment into the system is equal to sediment leaving the system. Additionally the coarse material (gravel) and the fine material (sand) are plotted separately to depict STR of each of these fractions individually. A) represents sediment transported during the entire hydrograph, whereas B) looks at the transported sediment during the peak discharge only.

For reference, the sediment transport ratios of the base case are 2.80 and 6.62 for the entire hydrograph and the peak discharge, respectively, which is higher than any of the

test cases. It should be noted that for the entire hydrograph, the sediment transport ratio was less than one for the highest density cases (Test Cases 1 and 2), indicating that there was more sediment stored than eroded in the system during the hydrograph.

Figure 22 also shows that the fine fractions have a greater sediment transport ratio than the coarse fractions for the highest density cases for both the entire hydrograph and at the peak flow. As the density of large particles decreases, the coarse sediment begins to have a higher ratio than the fine sediment. For the entire hydrograph, the STR of the coarse and fine material nearly reaches equivalency during Test Case 4, meaning that the fine and coarse material are similarly eroded out or deposited within the flume bed. When looking at the peak discharge only, equity is achieved between $\lambda/D = 1.92$ and $\lambda/D = 2.63$.

The results presented in Figure 22 confirm than an adequate range in large immobile particle density was tested. Ghilardi (2014) ensured that large particle densities between $\lambda/D = 2$ and 3 were used to capture the significant drop in sediment transport within this range. The results presented in Figure 22 show that this study was able to capture this significant drop which appears between Test Case 2 and Test Case 3.

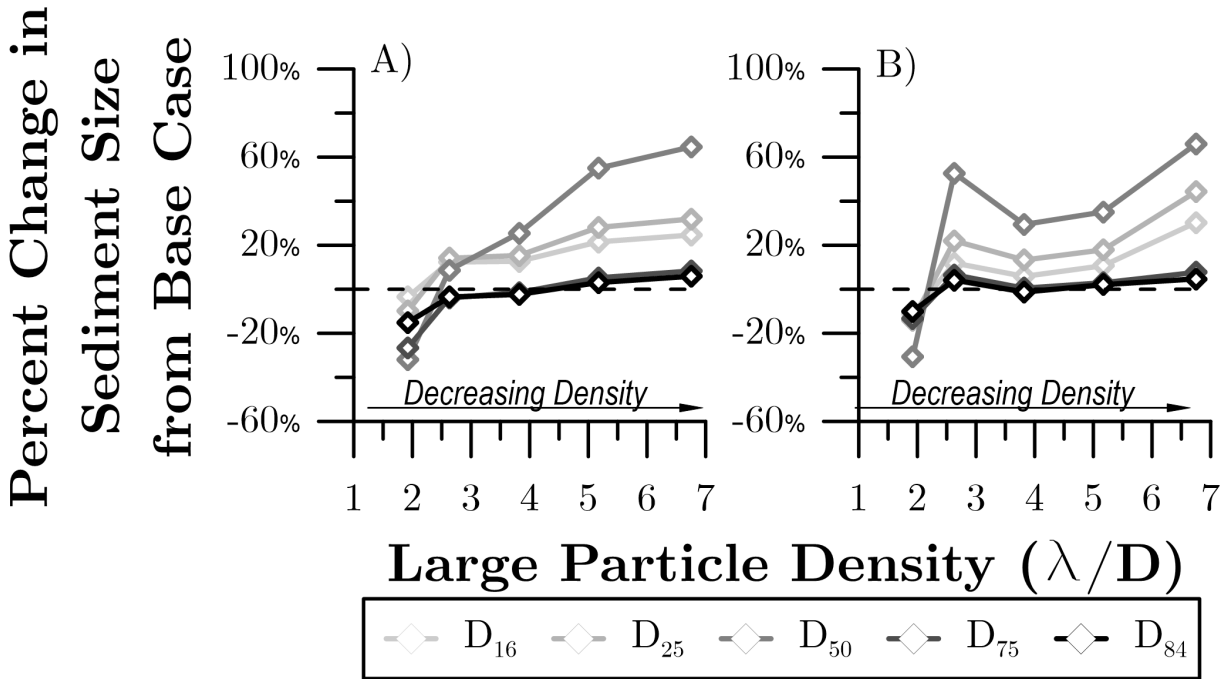

Figure 23: Change in the sediment size of transported material presented as a percent change in size fractions from the base case (ie. if the D_{50} is 1 mm for the base case, and 2 mm for the test case, this would be represented on the plot as 100%). The horizontal dashed line represents no change from the base case. A) represents all sediment collected during the entire hydrograph, and B) shows only sediment collected during the peak discharge

Figure 23 shows the change in transported sediment size from the base case, for both the cumulative data over the entire hydrograph (Figure 23A) and for the isolated peak discharge (Figure 23B). The overall trend is that the addition of large particles causes

an increase in the transported material size until the highest tested densities, as shown by values of <0%. As λ/D decreases (large particle density increases), the transported material size becomes smaller. For both the cumulative hydrograph and for the isolated peak, the highest density cases (Test Cases 1 and 2) relate to a decrease in particle size of all fractions. At the highest density case, all particle size fractions are smaller than the base case over the entire hydrograph and at the peak discharge. However, for all cases other than the highest density case, the particle size is generally increased when compared to the base case. The increase in particle size from a large particle density of $\lambda/D = 1.92$ and $\lambda/D = 2.63$ is a much greater increase than the increases in transported particle size found at lower large particle densities. As Figure 23 shows, the impact of large particle density on the transported particle size has the greatest effect on the median particle size (D_{50}). Additionally, the fine fractions are more impacted by the large particle densities than the coarse fractions.

4.2 Bed material size

Figure 24 depicts the difference in bed material size found after the hydrograph for each test case relative to the base case. The bed material gradations can be found in Appendix B. The highest density case (Test Case 1) yields results of nearly equivalent to that of the base case, with the bed material increasing as the density of the large particles decreases.

Figure 24 illustrates that the percentage change is lower in magnitude for the coarser percentiles for nearly all of the test cases, with the exception of Test Case 1, where all percentiles were approaching the same sizes found during the base case. Additionally, the D_{60} and D_{84} of the bed material are both larger during all test cases than the respective size classes during the base case, whereas the D_{30} and D_{50} experience decreases in particle size during the highest density test case. The results show that the coarsest particle size fraction is less impacted by changes in large particle density than the other size classes. There does appear to be a maximum in the bed material size during Test Case 4. This maximum is shown in the D_{30}, D_{50} and D_{60}, but the D_{84} and D_{90} experience a maximum at the lowest large particle density.

4.3 Erosion and Slope Change

Using the composite profile data from each test, erosional and depositional trends of the channel bed and changes in slope within the study reach were able to be determined. Figure 25 presents the results of this analysis. The profile plots for all test cases and the base case can be found in Appendix C. Changes in both elevation and slope (Figure 25) are less at the lower density cases (Test Cases 3,4 and 5) than the differences found in the higher density cases (Test Cases 1 and 2). The elevation drops are 35% and 39% of the base case for Test Case 1 and Test Case 2, respectively, compared to 133%, 98%, and 78% of the other 3 test cases. Correspondingly, the final bed slopes for Test Case 1 and Test Case 2 are 61% and 41% steeper than the base case, respectively, whereas the other 3 test cases are 12%, 7% and 17% steeper. These results mean that the higher density cases

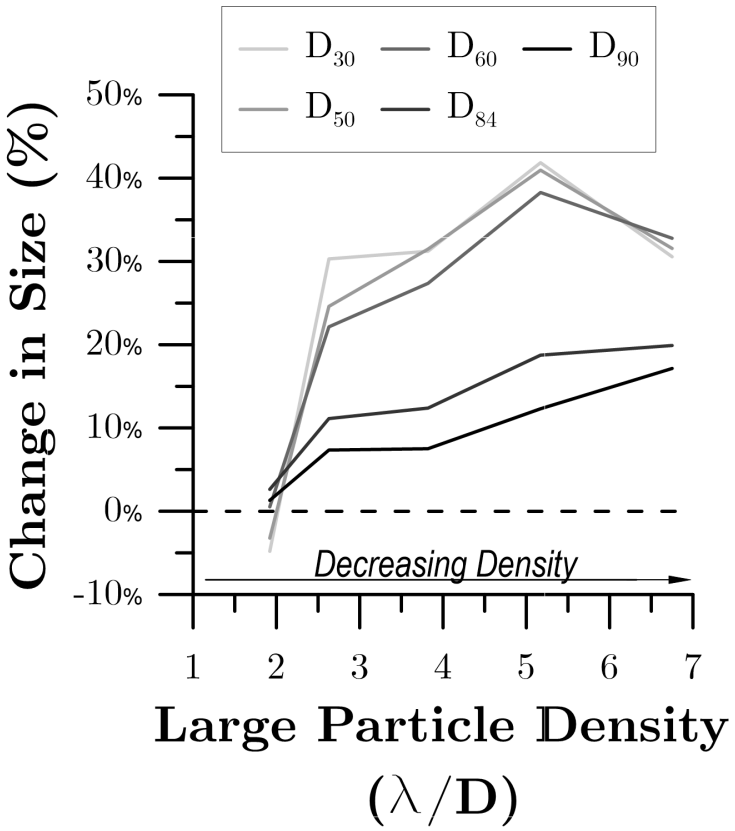

Figure 24: Increase in bed material size fractions found after the hydrograph with decreasing density, represented as percent change from the results of the base case. The horizontal dashed line represents no change from the base case value.

experienced more bed erosion and a greater increase in bed slope within the study reach than the lower density cases.

The impact of the large immobile particles on the channel slope are readily apparent until the density of the large particles reach $\lambda/D = 3.82$, after which lower densities of large particles show little difference in slope from the base case. The change in channel bed elevation over the hydrograph is reduced for Test Cases 1 and 2, with a small increase in the observed change for Test Case 3, near equal change as the base case for Test Case 4, and a lesser reduction in change for Test Case 5.

4.3.1 Particle Clustering Analysis

The results of the particle density analysis show that there is an increase in coarse particle clustering as the density of the large immobile particles decreases. Figure 26 depicts this trend by showing the particle clustering with 3 different metrics used in the analysis: the sum ratio, the increasing/decreasing area ratio and the mean ratio. Images showing the clustering analysis for each of the test cases and the base case can be found in Appendix D.

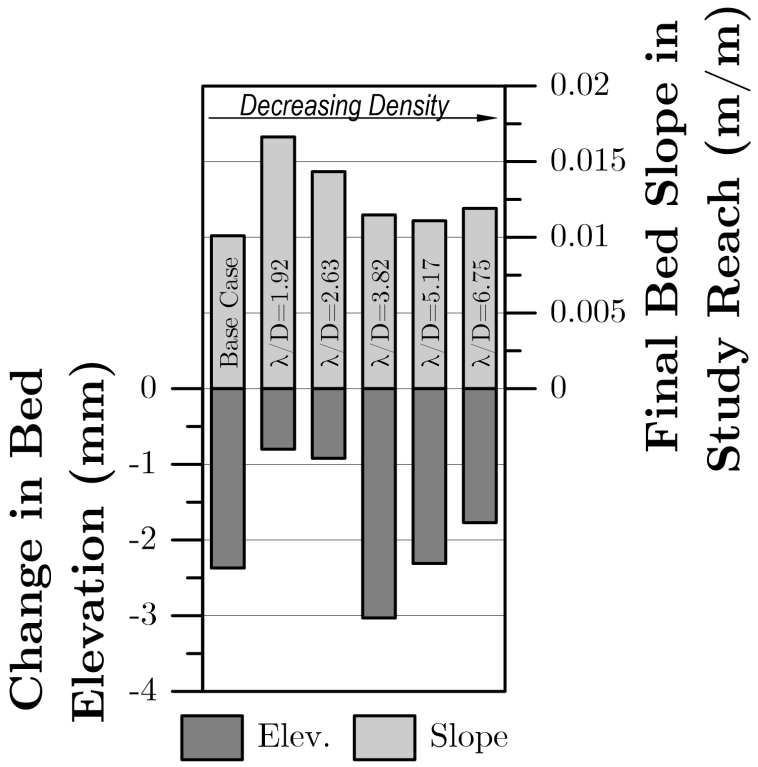

Figure 25: The change in bed elevation (dark grey) over the course of the hydrograph, and the final bed slope at the end of the experiment (light grey).

The increasing trend in coarse material density is consistent through all of the test cases except for Test Case 4, which is below both Test Case 3 and Test Case 5 cases. If either Test Case 3 or Test Case 4 were removed, the trend of increasing coarse material clustering while large particle density decreases would hold, with the deviation likely being due to experimental variability. The base case shows a decrease in coarse particle clustering, which is opposite to the results of all of the test cases, however, the decrease is very slight.

4.4 Bedload hysteresis

The bedload hysteresis analysis, which focuses on the difference in sediment transport rates between the rising and falling limbs of each hydrograph, resulted in a clockwise loop trend (greater transport during the rising limb) during the base case and for nearly all of the test cases as shown by Test Case 3 in Figure 27. This is consistent with the previous findings of Mao (2012) where clockwise hysteresis loops were found for every hydrograph of a laboratory experiment. Interestingly, this is opposite the result from Waters and Curran (2015), where a counterclockwise hysteresis was found on the first hydrograph of their lab experiments. The dominance of clockwise hysteresis trends indicates that the sediment supply is greater on the rising limb or that an armour layer forms, making sediment less available on the falling limb (Williams, 1989). The only exception to the clockwise hysteresis loop trend is Test Case 4, which shows a figure eight trend, with a

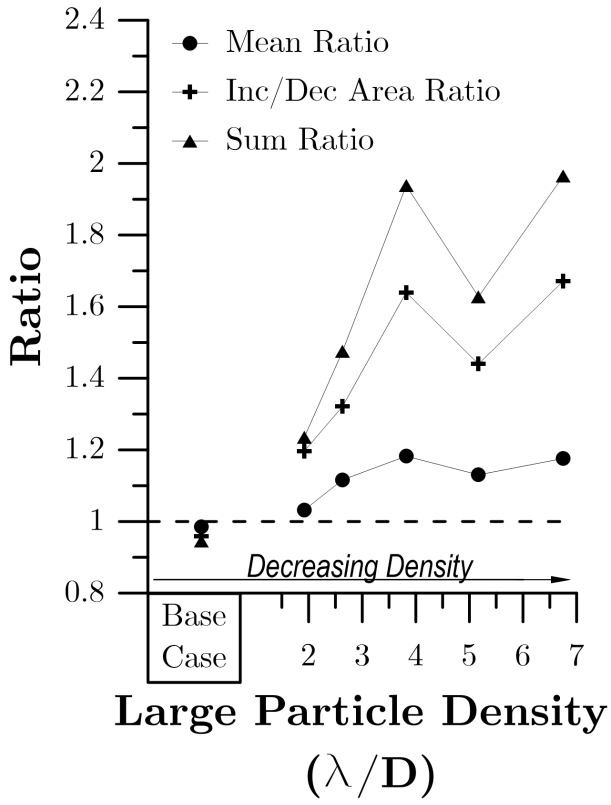

Figure 26: Results of the particle clustering analysis, displaying the mean ratio (circles), the increasing/decreasing area ratio (crosses), and the sum ratio (triangles). The horizontal dashed line represents values where the particle clustering is equivalent between the beginning and completion of each hydrograph.

clockwise trend dominating the higher flows in the hydrograph. A figure eight trend could be an indication of an armour layer breakup on the falling limb (Williams, 1989).

The base case has a sediment transport ratio of greater than 1 for the first step of the rising limb (Figure 27), whereas the test cases do not, with the exception of Test Case 5. The general trend observed was that the sediment transport characteristics of Test Cases 1 to 5 approached that of the base case with decreasing large immobile particle density. Additionally, for all but one of the test cases and the base case, the maximum STR occurs during the peak discharge. The differences in STR between the peak discharges and steps before each peak discharge become smaller as the density of the large immobile particles increased. Accordingly, during the highest density case (Test Case 1), the STR of the discharge step before the peak discharge exceeds that of the peak.

The hysteresis of each case was summarized in Figure 28, which presents the results as a hysteresis ratio. The hysteresis ratios have clear decreasing trends with decreasing large immobile particle density. Additionally, all test cases have a higher hysteresis ratio than the base case. Test Case 4 exhibits an outlying figure-eight hysteresis trend which does not follow the decreasing trend as shown in the other test cases. The highest density case has a hysteresis ratio that is 50% greater than the base case, with all cases (excluding Test Case

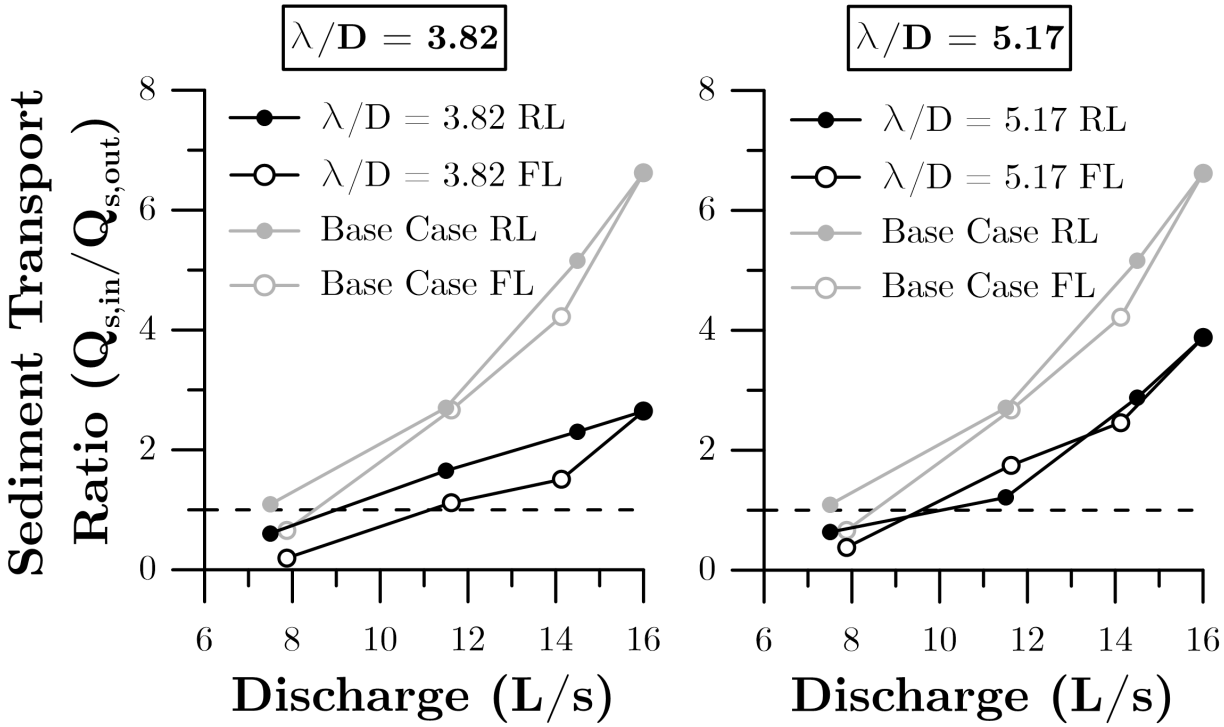

Figure 27: Bedload hysteresis plots for two representative cases, Test Case 3 (left) and Test Case 4 (right), depicted as the sediment transport ratio at various steps of the hydrograph. The base case is plotted against both test cases for scale and comparison. The horizontal dashed line represents equal sediment entering and exiting the system of the course of the hydrograph step. Filled symbols indicate steps on the rising limb of each hydrograph, hollow symbols identify falling limb observations. Plots for all cases are found in Appendix E.

4) being substantially higher than the base case. It is notable that all cases, including the base case, have a hysteresis ratio greater than 1.5. This result indicates that the sediment transport on the rising limb of each hydrograph is much greater than that of the falling limbs.

As Figure 28 shows, Test Case 4 ($\lambda/D = 5.17$) is lower than would be expected based on the results of the other 4 test cases. A possible explanation for this result is that the armour layer broke up during that test case, which would lead to an increased sediment transport rate on the falling limb as the armour layer began to redevelop. This is supported by Figure 26 which shows less coarse material clustering over the hydrograph, Figure 25 which shows that Test Case 4 experienced the most erosion of all the test cases, Figure 22 which depicts that Test Case 4 has the highest sediment transport rates of all of the test cases.

4.4.1 Fractional transport analysis and dimensionless bedload rating curve

The dimensionless unit bedload flux (q^*_{bi}) was calculated for each step of the hydrograph for all test cases and the base case. These data were then compiled into dimensionless

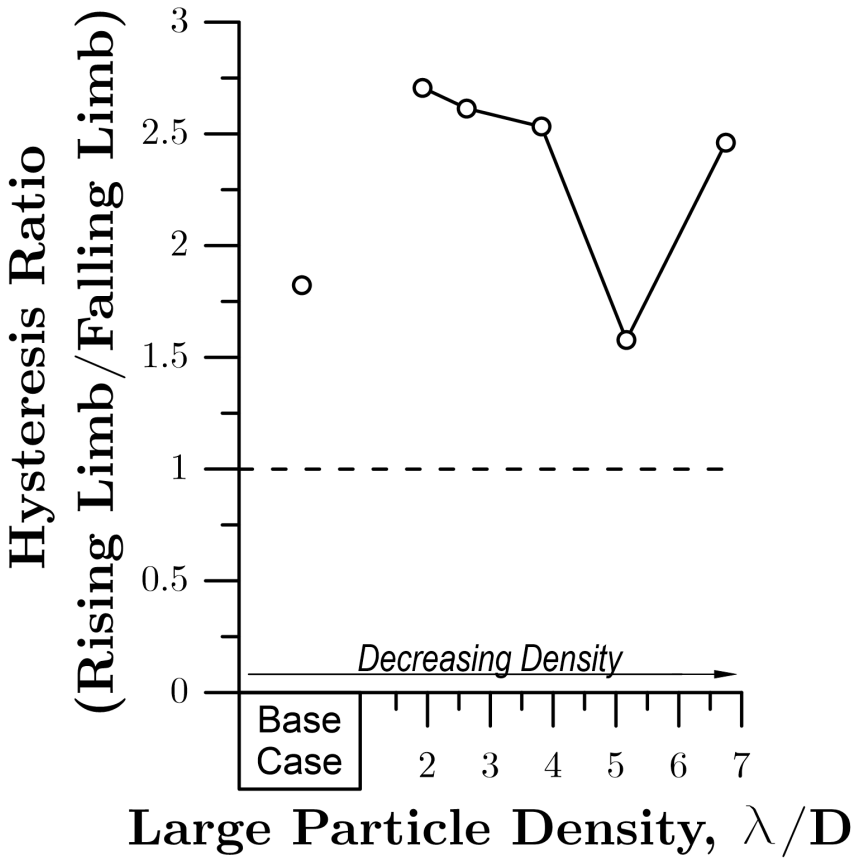

Figure 28: Hysteresis ratio versus large immobile particle density. The horizontal dashed line represents the conditions where an equivalent amount of sediment is transported on each limb. The base case has been plotted on the left for comparison to the test cases.

bedload rating curves by comparing the bedload flux to the dimensionless shear stress by employing Equations 14-16, with results shown in Figure 29. The dimensionless bedload rating curves were plotted against the rating curves generated by applying the modified form of the Meyer-Peter and Muller bedload transport equation (Wong and Parker, 2006). The bedload transport rates were observed to be lower for increases in large immobile particle density for most particle sizes in transport. The exception appears to be that of the largest and smallest particle sizes which appear to be unaffected by changes in large particle density. In all cases, the modified M-PM bedload transport equation over predicts the transport of fine-grain material fractions and under predicts the transport of coarse material fractions. The dimensionless bedload flux for the median particle sizes (from 1 mm to 2.8 mm) was noted to be lower than those for slightly coarser or finer material fractions.

The fractional transport analysis for each test case and the base case determined both the fractional transport ratios and the scaled fractional transport rates and are shown in Figures 30 and 31 respectively. The fractional transport ratios (Figure 30) show that the coarse material fractions are less represented in the bedload in the final discharge

steps of the falling limbs. Variability in the fractional transport ratios is less for the finer material, and greater for the coarser material as the large immobile particle density increases indicating a trend in the partial transport (Ashworth and Ferguson, 1989; Wilcock and McArdell, 1997). Excluding the first and last stages of each hydrograph, lower densities of large particles correspond to conditions close to unity in the fractional transport ratio across all size classes. In cases where higher large immobile particle densities were tested, the size selectivity towards the fine to medium particle sizes increases (Figure 30). Further, the fine material is mobilized more during the rising limbs and have values closer to 1, with much lower fractional transport ratios for the fine material during the falling limbs.

Based on the scaled fractional transport rate (Figure 31), the first and second steps of the rising limb are similar, with increasing large immobile particle densities having reduced transport rates for all other steps of the hydrograph. Additionally, the changes in scaled fractional transport at the coarser sediment sizes (greater than 1 mm) is greater than the changes seen in the finer fractions. All of the test cases and the base case show a decrease in scaled fractional transport rate around the median particle size of 2 mm. The scaled fractional transport rates for the falling limbs decreased more as the sediment size increased than the rising limb. This effect is more noticeable in the higher density cases, but is present in all cases. The spread of the finest particle size in terms of the scaled fractional transport rate is the greatest for the base case, with the spread becoming less as the large particle density increases. Finally, the peak discharge displays a clear drop in the fractional transport rate for the range of sediment size from 2 mm to 8 mm as the large particle density increases, with a drop being observed in nearly all sediment sizes, but not as evident.

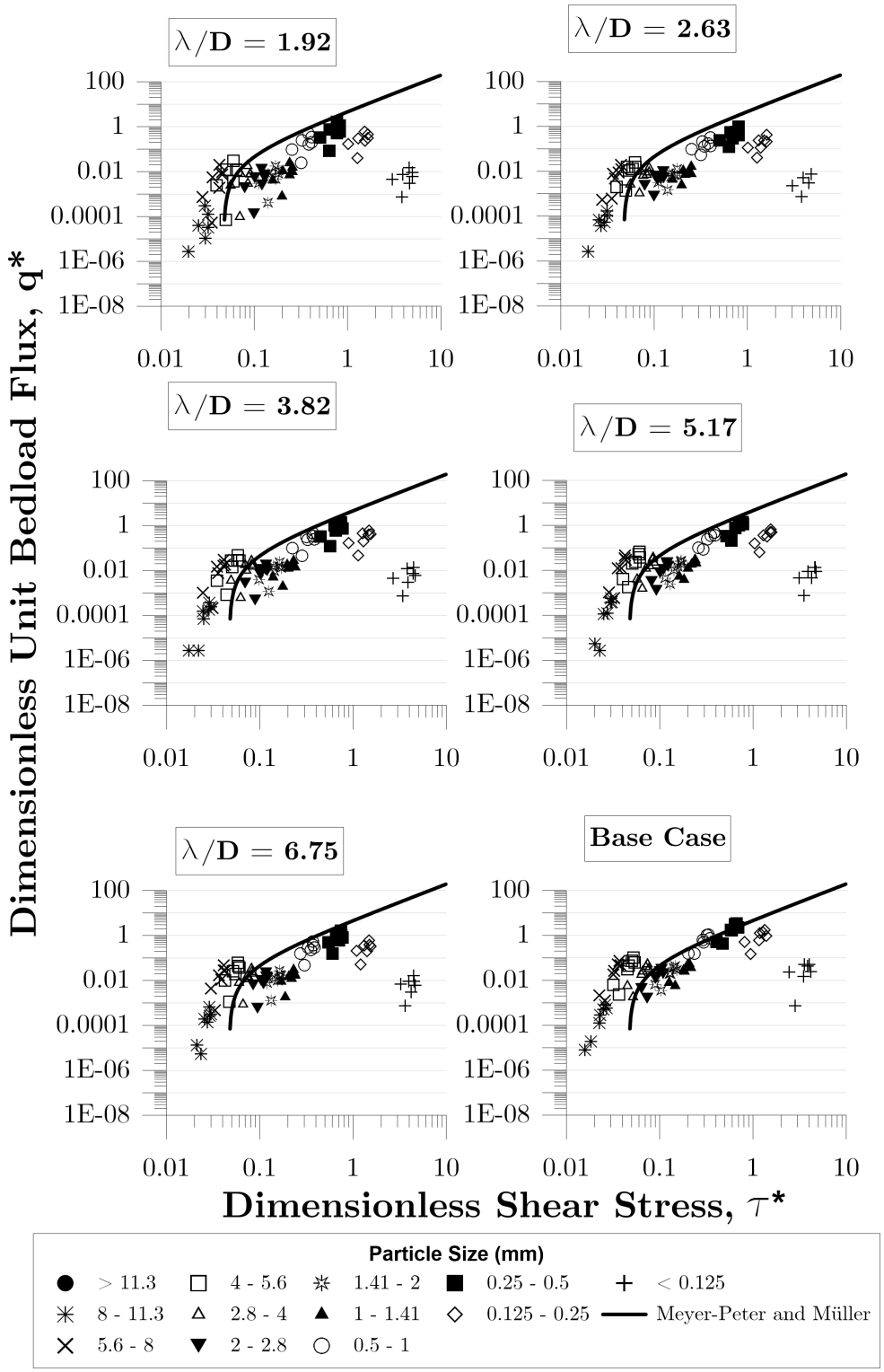

Figure 29: Dimensionless bedload rating curve for all cases. The modified form (Wong and Parker, 2006) of the Meyer-Peter and Muller bedload transport equation (Meyer-Peter and Müller, 1948) has been plotted for comparison (solid line).

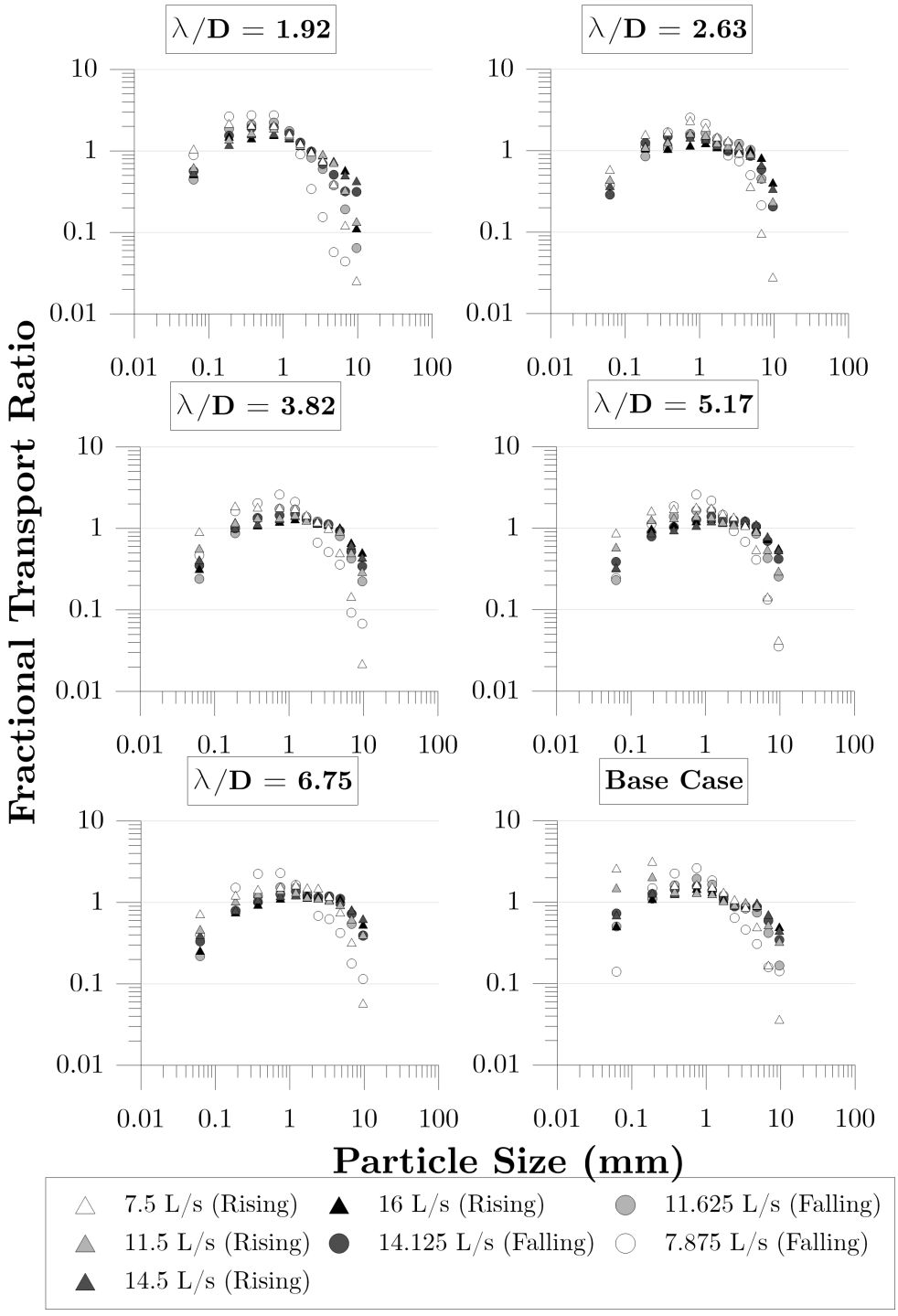

Figure 30: Fractional transport ratio for for all cases. Fractional transport ratio compares the representation of a material in the bedload compared to the same materials representation in the bed material mixture. Triangular symbols represent steps of the hydrograph on the rising limb, whereas circular symbols represent steps on the falling limb.

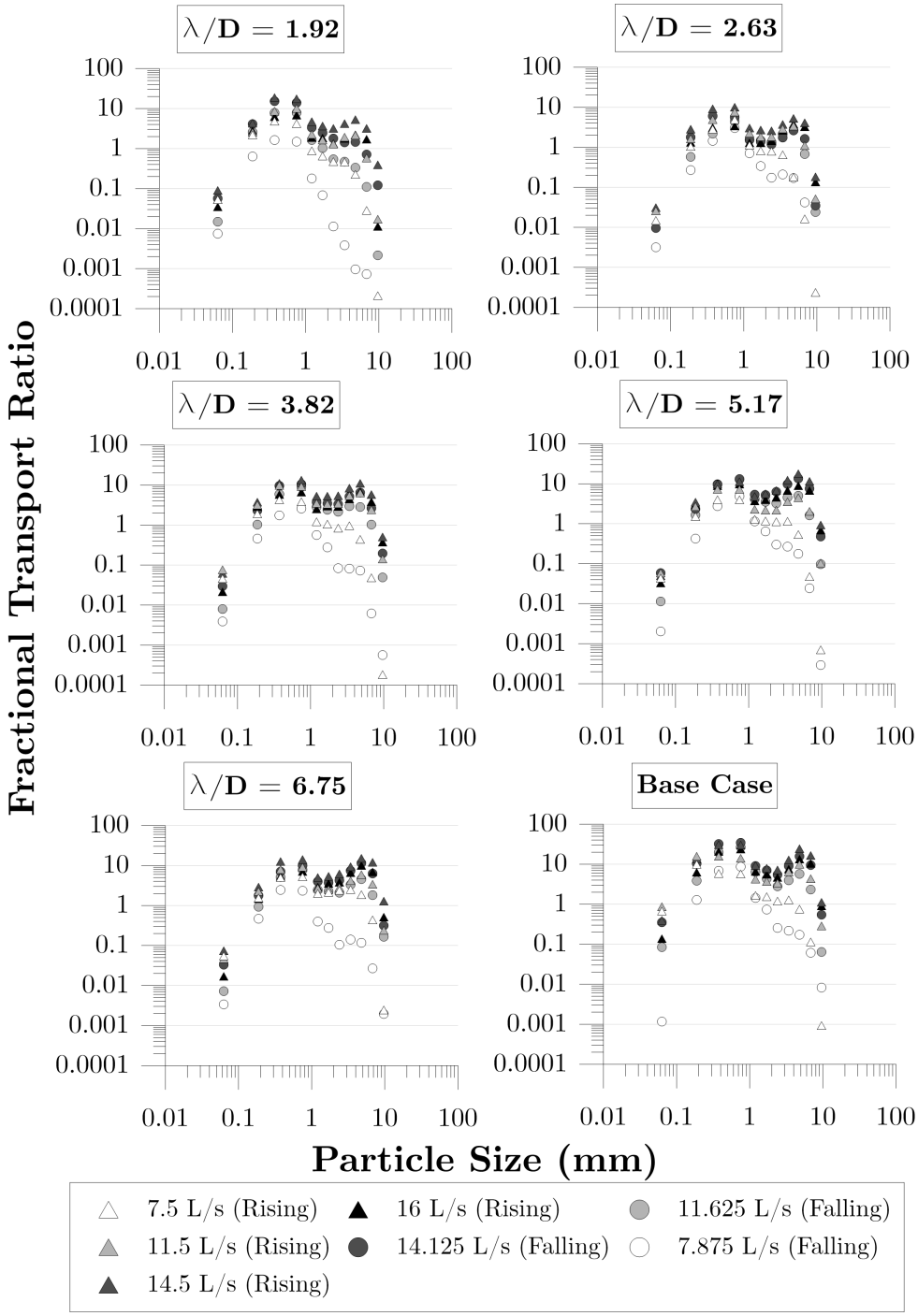

Figure 31: Scaled fractional transport rates for for all cases. Triangular symbols represent steps of the hydrograph on the rising limb, whereas circular symbols represent steps on the falling limb.

5 Discussion

The common interpretation in systems with large particles protruding from the channel bed is that there is a general drop in shear stress on the channel bed resulting in a reduced sediment transport capacity (Ghilardi, 2014; Brayshaw et al., 1983; Hassan and Reid, 1990; Yager et al., 2007). While this phenomena has been readily supported by the findings within this study, it does not encapsulate the full range of effects that large immobile particles have on sediment transport and channel morphology. While it appears that the average force being exerted on mobile bed sediments is being reduced as the density of large immobile particles increases, the results within this study do not all agree with what would initially be expected of an overall drop in bed shear stress. This is shown through changes in sediment transport and bed morphology.

It was suspected that the introduction of large immobile particles would cause decreased shear stress, and it would then be expected that the size of the transported material during the base case would always be coarser than material being transported during cases with large particles present. While the sediment transport rate does decrease as the density of the large immobile particles increases as predicted (Ghilardi, 2014; Brayshaw et al., 1983; Hassan and Reid, 1990; Yager et al., 2007), the size of the transported material is not finer in these high density cases as a typical sediment transport model would predict. Instead, the size of the transported material at the highest density cases (Test Case 1 and 2) is very similar to that of the case where no obstructions are present. The trend shows that the transported particle size increases as the density of the large particles decreases. Not only is this trend shown in Figure 23, it is also shown in Figure 22 in which the fraction of coarse material being transported decreases as the density of large particles increase.

The bed texture results also do not follow the expected trends. The expected result would be that as the large immobile particles cause an increase in bed roughness and a decrease in shear stress on mobile sediments, finer material would be maintained on the channel bed as it would not be able to be entrained (Ghilardi, 2014; Brayshaw et al., 1983; Hassan and Reid, 1990; Yager et al., 2007). However, the results of this study show that the channel bed is immediately coarser by 20 to 30% at the highest density case, then shows an increase in bed material size as the large particle density increases to $\lambda/D = 5.17$ (Test Case 4), followed by a decrease in particle size until the maximum tested density of $\lambda/D = 1.92$ (Test Case 1), which had bed material consistent in size with the base case. It should be noted that the increase in bed material size from Test Case 1 to Test Case 2 was the greatest increase in particle size between test cases, indicating that this might relate to the densities in which flow structures are being impacted the most. A drop in shear stress does not adequately provide an explanation for the process that causes an increase in bed material size due to the presence of large immobile particles.

The trends in sediment transport and bed texture clearly showed the ineffectiveness of the simple explanation that increasing large immobile particle density causes reduced shear stress and increased resistance to flow. Rather, the sediment transport and bed texture data support a more complex explanation that can be developed from existing literature (Brayshaw et al., 1983; Tan and Curran, 2012; Hassan and Reid, 1990). Brayshaw et al. (1983) found that isolated obstructions on a channel bed created localized areas of increased

total kinetic energy and turbulence in the horizontal plane on the lee side (downstream side) of the particles, as shown in Figure 10. If unaffected by downstream obstructions, this would result in increased shear stress and scour holes on the downstream side of the particles (ie. the processes leading to imbrication). These isolated obstructions also provide areas that are protected from high energy flows where material could deposit. Hassan and Reid (1990) identified that at high densities of large particles, the flow skimmed over the tightly spaced particles. This high energy skimming flow created powerful eddies that acted on the channel bed in the larger gaps of the randomly placed particles. Tan and Curran (2012) found that when particle clusters were at a specific spacing, the flow patterns of the clusters amplified each other, resulting in an increase in the power of the turbulence structure between them. When the clusters were spaced further apart, the flow patterns began to resemble isolated clusters. Alternatively, spacing the clusters closer together resulted in the flow patterns interfering with each other and reducing the energy of the turbulence cells.

To summarize, the more complex explanation of the trends in sediment transport and bed morphology is made up of three key points:

1. isolated large immobile particles create localized areas of increased erosive forces, and localized protected areas (Brayshaw et al., 1983);
2. at a narrow range of large immobile particle spacings, flow structures build upon each other and amplify their erosive forces (Tan and Curran, 2012); and
3. densely spaced large immobile particles cause high energy skimming flow that is able to create powerful eddies in gaps between the large particles (Hassan and Reid, 1990).

This complex explanation can be used to explain the trends observed in the current study in sediment transport rate, size of transported material, and bed texture. During the low density cases, coarser material was transported than the base case and the bed surface was coarser. This is explained through the study presented by Brayshaw et al. (1983). Low densities of large immobile particles provided isolated areas of increased energy that allowed for the mobilization of material that could not be mobilized during the base case, which caused the increase in transported material size. The scour holes created in this process would contain the coarse material that the increased energy could not mobilize, resulting in an increased bed material size. As the large immobile particle density increases to the intermediate tested densities, the sediment transport rate peaks then decreases, the size of transported material decreases and the bed material size peaks then decreases. The peaks in sediment transport rate are indicative of the large particle density passing the range in which the flow structures build upon each other and create more erosive force, mobilizing more material and creating larger scour pools armoured with coarse material (Tan and Curran, 2012). The drop in the size of the transported material is likely a result of the coarse material that is mobilized in the scour pools being deposited in the increasing number of areas where the large particles shield the bed from the flow (Brayshaw et al., 1983). At the highest density, the size of the transported material and the bed material size is nearly equivalent to that found in the base case. This can be attributed to these parameters reaching a balance caused by the skimming flow (Hassan and Reid, 1990). The

bed areas experiencing skimming flow are well protected from the high energy flow which would allow fine material to deposit in the tight spaces between the large particles. This also contributes to the drop in sediment transport rate. In the areas where there is a bigger gap between the large particles and the high energy flow is able to impinge on the channel bed, scour holes are formed exposing coarse material. While a greater proportion of coarse material is likely able to be mobilized than during the base case as a result of this high energy flow, this coarse material would likely be deposited prior to reaching the sediment trap. For the size of transported material, a balance is reached between coarse material that is mobilized from the scour holes and the coarse material that is deposited in lower energy areas, resulting in similar results to the base case. Similarly, the bed material is a balance between the coarse material present in the scour holes and the fine material trapped between the densely spaced particles, which results in a similar surface texture to the base case. It is predicted, that if the density of large particles increases past that tested in this study, the areas in which the eddies could impinge would reduce or cease to exist, resulting in a fining of both the transported material and the bed material in relation to the base case. Therefore, it is clear that the findings from these three pieces of existing literature are sufficient to explain the trends from this experiment in sediment transport rate, size of transported material and bed material texture. The use of these findings will be continued within the discussion of other results found within this study.

Interestingly, the density of large immobile particles on the channel bed had less impact on the finest and coarsest size fractions of the transported material than the impacts on the inter-quartile size fractions, as shown by Figure 23. While the limited change in the extreme fine and coarse fractions could be attributed to sediment availability (ie. once the fines have been washed off the bed surface, other material will need to be eroded for more fine material to become available), the fractional transport analysis as shown in Figure 30 depict that availability is not the cause of this due to their under-representation in the transported sediment. When comparing the fractional transport at the higher discharges of 14.5 L/s and 16 L/s on the rising limb and 14.25 L/s on the falling limb, the material around 2-3 mm exhibits the greatest changes between the different test cases. In contrast, the fine and coarse material fractions stay relatively constant between all cases. The effects predicted by Hassan and Reid (1990), which can be used to explain many of the other phenomena within this study, can also be applied here. During the base case, it is likely that as the finer material is eroded, the channel bed becomes armoured. The inclusion of the large particles and their resultant eddies will produce an increased transport capacity in localized areas and will provide for the ability to mobilize some of this coarser armour material. It has been previously identified that material on the downstream side of an obstruction or particle cluster is more frequently mobilized, and once mobilized, this material has shorter travel distances (Brayshaw et al., 1983). This could cause the coarse material that forms the armour layer to be mobilized due to the powerful eddies acting on the bed, allowing more easily transported material to be conveyed, with the coarse material being deposited in lower energy areas shortly downstream. With the deposition of this coarser material, it allows for the increased storage of fine materials in the interstitial spaces created. Despite the coarse material being mobilized, the low transport distances is a possible explanation for the lack of representation due to the material's inability to reach the bedload trap in

the flume.

The clustering of coarse particles has similar trends (Figure 26) to that shown in the transported material size and the bed material size, where it appeared that more particle clustering occurred at the lower densities of large particles, with the base case having the least amount of clustering and the higher the density of large particles approaching similar results to the base case. It is hypothesized that the scour holes behind the large immobile particles would provide a source of coarse material clustering due to the fines being washed away in those areas, however the large particles would also provide protected areas for fine material to cover the channel bed and reduce any coarse material clustering in those areas (Brayshaw et al., 1983). Additionally, the destructive flow patterns of large particles spaced closely together in the higher density cases would reduce the size of the scour holes (Tan and Curran, 2012). As such, it seems logical that the cases with lower densities of large immobile particles had the larger, more well developed scour holes overall, resulting in the greatest increase in coarse material clustering. Whereas the cases with high large particle densities would have more area where fines were trapped on the bed surface, as well as a greater number of poorly developed scour holes due to destructive flow patterns, resulting in a reduced amount of clustering.

The bedload hysteresis is generally increasing with large particle density (with positive values being in reference to clockwise hysteresis, or more sediment transport on the rising limb than the falling limb). Test Case 4 was an exception to this, experiencing a figure 8 trend. As discussed previously, this could be the result of an armour layer breakup, resulting in increased sediment transport rates during the falling limb (Orrú et al., 2016). This supports the proposed concept that large particles on the channel bed create more powerful eddying effects in the small scour holes on the downstream side of the particles (Hassan and Reid, 1990). During the rising limb, since it is the first time the channel bed has experienced flows above a low flow, material is being eroded from the scour holes. On the falling limb, these scour holes begin to fill with material as the scouring force is decreased to a point where material can deposit and the transport capacity in these areas is decreased. Additionally, the highest density cases likely have the highest hysteresis due to the much higher percentage of the mobile bed experiencing this effect compared to the lower density cases or the base case.

Some very clear trends were observed within the bed profile results. The most obvious observed trend was that the test cases with higher densities of large immobile particles experienced less erosion over the hydrograph, and that all supplemental cases experienced overall degradation of the channel bed. This overall erosion trend is likely a result of the bed material experiencing flows of the tested magnitudes for the first time during the hydrograph, causing the washout of unsettled and unstable material prior to an armour layer forming (Plumb, 2017). The lower level of erosion present at the highest densities is in line with other studies that suggest that large particle density is proportional to the overall bed resistance (Hassan and Reid, 1990; Tan and Curran, 2012). An interesting result is that the erosion does not increase with a decrease in large particle density as expected. From a density of $\lambda/D = 3.82$ to $\lambda/D = 6.75$, the bed experiences a decreasing amount of erosion. This is unexpected as the anticipated relationship between large particle density and resistance would suggest that as large particle density decreases, the erosion amount

would increase, approaching a maximum value at the base case. A possible explanation for this may be that at a density between $\lambda/D = 2.63$ and $\lambda/D = 5.17$, there is a point where the large particle spacing corresponds to the ideal spacing required for flow structures to build upon each other (Tan and Curran, 2012). This spacing would represent the case with the greatest number of well developed scour holes and the least amount of interfering flow patterns, leading to the greatest amount of erosive force.

The bed profile slope does not follow a similar trend as the bed elevation. The bed slope after the hydrograph is the steepest at the highest density case (Test Case 1), with the slope decreasing as the large particle density decreases until the base case, which has the shallowest slope. This trend is likely a result of material being deposited in the upstream section of the study reach as the flow enters into the large particle lined reach which has a larger resistance and a lower velocity, resulting in a decrease in sediment transport capacity. This reaction will likely continue until a balance is reached such that the slope has increased to a point where sediment transport continuity can be reached (ie. sediment in = sediment out). This continuity would be reached when the increased slope causes an increase in transport capacity, coupled with the reduced protrusion of the large immobile particles lowering their reduction to bed shear stress. Additionally, if the sediment inflow were to be increased, it would be expected that the slope found after the hydrograph would be greater for all cases.

The fractional transport analysis helps explain the evolution of the bedload composition as well as addressing other anomalous observations. For instance, as Figure 29 depicts, the Meyer-Peter and Muller bedload transport equation is more applicable to the finer material during the base case. However, for this experimental setup, the coarser material corresponded more readily with what was expected in terms of trends in sediment transport rates. Figure 30 shows that the changes due to the large particles being present in the channel were more noticeable in the coarse material than in the fine fractions. It was found that the fraction of coarse material present in the bedload was inversely proportional to the large particle density. This trend was more apparent during the falling limb. This characteristic would show that once an armour layer has developed, the coarse bed material is not as easily moved as the density of large particles is increased. This drop in the coarse material also indicates that as the large particle density increases, the system moves away from equal mobility and towards size selectivity of the finer fractions. Additionally, the first stages of the rising limb see little effect from the changes in particle density, as this is likely due to the material being in non-stable conditions as they have not been able to adjust to high flow conditions.

Figure 32 shows the fractional transport ratio for a select representative sample of the density cases at the peak discharge only. Interestingly, in all cases, there is a distinct drop in fractional transport ratio as the particle size increases past approximately 2 mm. However, this drop is clearly more noticeable in the base case and in Test Case 1, with the lowest density cases having the smallest decrease in fractional transport ratio of the coarse material. Two main points are clearly apparent. First, the base case and the highest density case are the most similar in terms of their fractional transport ratios, with the less dense cases showing an increase in representation of the coarse material. Second, equal mobility of the sediment is most apparent at an intermediate large particle density, with a

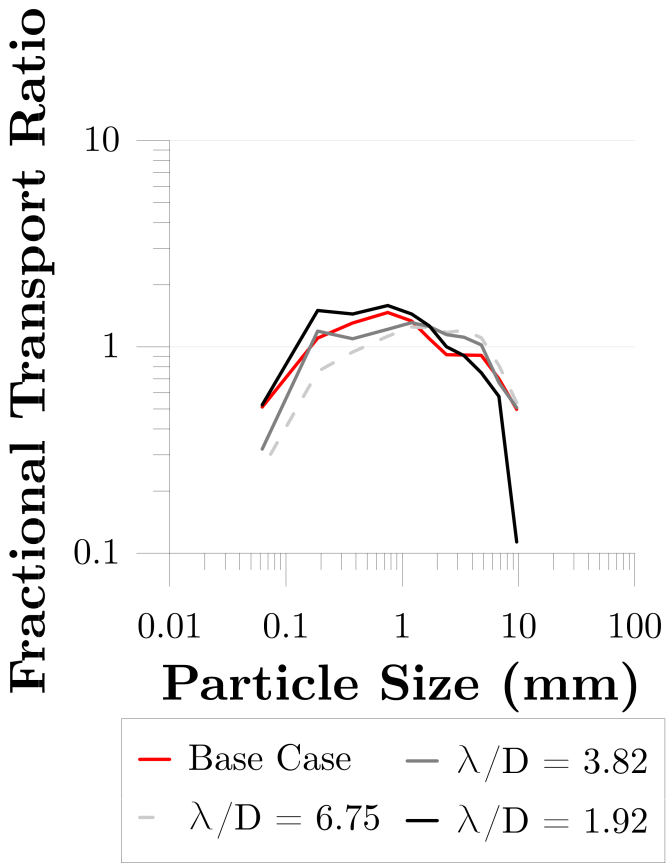

Figure 32: Fractional transport rates at peak discharge for selected test cases and the base case.

much more even distribution of size fractions being present in Test Case 3. The increase in equal mobility at intermediate size fractions can be explained by Tan and Curran (2012), where the intermediate large particle spacing causes the amplification of flow structures, and the resultant mobilization of the coarse particle size fractions.

6 Future Work and Practical Applications

To continue this research, it would be beneficial to conduct a similar study to examine a wider range of large particle densities, as well as more iterations of the same densities. Since protrusion of the large immobile particles was not incorporated into this study, it would be useful to monitor it as another variable if this study were to be continued. Additionally, it would be valuable to examine the long term effects of large particle density by conducting consecutive hydrographs to observe the morphological development of the channel in response to the large immobile particles. Finally, obtaining higher resolution sediment transport data would be beneficial to analyze more detailed trends in the sediment transport data. This was not completed during this experiment due to limited time and personnel.

The results and relationships presented within this study provide a framework for predicting the response to failed channel stabilization works. A summary of these relationships is found within Figure 33, which can be used as a guide to initial channel response resulting from the introduction of large immobile particles to a stream bed. For instance, a practitioner can qualitatively assess the density of the introduced material, and use this guide to predict changes in bed material size, bed slope, erosional trends, etc..

Further to using the information provided in Figure 33 to predict channel bed adjustments, this information could be used to inform the design of channel features aimed at remedying channel processes. A good example of this would be the design of a riffle feature with protruding keystones to limit the impacts of fine sediment being introduced through upstream construction activities. A riffle feature with a low density of protruding keystone particles would effectively reduce the sediment transport rate, while increasing the size of the transported material. Alternatively, in a scenario where land use changes cause channel instability and increased sediment load to downstream reaches, a riffle or series of riffles with a high density of protruding keystone particles could be used. This would act to temporarily reduce the sediment transport rates while maintaining the size of the transported material. Eventually, once the slope of these features increased to an equilibrium, they would cease their storage of sediment and maintain sediment continuity through the reach. While this research is able to provide a rough framework for the design of in-channel features, further research would be required to ensure that the relationships presented in Figure 33 are applicable in a natural river setting. Further research would also be useful to establish design criteria for features such as the riffles containing protruding keystone particles.

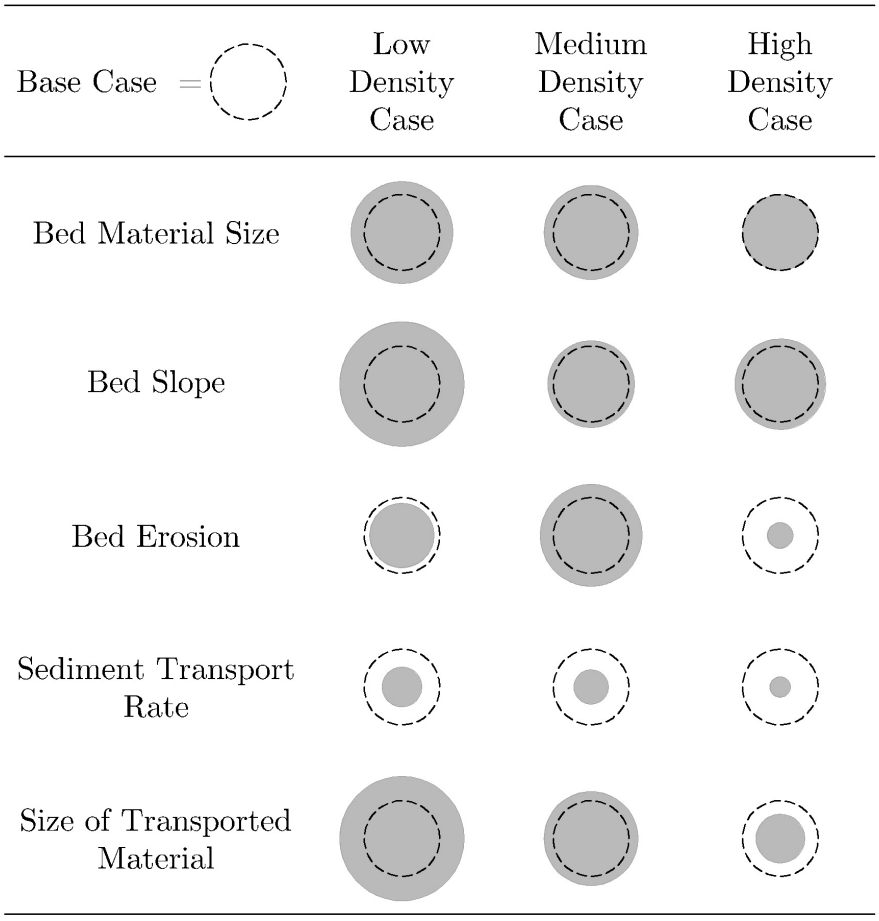

Figure 33: Relative changes in key parameters relative to the base case. Shaded circle scaled to represent change relative to the base case (shown as dashed circle).

7 Conclusions

This study investigated the effects of varying spatial densities of large immobile particles on sediment transport and bed morphology of a gravel-bed channel. A laboratory experiment was conducted to study this relationship by simulating a hydrograph over an alluvial bed in a flume. This research was aimed to present a more detailed look at the effects of large immobile particles on a channel bed, and to provide a more holistic overview to consolidate the findings of previous studies.

The results showed that the test cases corresponding to low densities of large immobile particles experienced a decrease in sediment transport rate, but an increase in the size of the transported material when compared to the base case. The bed in these cases experienced an increase in bed material size and an increase in coarse material clustering. These cases also experienced a more distinct clockwise hysteresis pattern with the coarse material comprising a greater fraction of the transported material.

As the experiments transitioned to the intermediate densities of large immobile particles, the sediment transport rates further decreased, and the size of the transported material also began to decrease. The channel bed experienced the greatest increase in bed material size during these cases, as well as experiencing the greatest amount of erosion. The hysteresis of these intermediate cases was an even stronger clockwise trend, while the sediment transport approached equal mobility.

Finally, at the highest densities of large immobile particles the size of transported material, the bed material size and the amount of coarse material clustering were all similar to the results presented in the base case. Despite these similarities, the bed experienced an increase in slope and decreased erosion compared to the base case. Additionally, the highest density cases experienced the strongest clockwise hysteresis trends and the greatest bias towards size selective transport.

The results presented within this study demonstrate that the effects of large immobile particles cannot be explained simply by relating keystone density to an increase in channel roughness and a decrease in transport capacity. However, the results are supported by a more holistic explanation using the results of existing literature, specifically the research completed by Brayshaw et al. (1983); Tan and Curran (2012); Hassan and Reid (1990). The overall holistic model is summarized in three points:

1. Isolated large immobile particles create localized areas of increased erosive forces, and localized protected areas (Brayshaw et al., 1983).
2. At a narrow range of large immobile particle spacings, flow structures build upon each other and amplify their erosive forces (Tan and Curran, 2012).
3. Densely spaced large immobile particles causes high energy skimming flow that is able to create powerful eddies in gaps between the large particles (Hassan and Reid, 1990).

While a substantial amount of research has been completed on the effects of large immobile particles on sediment transport and bed morphology, the previous studies were

often overly simplified or were conducted under a set of conditions that were not applicable to moderate gradient gravel-bed streams. The research presented in this study is able to consolidate the findings of existing literature to provide a more holistic understanding and explanation of the effects that large immobile particles have on a natural gravel-bed stream.

This thesis provides a framework for predicting or understanding the impacts to a natural channel system caused by the introduction of large immobile material. Additionally, the results of this study can be used to further research and develop design criteria for engineered in-channel structures to remedy imbalanced channel processes.

References

Andrews, E. D. (1983). Entrainment of gravel from naturally sorted riverbed material. *GSA Bulletin*, 94(10):1225.

Annable, W. K. (2010). *Quasi-equilibrium conditions of urban gravel-bed stream channels in Southern Ontario, Canada, and their implications for urban-stream restoration*. PhD thesis, Colorado State University.

Annable, W. K., Watson, C. C., and Thompson, P. J. (2012). Quasi-equilibrium conditions of urban gravel-bed stream channels in southern ontario, canada. *River Research and Applications*, 28(3):302–325.

Aristide Lenzi, M., Mao, L., and Comiti, F. (2006). When does bedload transport begin in steep boulder-bed streams? *Hydrological Processes*, 20(16):3517–3533.

Ashida, K. and Michiue, M. (1972). Study on hydraulic resistance and bed-load transport rate in alluvial streams. *Proceedings of the Japan Society of Civil Engineers*, 1972(206):59–69.

Ashworth, P. J. (1987). *Bedload transport and channel change in gravel-bed rivers*. PhD thesis, University of Stirling.

Ashworth, P. J. and Ferguson, R. I. (1986). Interrelationships of channel processes, changes and sediments in a proglacial braided river. *Geografiska Annaler. Series A, Physical Geography*, 68(4):361–371.

Ashworth, P. J. and Ferguson, R. I. (1989). Sizeselective entrainment of bed load in gravel bed streams. *Water Resources Research*, 25(4):627–634.

Blodgett, J. and McConaughy, C. (1986). Rock riprap design for protection of stream channel near highway structures, volume 2 - evaluation of riprap design procedures. report 89-4128, U.S. Geological Survey.

Booth, D. B. (1990). Stream-channel incision following drainage-basin urbanization1. *JAWRA Journal of the American Water Resources Association*, 26(3):407–417.

Brayshaw, A. C., Frostick, L. E., and Reid, I. (1983). The hydrodynamics of particle clusters and sediment entrapment in coarse alluvial channels. *Sedimentology*, 30(1):137–143.

Buffin-Blanger, T., Roy, A. G., and Kirkbride, A. D. (2000). On large-scale flow structures in a gravel-bed river. *Geomorphology*, 32(3):417 – 435.

Chin, A. (2006). Urban transformation of river landscapes in a global context. *Geomorphology*, 79(3):460 – 487. 37th Binghamton Geomorphology Symposium.

Church, M. and Hassan, M. A. (2002). Mobility of bed material in harris creek. *Water Resources Research*, 38(11):19–1–19–12. 1237.

Church, M., Hassan, M. A., and Wolcott, J. F. (1998). Stabilizing self-organized structures in gravel-bed stream channels: Field and experimental observations. *Water Resources Research*, 34(11):3169–3179.

Colorado Department of Transportation (2004). *Drainage Design Manual*.

Cowan, W. (1956). Estimating hydraulic roughness coefficients. *Agricultural Engineering*, 37(7):473–475.

Detert, M. and Weitbrecht, V. (2013). User guide to gravelometric image analysis by basegrain. *Advances in River Sediment Research*.

Du Buat, P. L. G. (1786). Principes d'hydraulique. *De l'Imprimerie de Monsieur*.

DuBoys, P. (1879). Le rhone et les rivieres a lit affouillable. *Annales de Ponts et Chausses*, 18:141–195.

Egiazaroff, I. V. (1965). Calculation of nonuniform sediment concentrations. *Journal of the Hydraulics Division*, 91:225–247.

Einstein, H. A. (1950). *The Bed-Load Function for Sediment Transportation in Open Channel Flows*.

Engelund, F. and Fredsøe, J. (1976). A sediment transport model for straight alluvial channels. *Hydrology Research*, 7(5):293–306.

Ferdowsi, B., Ortiz, C. P., Houssais, M., and Jerolmack, D. J. (2017). River-bed armouring as a granular segregation phenomenon. *Nature Communications*, 8:1363.

Finkenbine, J. K., Atwater, J. W., and Mavinic, D. S. (2000). Stream health after urbanization1. *JAWRA Journal of the American Water Resources Association*, 36(5):1149–1160.

Friedman, G. M. and Sanders, J. L. (1978). *Principals of Sedimentology*. John Wiley and Sons, Inc., United States of America.

Ghilardi, T. (2014). *Sediment transport and flow conditions in steep rivers with large immobile boulders*. Communication (Laboratoire de constructions hydrauliques, Ecole polytechnique fdrale de Lausanne). EPFL - LCH, Lausanne.

Graf, W. (1984). *Hydraulics of Sediment Transport*. Water Resources Publications.

Gregory, K. (2011). Wolman mg (1967) a cycle of sedimentation and erosion in urban river channels. geografiska annaler 49a: 385395. *Progress in Physical Geography: Earth and Environment*, 35(6):831–841.

Hammer, T. R. (1972). Stream channel enlargement due to urbanization. *Water Resources Research*, 8(6):1530–1540.

Hassan, M. A. and Church, M. (2000). Experiments on surface structure and partial sediment transport on a gravel bed. *Water Resources Research*, 36(7):1885–1895.

Hassan, M. A. and Reid, I. (1990). The influence of microform bed roughness elements on flow and sediment transport in gravel bed rivers. *Earth Surface Processes and Landforms*, 15(8):739–750.

Hawley, R. and Bledsoe, B. (2011). How do flow peaks and durations change in suburbanizing semi-arid watersheds? a southern california case study. *Journal of Hydrology - J HYDROL*, 405:69–82.

Hawley, R. and Bledsoe, B. (2013). Channel enlargement in semiarid suburbanizing watersheds: A southern california case study. *Journal of Hydrology*, 496:17 – 30.

Hawley, R. J., MacMannis, K. R., and Wooten, M. S. (2013). Bed coarsening, riffle shortening, and channel enlargement in urbanizing watersheds, northern kentucky, usa. *Geomorphology*, 201:111 – 126.

Hollis, G. E. (1975). The effect of urbanization on floods of different recurrence interval. *Water Resources Research*, 11(3):431–435.

Humphries, R., Venditti, J. G., Sklar, L. S., and Wooster, J. K. (2012). Experimental evidence for the effect of hydrographs on sediment pulse dynamics in gravel-bedded rivers. *Water Resources Research*, 48(1).

IOWA Department of Natural Resources (2006). *How to Control Streambank Erosion*.

J Nelson, E. and Booth, D. (2002). Sediment sources in an urbanizing, mixed land-use watershed. *Journal of Hydrology*, 264:51–68.

J. Walsh, C., Roy, A., W. Feminella, J., Cottingham, P., Groffman, P., and Morgan II, R. (2005). The urban stream syndrome: Current knowledge and the search for a cure. *Am. Benthol. Soc*, 24:706–723.

Julien, P. Y. (2002). *River Mechanics*. Cambridge University Press.

Kuhnle, R. A. (1982). Bed load transport during rising and falling stages on two small streams. *Earth Surface Processes and Landforms*, 17(2):191–197.

Luque, R. F. and Beek, R. V. (1976). Erosion and transport of bed-load sediment. *Journal of Hydraulic Research*, 14(2):127–144.

Manning, R. (1891). On the flow of water in open channels and pipes. *Transactions of the Institution of Civil Engineers of Ireland*, 20:161–207.

Mao, L. (2012). The effect of hydrographs on bed load transport and bed sediment spatial arrangement. *Journal of Geophysical Research: Earth Surface*, 117(F3):n/a–n/a. F03024.

Marion, D. A. and Weirich, F. (2003). Equal-mobility bed load transport in a small, step-pool channel in the ouachita mountains. *Geomorphology*, 55(1):139 – 154. Mountain Geomorphology - Integrating Earth Systems, Proceedings of the 32nd Annual Binghamton Geomorphology Symposium.

Melville, B. and Chin, C. (1986). Stream bed armouring. *9th Australasian Fluid Mechanics Conference*.

Meyer-Peter, E. and Müller, R. (1948). Formulas for bed-load transport. *International Association for Hydro-Environment Engineering and Research*, IAHSR 2nd meeting, Stockholm.

Morris, H. M. (1955). Flow in rough conditions. *Transactions American Society of Civil Engineers*, 120:373–398.

MTO (1997). Mto drainage management manual. *Drainage and Hydrology Section, Ministry of Transportation, Ontario, Canada*.

New Jersey State Soil Conservation Committee (2014). *The Standards for Soil Erosion and Sediment Control in New Jersey*. New Jersey Department of Agriculture.

Nezu, I., Nakagawa, H., and H. Jirka, G. (1993). Turbulence in openchannel flows. *Journal of Hydraulic Engineering*, 120:1235–1237.

Orrú, C., Blom, A., and Uijttewaal, W. S. J. (2016). Armor breakup and reformation in a degradational laboratory experiment. *Earth Surface Dynamics*, 4(2):461–470.

Parker, G. (1979). Hydraulic geometry of active gravel rivers. *ASCE J Hydraul Div*, 105.

Parker, G., Klingeman, P., and McLean, D. (1983). Bedload and size distribution in paved gravel-bed streams. *Journal of Hydraulic Engineering*, 109(5):793–794.

Petit, F. (1994). Dimensionless critical shear stress evaluation from flume experiments using different gravel beds. *Earth Surface Processes and Landforms*, 19(6):565–576.

Pizzuto, J. E., Hession, W. C., and McBride, M. (2000). Comparing gravel-bed rivers in paired urban and rural catchments of southeastern pennsylvania. *Geology*, 28(1):79.

Plumb, B. (2017). *Impacts of Hydromodification and Sediment Supply Alterations on Bedload Transport and Bed Morphology in Urbanizing Gravel-bed Rivers*. PhD thesis, University of Waterloo, Waterloo, Ontario, Canada.

Polster Environmental Services Ltd. (2003). Alternatives for bank stabilization - literature review. *Fisheries and Oceans Canada*, page 4.

Province of British Columbia (2000). *Riprap Design and Construction Guide*.

Reid, I., Frostick, L. E., and Layman, J. T. (1985). The incidence and nature of bedload transport during flood flows in coarse-grained alluvial channels. *Earth Surface Processes and Landforms*, 10(1):33–44.

Scottish Environment Protection Agency (2008). *Bank Protection: Rivers and Lochs*. Engineering in the Water Environment Good Practice Guide. EPFL - LCH.

Shields, A. (1936). Application of similarity principles and turbulence research to bed-load movement. *Soil Conservation Service, Cooperative Laboratory*.

Strom, K., Papanicolaou, A. N., Evangelopoulos, N., and Odeh, M. (2004). Microforms in gravel bed rivers: Formation, disintegration, and effects on bedload transport. *Journal of Hydraulic Engineering*, 130(6):554–567.

Sutton, H. (2008). Shoreline erosion control failures and how to avoid them. report, Illinois Lake Management Association and Lake Rip Rap, Inc.

Tan, L. and Curran, J. C. (2012). Comparison of turbulent flows over clusters of varying density. *Journal of Hydraulic Engineering*, 138(12):1031–1044.

Te Chow, V. (1959). *Open-channel hydraulics*. McGraw-Hill civil engineering series. McGraw-Hill.

Transport Association of Canada (2001). *Guide to Bridge Hydraulics*. Thomas Telford Publishing, second edition edition.

Trimble, S. W. (1997). Contribution of stream channel erosion to sediment yield from an urbanizing watershed. *Science*, 278(5342):1442–1444.

Tritico, H. M. and Hotchkiss, R. H. (2005). Unobstructed and obstructed turbulent flow in gravel bed rivers. *Journal of Hydraulic Engineering*, 131(8):635–645.

United States Geological Survey (1986). *Rock Riprap Design for Protection of Stream Channels near Highway Structures*. Water-Resources Investigations Report 86-4128. Federal Highway Administration.

U.S. Department of Transportation, Federal Highway Administration (1989). Design of riprap revetment. *HEC 11*.

Vermont Department of Environmental Conservation (2013). *Resloping, rock toe and rip rap, Bank stabilization*.

Wang, L., Cuthbertson, A. J., Pender, G., and Cao, Z. (2015). Experimental investigations of graded sediment transport under unsteady flow hydrographs. *International Journal of Sediment Research*, 30(4):306 – 320.

Waters, K. A. and Curran, J. C. (2015). Linking bed morphology changes of two sediment mixtures to sediment transport predictions in unsteady flows. *Water Resources Research*, 51(4):2724–2741.

Wilcock, P. R. and DeTemple, B. T. (2005). Persistence of armor layers in gravel-bed streams. *Geophysical Research Letters*, 32(8).

Wilcock, P. R. and McArdell, B. W. (1997). Partial transport of a sand/gravel sediment. *Water Resources Research*, 33(1):235–245.

Wilcock, P. R. and Southard, J. B. (1988). Experimental study of incipient motion in mixedsize sediment. *Water Resources Research*, 24(7):1137–1151.

Williams, G. P. (1989). Sediment concentration versus water discharge during single hydrologic events in rivers. *Journal of Hydrology*, 111(1-4):89–106.

Wong, M. and Parker, G. (2006). Reanalysis and correction of bed-load relation of meyer-peter and muller using their own database. *Journal of Hydraulic Engineering-asce - J HYDRAUL ENG-ASCE*, 132.

Yager, E. M., Kirchner, J. W., and Dietrich, W. E. (2007). Calculating bed load transport in steep boulder bed channels. *Water Resources Research*, 43(7):n/a–n/a. W07418.

Yager, E. M., Turowski, J. M., Rickenmann, D., and McArdell, B. W. (2012). Sediment supply, grain protrusion, and bedload transport in mountain streams. *Geophysical Research Letters*, 39(10):n/a–n/a. L10402.

Appendix

A Sediment Transport Data

λ/D = 1.92																							
Hydrograph Step	1	2	3	4	5	6	7	8	9	10	11	12	13	14	15	16	17	18	19		%Finer
Flow Rate (L/s)	6.0	7.0	8.0	9.0	10.0	11.0	12.0	13.0	14.0	15.0	16.0	14.8	13.5	12.3	11.0	9.8	8.5	7.3	6.0	Total	Than
Sample Total (g)		301		707		926		1888		3311	694	1883		801		153		51		10715	
Combined Total (g)		1008				2814				3311	694	1883		801			204			10715	
Sample Masses on Sieve (g)																					
11.3		0				0				0	0	0		0			0			0	*100%*
8		1				15				55	3	23		2			0			99	*99%*
5.6		28				212				377	89	136		35			2			879	*91%*
4		69				356				429	89	169		53			2			1167	*80%*
2.8		74				251				284	60	126		47			3			845	*72%*
2		58				161				192	40	109		39			4			603	*66%*
1.41		63				166				190	43	119		50			9			640	*60%*
1		65				174				193	39	123		56			13			663	*54%*
0.5		247				639				645	129	436		213			65			2374	*32%*
0.25		275				617				696	128	472		221			71			2480	*9%*
0.125		6				217				216	56	159		83			29			881	*1%*
pan		1007				10				10	2	6		2			1			37	*0%*

λ / D = 2.63																					
Hydrograph Step	1	2	3	4	5	6	7	8	9	10	11	12	13	14	15	16	17	18	19		
Flow Rate (L/s)	6.0	7.0	8.0	9.0	10.0	11.0	12.0	13.0	14.0	15.0	16.0	14.8	13.5	12.3	11.0	9.8	8.5	7.3	6.0	Total	
Sample Total (g)	269		641		726		2094		2439		628	1241		873		365		106		9382	%Finer Than
Combined Total (g)	910				2820				2439		628	1241		873		471				9382	
Sample Masses on Sieve (g) *11.3*	0				0				0		0	0		0		0				0	*100%*
8	1				26				32		10	10		7		0				86	*99%*
5.6	20				291				365		118	166		90		23				1073	*88%*
4	58				449				363		112	186		156		41				1365	*73%*
2.8	83				309				229		70	113		104		34				942	*63%*
2	71				190				147		40	72		64		24				608	*57%*
1.41	67				176				139		35	72		62		31				582	*50%*
1	70				174				132		31	67		57		40				571	*44%*
0.5	254				553				417		87	223		168		143				1845	*25%*
0.25	201				466				412		87	241		123		103				1633	*7%*
0.125	79				173				150		37	85		41		29				594	*1%*
pan	3				7				5		0	2		0		1				18	*1%*

λ/D = 3.82																					
Hydrograph Step	1	2	3	4	5	6	7	8	9	10	11	12	13	14	15	16	17	18	19		
Flow Rate (L/s)	6.0	7.0	8.0	9.0	10.0	11.0	12.0	13.0	14.0	15.0	16.0	14.8	13.5	12.3	11.0	9.8	8.5	7.3	6.0	Total	
Sample Total (g)	308		862		1454		3514		3877		1117	2538		1481		256		123		15530	%Finer Than
Combined Total (g)	1170				4968				3877		1117	2538		1481		379				15530	
Sample Masses on Sieve (g) *11.3*	0				0				0		0	0		0		0				0	*100%*
8	1				57				67		22	34		13		1				195	*99%*
5.6	39				568				551		170	300		144		8				1780	*87%*
4	103				808				671		199	415		209		24				2429	*72%*
2.8	114				560				433		121	277		160		19				1684	*61%*
2	83				343				271		75	173		106		15				1066	*54%*
1.41	86				315				246		70	163		103		25				1008	*47%*
1	82				289				220		58	151		100		32				932	*41%*
0.5	253				809				609		162	439		308		119				2699	*24%*
0.25	280				875				578		159	436		261		102				2691	*7%*
0.125	121				323				217		73	139		71		34				978	*0%*
pan	6				16				9		2	5		2		1				41	*0%*

λ/D = 5.17																					
Hydrograph Step	1	2	3	4	5	6	7	8	9	10	11	12	13	14	15	16	17	18	19		
Flow Rate (L/s)	6.0	7.0	8.0	9.0	10.0	11.0	12.0	13.0	14.0	15.0	16.0	14.8	13.5	12.3	11.0	9.8	8.5	7.3	6.0	Total	
Sample Total (g)	435		786		1547		2089		4859		1636	4143		2313		559		168		18535	%Finer Than
Combined Total (g)	1221				3636				4859		1636	4143		2313		727				18535	
Sample Masses on Sieve (g) *11.3*	0				0				0		0	0		0		0				0	*100%*
8	2				42				102		36	68		23		1				274	*99%*
5.6	40				451				866		273	656		227		22				2535	*85%*
4	117				580				947		274	763		348		52				3081	*68%*
2.8	128				386				591		179	488		249		48				2069	*57%*
2	98				237				337		115	304		163		39				1293	*50%*
1.41	93				219				284		99	255		156		53				1159	*44%*
1	86				199				235		85	229		151		63				1048	*38%*
0.5	263				612				624		238	626		459		225				3047	*22%*
0.25	275				638				603		238	557		419		176				2906	*6%*
0.125	110				253				234		88	179		112		45				1021	*1%*
pan	6				12				9		3	9		3		1				43	*0%*

λ/D = 6.75																					
Hydrograph Step	1	2	3	4	5	6	7	8	9	10	11	12	13	14	15	16	17	18	19		
Flow Rate (L/s)	6.0	7.0	8.0	9.0	10.0	11.0	12.0	13.0	14.0	15.0	16.0	14.8	13.5	12.3	11.0	9.8	8.5	7.3	6.0	Total	
Sample Total (g)	699		1504		1857		2683		4912		1390	3224		1630		386		57		18342	%Finer Than
Combined Total (g)	2203				4540				4912		1390	3224		1630		443				18342	
Sample Masses on Sieve (g) *11.3*	0				2				3		0	0		0		0				5	*100%*
8	5				71				121		29	49		25		2				302	*98%*
5.6	162				646				894		257	529		202		18				2708	*84%*
4	292				746				879		269	627		279		33				3125	*67%*
2.8	255				471				520		163	375		178		27				1989	*56%*
2	193				301				328		96	221		110		18				1267	*49%*
1.41	168				263				282		86	190		106		27				1122	*43%*
1	144				240				242		69	175		98		29				997	*37%*
0.5	408				767				710		187	483		300		122				2977	*21%*
0.25	414				754				696		171	425		257		130				2847	*5%*
0.125	150				259				216		58	138		71		37				929	*0%*
pan	9				12				11		2	6		2		1				43	*0%*

Base Case																					
Hydrograph Step	1	2	3	4	5	6	7	8	9	10	11	12	13	14	15	16	17	18	19		
Flow Rate (L/s)	6.0	7.0	8.0	9.0	10.0	11.0	12.0	13.0	14.0	15.0	16.0	14.8	13.5	12.3	11.0	9.8	8.5	7.3	6.0	Total	
Sample Total (g)	646		1461		2597		5529		8671		2781	7111		3529		1116		305		33746	%Finer
Combined Total (g)	2107				8126				8671		2781	7111		3529		1279				33604	Than
Sample Masses on Sieve (g) *11.3*	0				0				0		0	0		0		0				0	*100%*
8	3				104				151		54	95		23		7				437	*99%*
5.6	81				975				1392		444	962		337		46				4237	*86%*
4	182				1298				1490		443	1086		458		68				5025	*71%*
2.8	178				783				808		248	614		286		57				2974	*62%*
2	133				440				467		150	370		187		48				1795	*57%*
1.41	140				423				455		153	386		214		75				1846	*52%*
1	129				407				437		148	391		231		93				1836	*46%*
0.5	413				1281				1375		489	1326		822		398				6104	*28%*
0.25	440				1420				1437		474	1334		742		371				6218	*10%*
0.125	369				913				620		169	494		213		104				2882	*1%*
pan	31				69				34		8	29		10		1				182	*1%*

B Bed Material Data

Particle Count

	λ/D = 1.92		λ/D = 2.63		λ/D = 3.82		λ/D = 5.17		λ/D = 6.75		Base Case	
Size Range	Pre	Post	Pre	Post	Pre	Post	Pre	Post	Pre	Post	Pre	Post
15 <	73	73	49	53	23	22	15	10	10	4	0	0
11.3 - 15	1	3	0	0	1	0	0	0	1	0	0	0
8 - 11.3	8	9	15	19	12	21	10	31	9	36	13	21
5.6 - 8	27	44	36	57	50	72	28	86	47	77	53	71
4 - 5.6	33	41	53	62	39	77	38	73	59	62	90	79
2.8 - 4	50	44	76	74	54	65	76	72	71	76	77	97
2 - 2.8	60	61	60	32	87	53	84	36	65	47	110	108
< 2	68	45	31	18	54	10	69	12	58	18	98	65
Total Count	320	320	320	315	320	320	320	320	320	320	441	441
Excluding Keystones	247	247	271	262	297	298	305	310	310	316	441	441

% Finer Excluding Keystones

	λ/D = 1.92		λ/D = 2.63		λ/D = 3.82		λ/D = 5.17		λ/D = 6.75		Base Case	
Size	Pre	Post	Pre	Post	Pre	Post	Pre	Post	Pre	Post	Pre	Post
15	100%	100%	100%	100%	100%	100%	100%	100%	100%	100%	100%	100%
11.3	100%	99%	100%	100%	100%	100%	100%	100%	100%	100%	100%	100%
8	96%	95%	94%	93%	96%	93%	97%	90%	97%	89%	97%	95%
5.6	85%	77%	81%	71%	79%	69%	88%	62%	82%	64%	85%	79%
4	72%	61%	62%	47%	66%	43%	75%	39%	63%	45%	65%	61%
2.8	52%	43%	34%	19%	47%	21%	50%	15%	40%	21%	47%	39%
2	28%	18%	11%	7%	18%	3%	23%	4%	19%	6%	22%	15%
0	0%	0%	0%	0%	0%	0%	0%	0%	0%	0%	0%	0%

Size Classes												
D16			2.14	2.57	1.95	2.54		2.82		2.53		2.03
D30	2.07	2.35	2.65	3.21	2.29	3.24	2.19	3.50	2.40	3.22	2.22	2.47
D50	2.73	3.23	3.45	4.15	2.94	4.38	2.79	4.70	3.29	4.39	2.97	3.33
D60	3.23	3.94	3.92	4.79	3.58	4.99	3.22	5.42	3.84	5.21	3.64	3.92
D84	5.40	6.40	6.04	6.93	6.25	7.01	5.09	7.41	5.92	7.48	5.51	6.24
D90	6.50	7.22	7.10	7.65	7.10	7.66	6.16	8.00	6.82	8.34	6.49	7.12

C Profile Plots

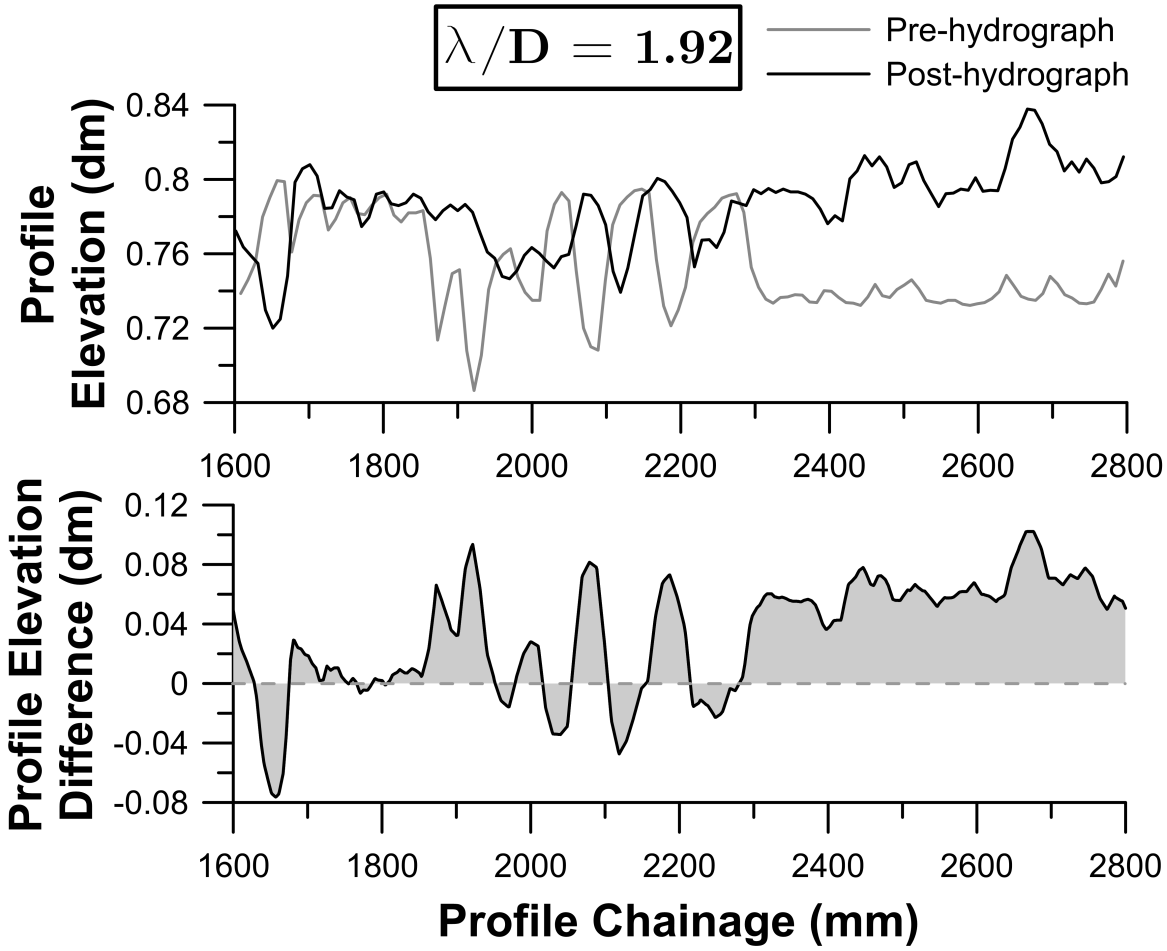

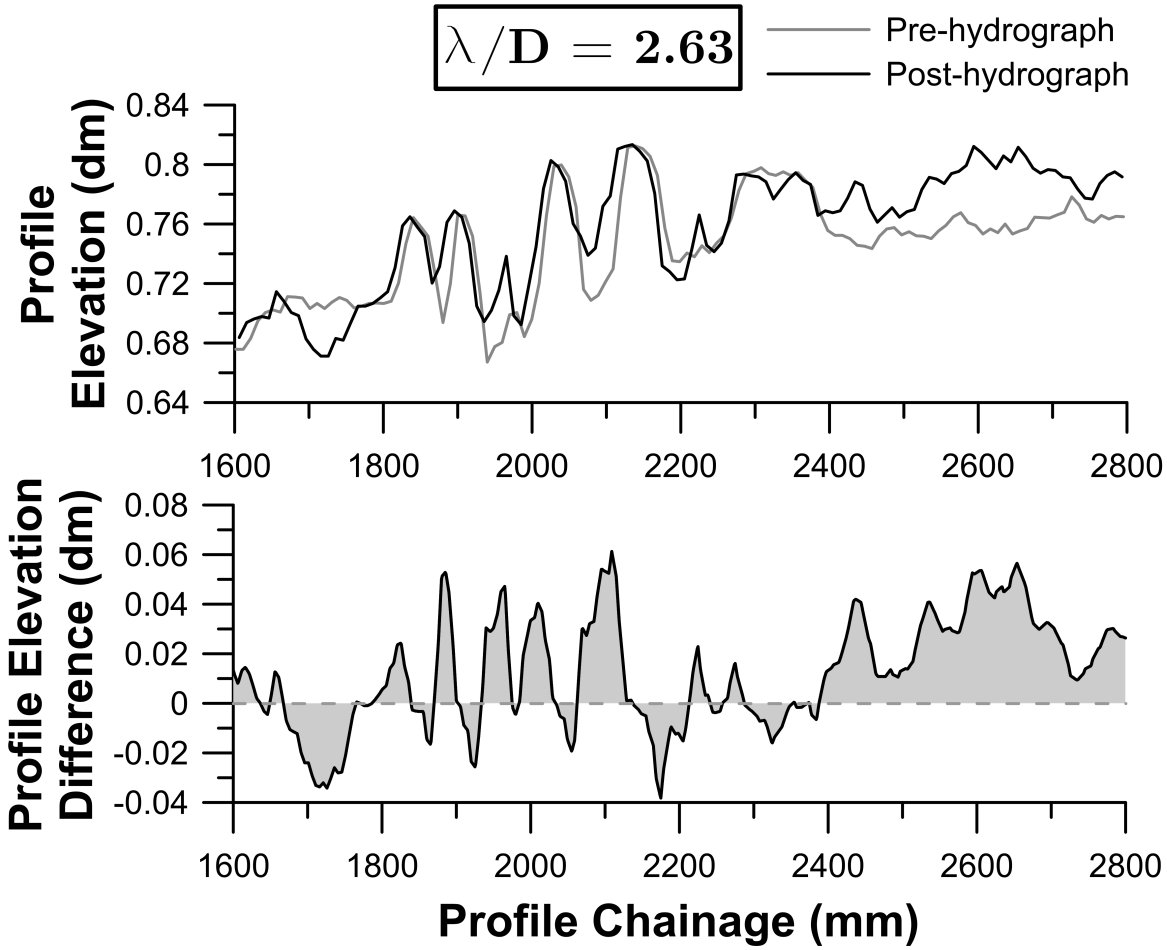
$\lambda/D = 2.63$
Pre-hydrograph
Post-hydrograph
Profile Elevation (dm)
0.84
0.8
0.76
0.72
0.68
0.64
1600
1800
2000
2200
2400
2600
2800
Profile Elevation Difference (dm)
0.08
0.06
0.04
0.02
0
-0.02
-0.04
1600
1800
2000
2200
2400
2600
2800
Profile Chainage (mm)

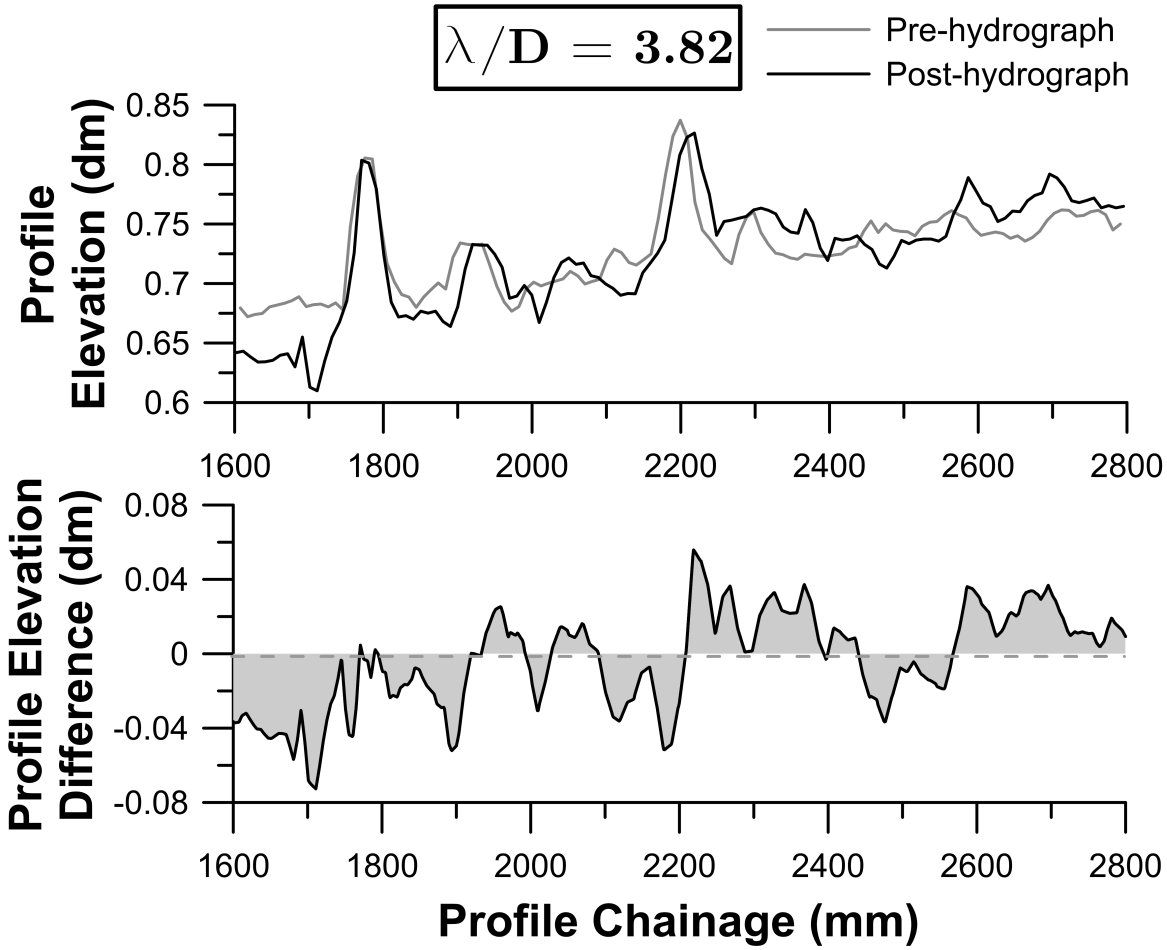
$\lambda/D = 3.82$
Pre-hydrograph
Post-hydrograph
Profile Elevation (dm)
0.85
0.8
0.75
0.7
0.65
0.6
1600
1800
2000
2200
2400
2600
2800
Profile Elevation Difference (dm)
0.08
0.04
0
-0.04
-0.08
1600
1800
2000
2200
2400
2600
2800
Profile Chainage (mm)

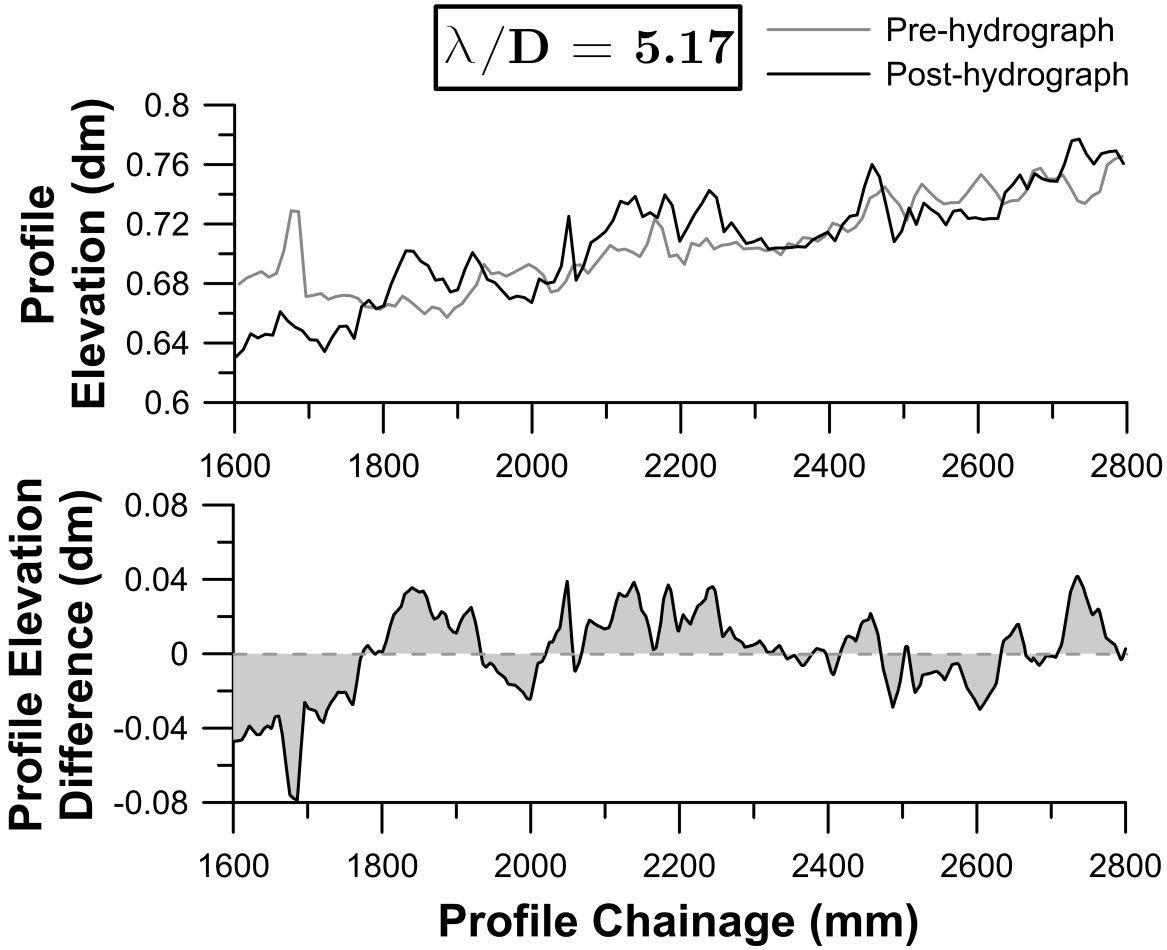
$\lambda/D = 5.17$
Pre-hydrograph
Post-hydrograph
Profile Elevation (dm)
0.8
0.76
0.72
0.68
0.64
0.6
1600
1800
2000
2200
2400
2600
2800
Profile Elevation Difference (dm)
0.08
0.04
0
-0.04
-0.08
1600
1800
2000
2200
2400
2600
2800
Profile Chainage (mm)

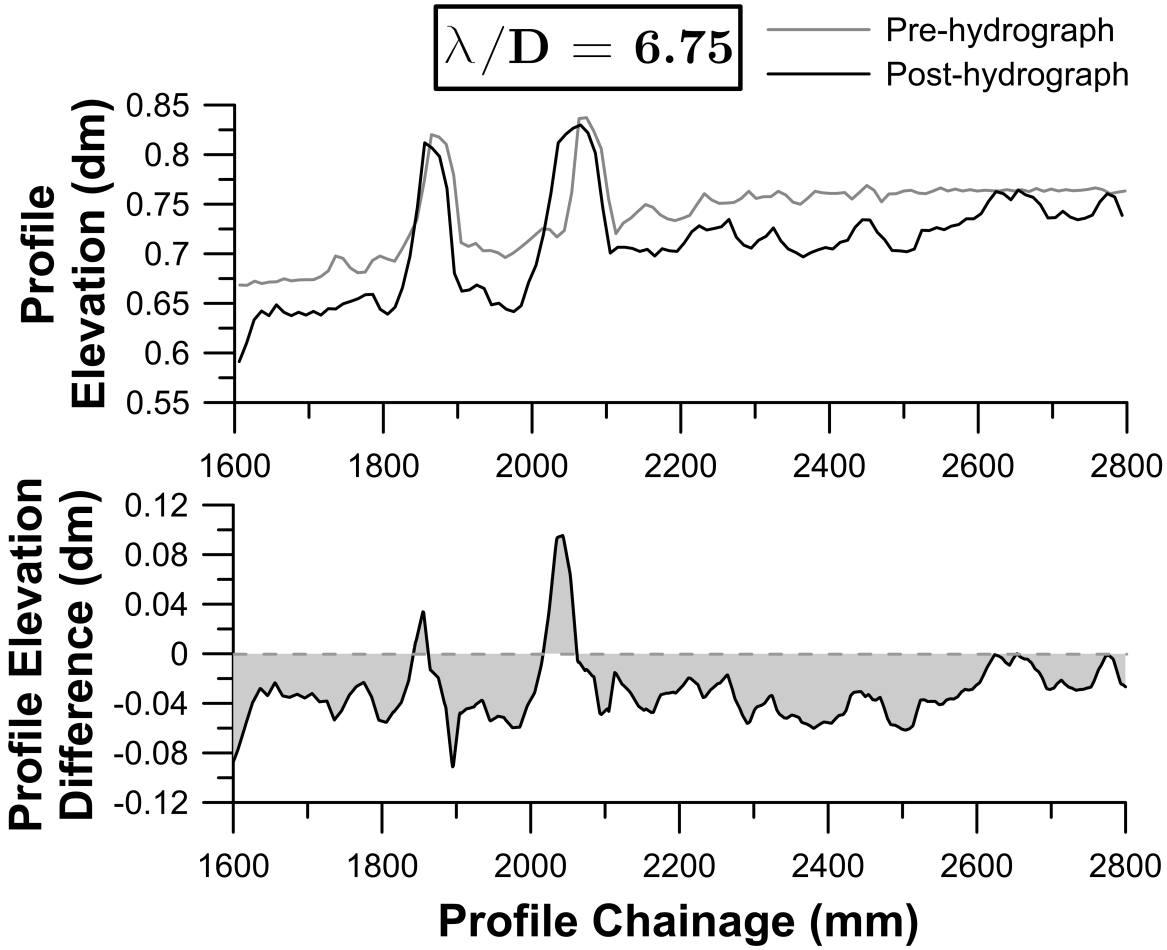
$\lambda/D = 6.75$
Pre-hydrograph
Post-hydrograph
Profile Elevation (dm)
0.85
0.8
0.75
0.7
0.65
0.6
0.55
1600
1800
2000
2200
2400
2600
2800
Profile Elevation Difference (dm)
0.12
0.08
0.04
0
-0.04
-0.08
-0.12
1600
1800
2000
2200
2400
2600
2800
Profile Chainage (mm)

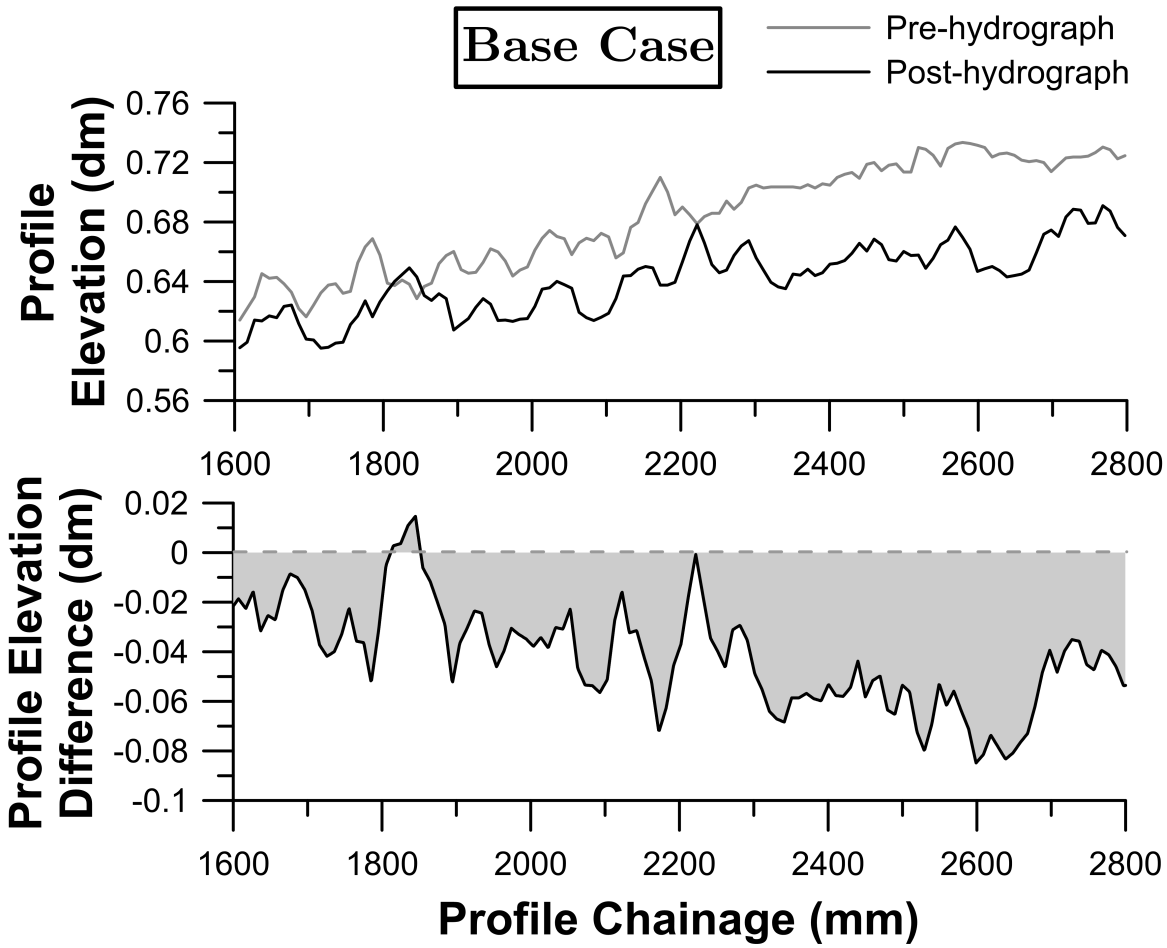
Base Case
Pre-hydrograph
Post-hydrograph
Profile Elevation (dm)
0.76
0.72
0.68
0.64
0.6
0.56
1600
1800
2000
2200
2400
2600
2800
Profile Elevation Difference (dm)
0.02
0
-0.02
-0.04
-0.06
-0.08
-0.1
Profile Chainage (mm)

D Particle Clustering Maps

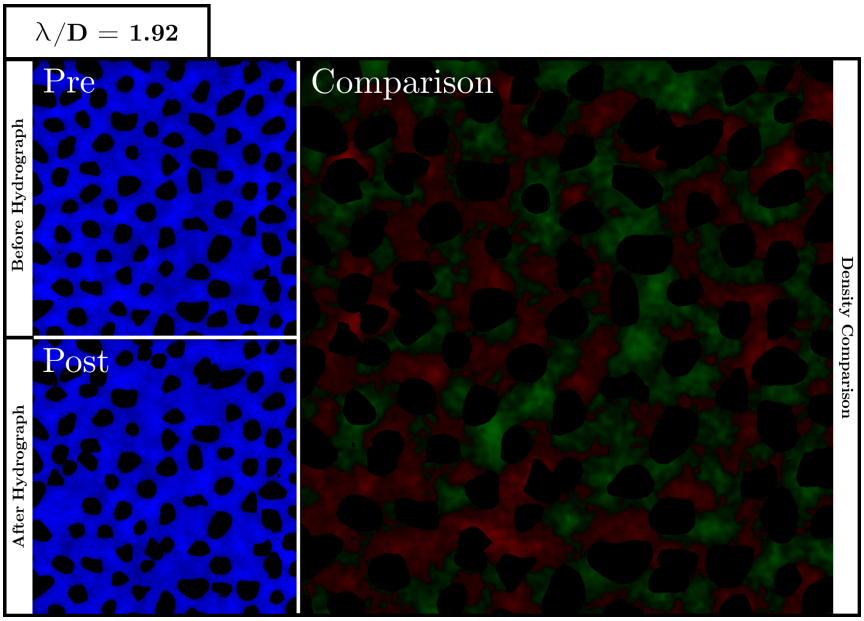

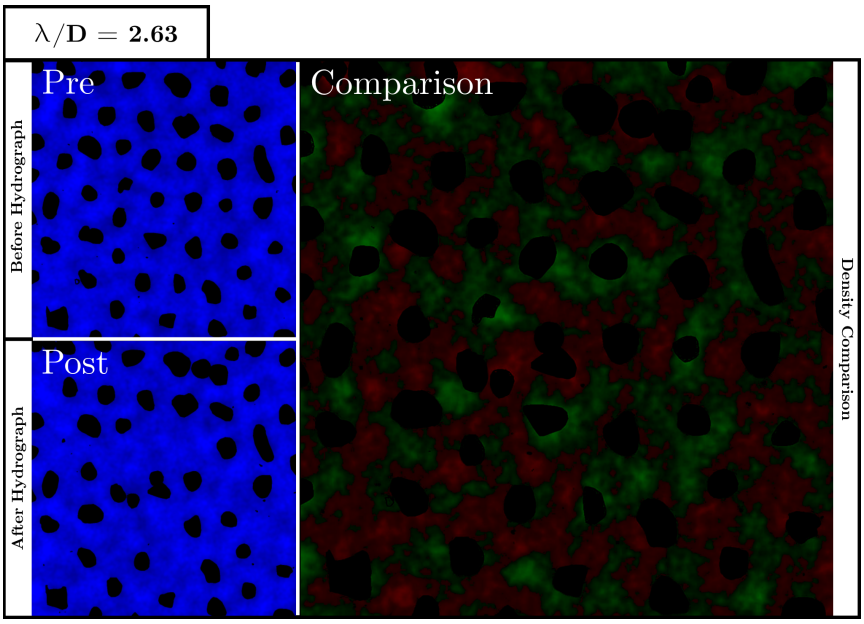

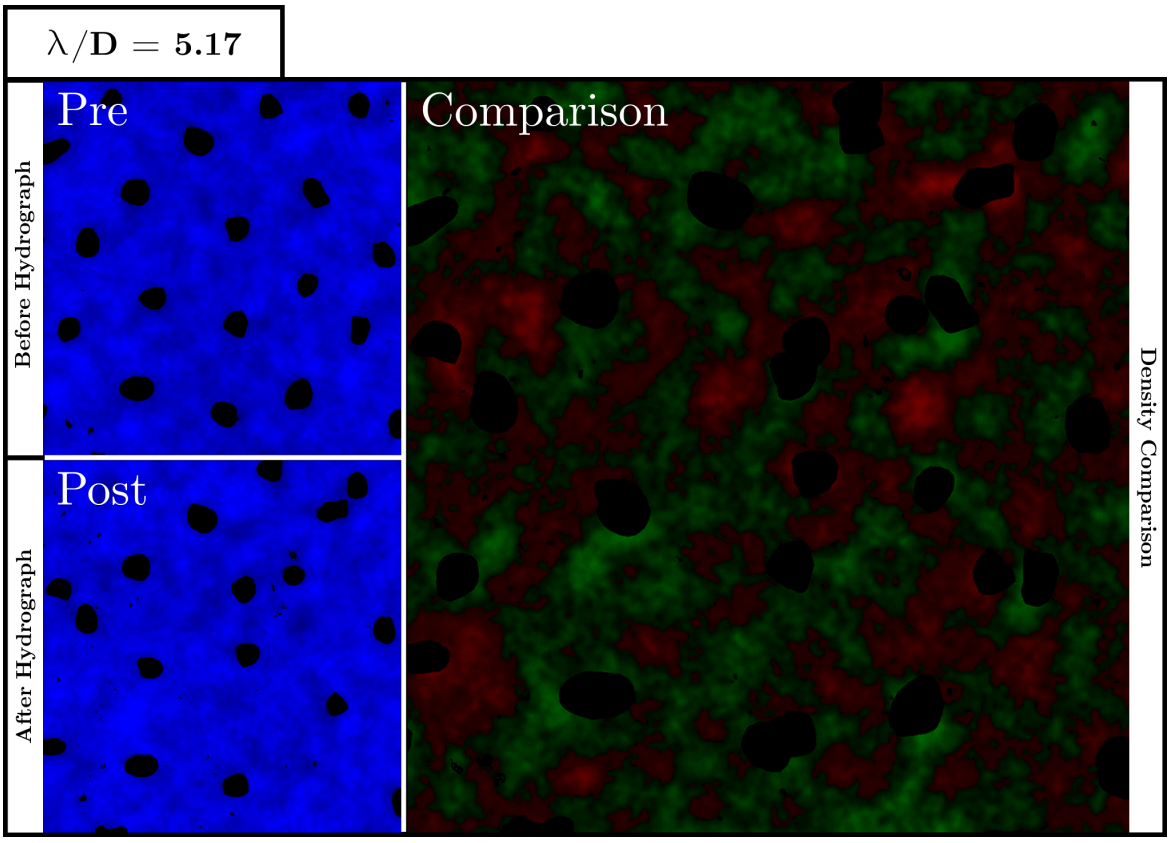
λ/D = 5.17
Pre
Post
Comparison
Before Hydrograph
After Hydrograph
Density Comparison

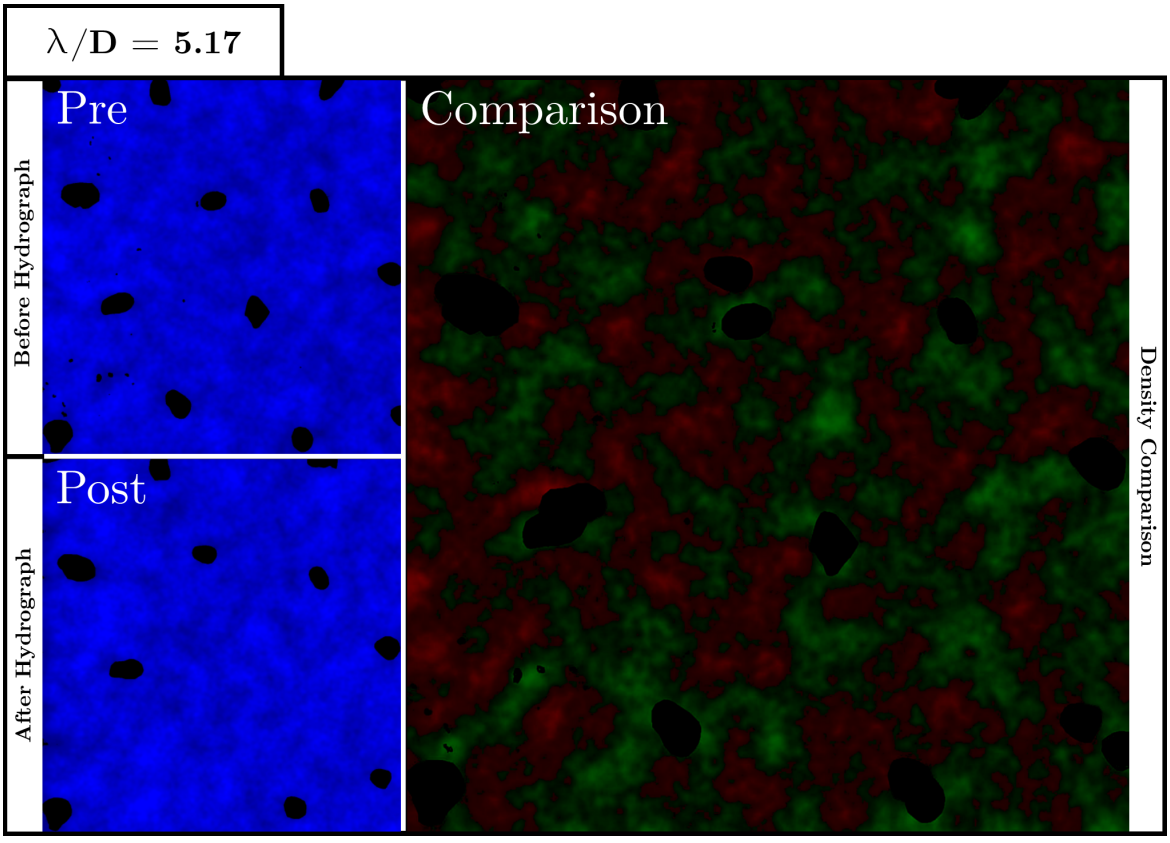
λ/D = 5.17
Pre
Post
Comparison
Before Hydrograph
After Hydrograph
Density Comparison

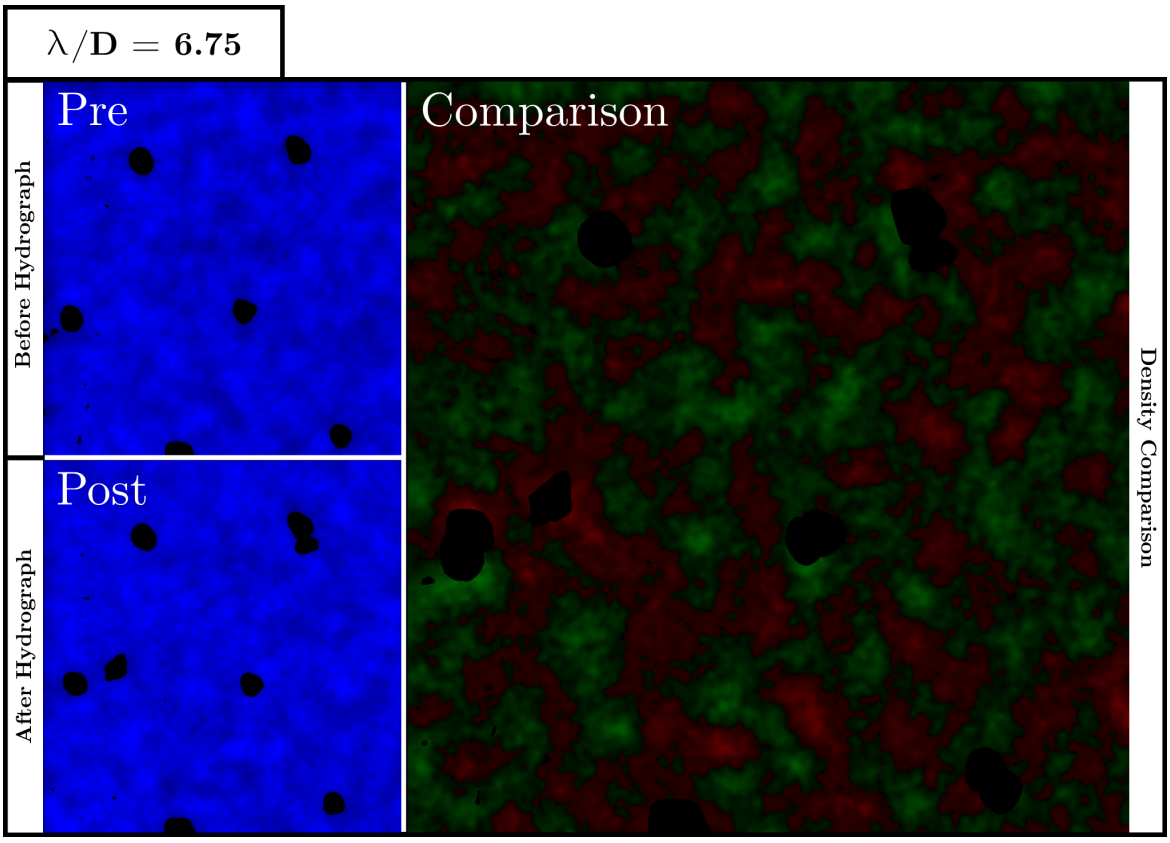
λ/D = 6.75
Pre
Comparison
Before Hydrograph
Post
After Hydrograph
Density Comparison

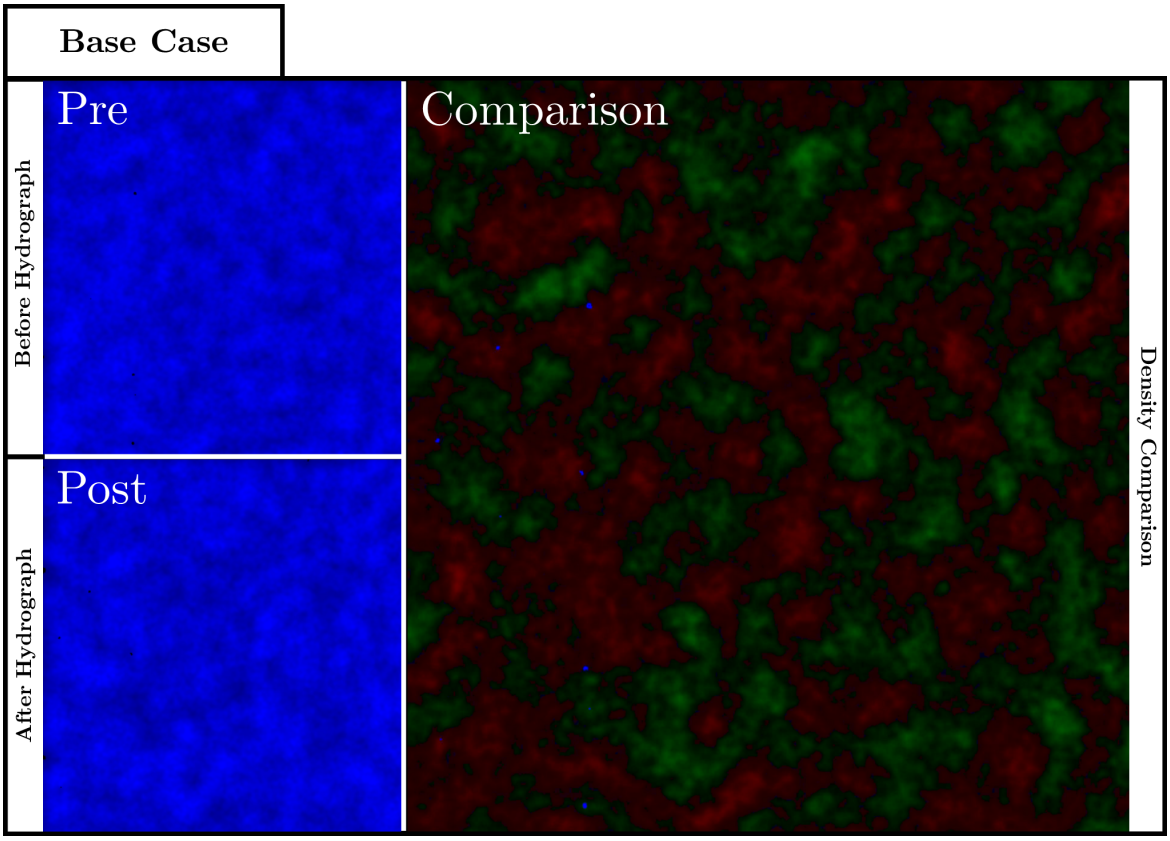
Base Case
Pre
Comparison
Before Hydrograph
Post
After Hydrograph
Density Comparison

E Hysteresis Plots

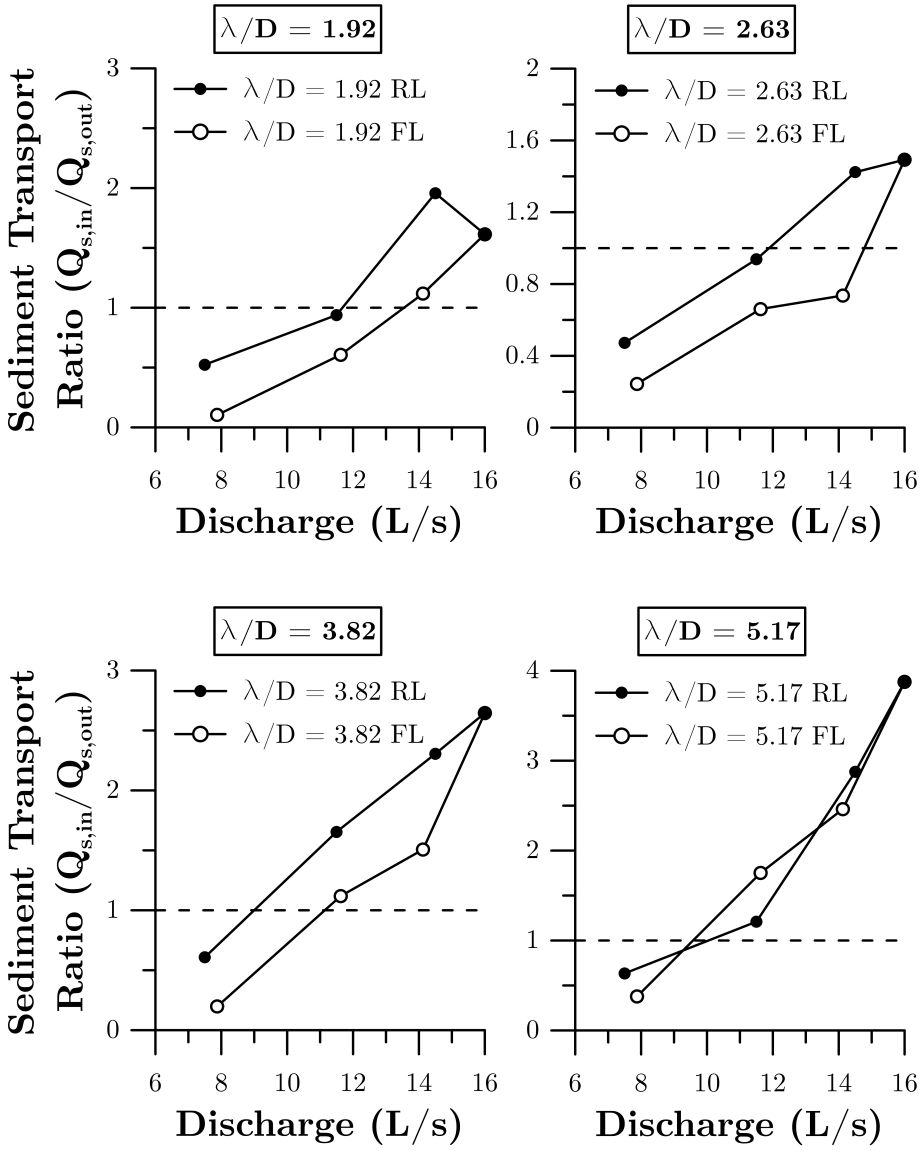

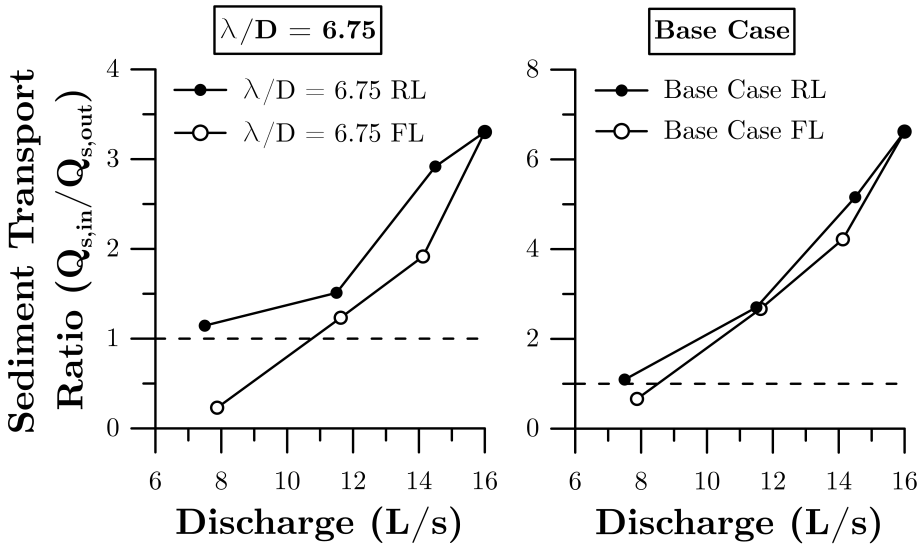
λ/D = 6.75
Base Case
Sediment Transport Ratio ($Q_{s,in}/Q_{s,out}$)
λ/D = 6.75 RL
λ/D = 6.75 FL
Base Case RL
Base Case FL
0
1
2
3
4
6
8
10
12
14
16
Discharge (L/s)
Discharge (L/s)